UNIVERSITÀ DI SIENA 1240

UNIONE EUROPEA
FSE REACT-EU

PhD Program developed with the financial support of the PON REACT-EU program

DEPARTMENT OF BIOTECHNOLOGY, CHEMISTRY AND PHARMACY

**PhD Program in Biochemistry and Molecular Biology**
**37° Cycle**
Coordinator: Prof. Lorenza Trabalzini

# Cadmium detoxification mechanisms in *Populus alba*: ecophysiological perspectives and the role of thiol-peptides

Academic discipline: BIOS-07/A

*Candidate*
Valentina Vitelli
Mass Spectrometry center, at St.Chiara Hospital, AOUP, Pisa, Italy

31/03/2025 12:11:01
VALENTINA VITELLI

Valentina Vitelli

*Supervisor*
Alessandro Saba
Department of Surgical, Medical, and Molecular Pathology and Critical Care Medicine, University of Pisa, Pisa, Italy

*Co-supervisor*
Andrea Andreucci
Department of Biology University of Pisa, Pisa, Italy

Academic year of the PhD
2023/24

University of Siena
PhD PROGRAM IN BIOCHEMISTRY AND MOLECULAR BIOLOGY
37° Cycle

*Date of the final exam*

*17 April 2025*

*Examining board*

*Prof. Giovanni Signore*
*PA - SSD BIOS-07/A – Department of Biology– University of Pisa, Pisa, Italy*

*Prof. Anna Solini*
*PA – SSD MEDS-05/A -Department of Surgical, Medical, and Molecular Pathology and Critical Care Medicine, University of Pisa, Pisa, Italy*

*Prof. Antonio Junior Lepedda*
*RTD – SSD BIOS-07/A – Department of Biomedical Science – University of Sassari*

*Dr. Amalia Gastaldelli-Expert member*
*Institute of Clinical Physiology – CNR - Pisa*

*Substitutes*

*Prof. Sandra Ghelardoni*
*PA – SSD BIOS-07/A - Department of Surgical, Medical, and Molecular Pathology and Critical Care Medicine, University of Pisa, Pisa, Italy*

*Prof. Stefano Luin*
*PA – SSD PHYS-03/A– Scuola Normale Superiore*

## TABLE OF CONTENTS

## Figure list

**Figure 17.** Leaf area (A), stems length (B), roots length (C), number of leaves per plant (D), and dry matter percentage (E) measured in *P. alba* samples treated with 0 (CTRL), 50, and 100 μM $Cd^{2+}$. Values are presented as mean ± SE. The abbreviation "ns" indicates no significant differences between different concentrations and organs (one-way ANOVA followed by Tukey's test, $p < 0.05$).

**Figure 18**. JIP-test parameters performed on *P. alba* samples treated with 0 (control), 50, and 100 μM $Cd^{2+}$: technical parameters (A), specific energy fluxes (B), phenomenological energy fluxes at time 0 (C), and phenomenological energy fluxes at the final time (D). Values are presented as mean ± SE. The abbreviation "ns" indicates no significant differences between different concentrations and organs (one-way ANOVA followed by Tukey's test, $p < 0.05$).

**Figure 19.** Chromatogram of standard mixture (500 ng/mL) of GSH, PC2, PC3, PC4 analytes in extraction buffer.

**Figure 20.** Intracellular GSH content in the three organs (leaves, stems, and roots) of *P. alba* samples treated with 0 (CTRL), 50, and 100 μM $Cd^{2+}$, expressed as nmol/g FW. Values are presented as mean ± SE. Different letters indicate significant differences between different concentrations and organs (two-way ANOVA followed by Tukey's test, $p < 0.05$).

**Figure 21.** Total intracellular PCn content in the three organs (leaves, stems, and roots) of *P. alba* samples treated with 0 (CTRL), 50, and 100 μM $Cd^{2+}$, expressed as nmol/g FW. Values are reported as mean ± SE. Different letters indicate significant differences between different concentrations and organs (two-way ANOVA followed by Tukey's test, $p < 0.05$).

**Figure 22**. Intracellular content in shoots (A) and roots (B) and extracellular presence (C) of GSH at 0 (CTRL), 5,10, 20, 36 μM $Cd^{2+}$ after 24-48-72 h as exposure times. Values are reported as mean ± SE. Different letters indicate significant differences between different concentrations and organs (two-way ANOVA followed by Tukey's test, $p < 0.05$).

**Figure 23**. Intracellular content in shoots (A) and roots (B) and extracellular presence (C) of PCn at 0 (CTRL), 5,10, 20, 36 μM $Cd^{2+}$ after 24-48-72 h as exposure times. Values are reported as mean ± SE. Different letters indicate significant differences between different concentrations and organs (two-way ANOVA followed by Tukey's test, $p < 0.05$).

**Figure 24.** Intracellular (in roots, A, B, C) and extracellular (D, E, F) phytochelatin oligomers PC2-3-4 (nmol/g FW) at 0 (CTRL), 5,10, 20, 36 μM $Cd^{2+}$ stressed condition, after 24-48-72 h as exposure times. Values are reported as mean ± SE (n = 3). Different letters indicate significant differences (two-way ANOVA followed by Tukey's test, $p < 0.05$).

**Figure 25.** JIP-test technical parameters performed on *P. alba* samples treated with 0 (CTRL), and 36 μM $Cd^{2+}$, both under 72 h of treatment.

**Figure 26:** Inhibition study on *P.alba* plasmalemma transporters: GSH values (nmol/g FW of root system) obtained by HPLC-MS/MS analysis of extracellular thiol-peptides at 0 (CTRL) and 36 µM $Cd^{2+}$ without inhibitor and with sodium orthovanadate 0.125mM (A) or 0.250 mM (B). PCn values (nmol/g FW of root system) obtained by HPLC-MS/MS analysis of extracellular thiol-peptides at 0 (CTRL) and 36 µM $Cd^{2+}$ without inhibitor and with sodium orthovanadate 0.125mM (C) or 0.250 mM (D). Values are reported as mean ± SE (n = 3). Different letters indicate significant differences (two-way ANOVA followed by Tukey's test, $p < 0.05$).

**Figure 27.** Relative percentages of GSH (A) and PCn (B) in shoots, roots, and media, with 100% representing the total sum of these three compartments, under 36 µM $Cd^{2+}$ stressed condition maintained for 48 and 72 h, with or without sodium orthovanadate (0.125-0.250 mM). Values are reported as mean ± SE (n = 3). The comparison of the percentage distribution of shoots, roots, and growth medium across different conditions was performed. Different letters indicate significant differences and the abbreviation "ns" indicates no significant differences (one-way ANOVA followed by Tukey's test, $p < 0.05$).

**Figure 28.** *In vivo* concentrations of phytochelatins (PCn, nmol/g FW) in *Marchantia polymorpha* gametophytes exposed for 6, 14, 24, 72, and 120 h to 80 µM (light blue bars) or 200 µM (blue bars) Zn (A) and to 80 µM (beige bars) or 200 µM (orange bars) Cu (B) and to 200 µM (pink bars) or 300 µM (amaranth bars) Fe (C). Values are reported as mean ± SE. Different letters indicate significant differences between different concentrations and organs (two-way ANOVA followed by Tukey's test, $p < 0.05$) [227]. Values are reported as mean ± SE. Different letters indicate significant differences between different concentrations and organs (two-way ANOVA followed by Tukey's test, $p < 0.05$).

**Figure 29.** *In vivo* phytochelatin oligomers PC2-3-4 (nmol/g FW) in *Marchantia polymorpha* gametophytes exposed for 6, 14, 24, 72, and 120 h and to 80 µM (light blue bars, A) or 200 µM (blue bars, B) Zn and to 80 µM (beige bars, C) or 200 µM (orange bars, D) Cu and to 200 µM (pink bars, E) or 300 µM (amaranth bars, F) Fe. Values are reported as mean ± SE. Different letters indicate significant differences between different concentrations and organs (two-way ANOVA followed by Tukey's test, $p < 0.05$) [227].

**Figure 30.** Extracellular concentrations of phytochelatins (PCn, nmol/g FW) in the ms ½ growth medium, where *Marchantia polymorpha* gametophytes were exposed for 24 and 72 h to 80 µM (light blue bars) or 200 µM (blue bars) Zn (A); 80 µM (beige bars) or 200 µM (orange bars) Cu (C); 200 µM (pink bars) or 300 µM (amaranth bars) Fe (E). Extracellular concentrations of GSH (nmol/g FW) in the MS ½ growth medium, where *M. polymorpha*

gametophytes were exposed for 24 and 72 h to 80 µM (light blue bars) or 200 µM (blue bars) Zn (B); 80 µM (beige bars) or 200 µM (orange bars) Cu (D); 200 µM (pink bars) or 300 µM (amaranth bars) Fe (F). Values are means ± SE (n = 3). Different letters indicate significant differences (two-way ANOVA followed by Tukey's test, $p < 0.05$) [227].

## Table list

## Abbreviation

ABC: ATP-binding cassette

ACN: Acetonitrile

ALMT14: Aluminum-activated malate transporter 14

As: Arsenic

BQB: ω-bromoacetonylquinolinium bromide

Ca: Calcium

CAD: Collision gas

$Cl^-$ : Chloride ion

CAT: Proteins like catalase

$Cd^{2+}$ : Cadmium divalent ion

$CdSO_4$ : Cadmium sulphate

CE: Collision energy

CET: Cation efflux transporter

$CH_3COO^-$: Acetate ion

CID: Collision-induced dissociation

CIPK23: CBL-interacting protein kinase 23

CTRL: Control condition

CXP: Collision cell exit potential

Co: Cobalt

Cr: Chromium

Cu: Copper

Cys: Cysteine

CUR: Curtain gas

DEPC: Diethylpyrocarbonate

DTNB: 5,5-dithiobis(2-ni- trobenzoic acid)

DP: Declustering potential

DTPA: Diethylenetriaminepentaacetic

DW: Dry weight

EDTA: Ethylenediaminetetraacetic acid

ESI: Electrospray ionisation

FA: Formica acid

Fe: Iron

FW: Fresh weight

γ-EC: γ-glutamylcysteine

Glu: Glutamic acid

GPx: Glutathione peroxidase

GR: Glutathione reductase

GRX: Glutaredoxin

GS1-2: Gas Source 1-2

GSH: Glutathione

$H_2O$: Water

HCl: Chloridic acid

$HCOO^-$ : Formate ion

Hg: Mercury

HILIC: Hydrophilic Interaction Liquid Chromatography

HLB: Hydrophilic-lipophilic balance

HM: Heavy metal

HMA: Heavy metal ATP-ase

HPLC: High-Performance Liquid Chromatography

HPLC-MS/MS: High-Performance Liquid Chromatography coupled with Tandem Mass Spectrometry

IDF1: IRT1 degradation factor 1 protein

IQ1: Focusing lens 1

IRT: Iron-regulated transporter-like protein

IS: Ion spray voltage

$K^+$ : Potassium ion

KOH: Potassium hydroxide

LIT: Linear ion trap

MeOH: Methanol

Mn: Manganese

MRM: Multiple reaction monitoring

MS: Mass spectrometry

MS: Murashige & Skoog Medium

MT: Metallothionin

MTP: Metal tolerance or transporter protein

$Na^+$: Sodium ion

$N_2$: Nitrogen

NAA: Alpha-naphthaleneacetic acid

$Na_3VO_4$: Sodium orthovanadate

$NH_4^+$: Ammonium ion

$NH_4OH$: Ammonium hydroxide

NRAMP: Natural resistance-associated macrophage protein

n-BuOH: Normal-butanol

NEG : Negative

NRAMP: Natural resistance and macrophage protein

$OH^-$: Hydroxy ion

Pb: Lead

PCn:  Phytochelatins

PCS: Phytochelatin synthase

PDR: Pleiotropic drug resistance transporter

POS: Positive

PSII: Photosystem II

QMF: Quadrupole mass filter

$Q_n$: Quadrupole

RBOHD: Respiratory burst oxidase homolog protein D

RNS: Reactive nitrogen species

ROS: Reactive oxigen species

RP: Reverse phase

RT-PCR: Real Time PCR

Sn: Tin

SOS2L1: Kinase salt overly sensitive 2-like1protein

SPE: Solid phase extraction

SRM: selected reaction monitoring

ST: Prefilter value

TCEP: Tris(2-chloroethyl)phosphate

TE: Source temperature

TMD: Transmembrane domain

$t_R$: Retention time

UHPLC: Ultra High-Performance Liquid Chromatography

Vitamin C: ascorbic acid

Vitamin E: ϱ-tocopherol

WAX: Weak anion exchange

WCX: Weak cation exchange

WPM: Woody plant medium

ZIP: Zinc-regulated transporter-like protein

## Abstract

Due to its exceptional toxicity to all biological systems, cadmium (Cd) is a heavy metal (HM) frequently released into the environment by both natural and man-made sources and is particularly pervasive in soils competing with the plant for nutrient uptake. In contrast to organic pollutants, HMs are non-biodegradable and tend to accumulate in living organisms. For these reasons HMs and specifically Cd are dangerous even at low concentrations as they can result in micronutrient deficiencies. This impactful problem of HM pollution in environment is a significant risk to public health worldwide. *Populus alba* has been identified as a promising phytoremediator due to its ability to withstand various HMs, employing different tolerance and detoxification mechanisms, including the production of phytochelatins (PCn), which are cysteine-rich oligopeptides synthesized from glutathione (GSH) by the enzyme phytochelatin synthase (PCS). The principal mechanism of intracellular HMs detoxification involves the formation of PCn-HM complexes, which are then sequestered in the vacuole for detoxification.

To investigate the thiol-peptides role in *Populus alba* HM detoxification, we developed an HPLC-MS/MS method for quantifying GSH and PCn in plant matrices under CTRL and $Cd^{2+}$-stressed conditions. The first experimental setup provided the evaluation of biometric parameters, fluorescence and photosynthetic efficiency, and thiol-peptide quantifications in *Populus alba* plants exposed to high $Cd^{2+}$ stressed conditions (50 and 100 μM $CdSO_4$) in a woody plant solid medium with vitamins (pH 5.85) for two months. To assess short-term responses of *Populus alba*, a second set of experiments was conducted: one-month-old plants were transferred to Gamborg's B5 liquid medium (pH 5.85) containing various concentrations of $CdSO_4$ (5, 10, 20, 36 μM) for exposure durations of 24-48-72 hours. The plants' shoots and roots were sampled and analysed to assess GSH and PCn levels at different exposure times and $Cd^{2+}$ concentrations. Concurrently, the growth medium was analysed to track the potential expulsion of GSH and PCn- $Cd^{2+}$ complexes from the roots. Preliminary results indicated an increase in both intracellular and extracellular GSH and PCn concentrations, which correlated with longer treatment durations and higher $Cd^{2+}$ concentrations. At the same time, to investigate whether thiol-peptide release observed in complex plants also occurs in simpler cellular organisms, we used immortalized *Arabidopsis thaliana* cells as a model. Cells were exposed to control conditions and varying concentrations of $Cd^{2+}$ (10, 20, and 36 μM) for 48 and 72 hours. Analytical evaluation of GSH and PCn demonstrated that eukaryotic cells effectively employ defence mechanisms against HM stress. Notably, at 20 μM $Cd^{2+}$ after 48 hours,

significant thiol-peptide production was observed both intracellularly and extracellularly. To investigate the release of thiol-peptides into the extracellular environment an inhibition study of hypothetical plasmalemma membrane PCn/ PCn- $Cd^{2+}$ transporters was conducted. This study highlights a remarkable ability of *Populus alba* to tolerate Cd stress, through the investigation of its detoxification mechanisms. Notably, the focus on PCn revealed their dual role: not only they chelate Cd at the intracellular level, but they also contribute to the formation of an extracellular barrier, further protecting the plant from metal toxicity.

# 1. INTRODUCTION

## 1.1 Heavy metals and cadmium stress in plants

Heavy metals (HMs) are elements characterized by an atomic number greater than 20, an atomic density exceeding 5 g/cm$^3$, and metallic properties. Transition metals, like cadmium (Cd), mercury (Hg), and chromium (Cr), elements in the bottom left section of the periodic table like lead (Pd) and tin (Sn), and certain metalloids like arsenic (As) are essentially what are referred to as HMs. The latter can be broadly classified into two categories: essential and non-essential HMs. The first ones are necessary for living organisms to perform fundamental processes such as growth, metabolism and organ development. Therefore, HMs such as iron (Fe), zinc (Zn), copper (Cu), and cobalt (Co), function as cofactors that support redox and protein structure processes, making them crucial for plant growth and development. The non-essential ones are dangerous because they can bind to a variety of functional groups in biomolecules, including amino, carboxylic acid, and sulphur-containing groups [1]. Moreover, they compete with the plant for nutrient uptake, they are dangerous even at low concentrations as they can result in macronutrient deficiencies [2]. Increased HMs buildup results in acute toxicity, growth inhibition, and ultimately plant death [2]. In contrast to organic pollutants, HMs are non-biodegradable and tend to accumulate in living organisms [3] and the pervasive problem of HM pollution in the environment is a significant risk to public health worldwide. Reports indicate that 20 million hectares of China's farmland, constituting roughly 20% of the nation's total agricultural area, are affected by HM pollution, notably Cd, Pb, As, and Hg. Within this affected area, 14,000 hectares are particularly afflicted by Cd contamination [1,4]. Groundwater, agricultural products, and crops alike will soon suffer the far-reaching consequences of the presence of Cd in soil [5]. Pollution of the environment by HMs can result from both natural processes and human activities. Among the latter, the primary artificial causes of soil contamination include farming practices, urban sprawl, industrial operations, mining activities [6] and the expansion of transport infrastructure [7]. Industrial operations contribute to ecological pollution since HMs and their numerous chemical combinations are frequently employed as catalysts in chemical reactions. Transportation wise, the emission of gases from tires, brakes, and gasoline fuel have shown to be the main contributors of Pb and Cd emissions to the air due to the increased traffic [8]. Mining activities, though less directly linked in some regions, can still impact soil quality indirectly. For instance, agricultural goods grown in roadside fields often exhibit higher levels of HM contamination than crops from other

areas, likely due to atmospheric deposition of pollutants [9]. Additionally, mining operations themselves exacerbate soil pollution through windborne metal particles and the transportation of minerals, further degrading the surrounding environment [10]. The proximity to mines can amplify HM accumulation in soil, influenced by climatic factors that enhance metal mobilization [10,11]. The expanding trash mounds have a negative effect on the surrounding areas of mining and potentially transform some agricultural regions into wasteland [12]. Besides, one of the primary causes of ecological contamination of these areas is the water utilized in the mining process. People living close to mines suffer from a variety of autoimmune and non-autoimmune disorders that can be fatal due to toxic HMs in the surrounding soil [12]. Furthermore, human-induced soil modifications, such as the standard agricultural methods used in different areas, cause crops to take in HMs. The most common causes of liquid-induced HM environmental pollution are the application of phosphate fertilizers and the irrigation of agricultural lands with dirty water [13].

One trace element that is not necessary for biological systems yet is present in large quantities in the environment is Cd. Due to its exceptional toxicity to all biological systems, Cd is a HM frequently released into the environment by both natural and man-made sources [14]. For these reasons, it is considered a major metal pollutant [15,16]. Cd and its compounds are soluble, making them more mobile than other metals in environmental matrices. They also have high bioavailability, which makes them easily absorbable by plants. Once inside the plant, Cd can interfere with important physiological processes [17,18]. Given that Cd is highly toxic, this poses a significant risk to human health, leading to cancer and extensive environmental harm [19]. According to numerous studies, dumps often contain Cd levels exceeding the permissible limit in soil [20–23]. With a global mean of 0.36 mg/kg, Cd usually occurs in soils at amounts ranging from 0.01 to 1 mg/kg [16], and can be found in soil water at up to 5 μg/L [24] and groundwater at up to 1 μg/L [25]. Increases in Cd concentrations in soils and groundwater, which are crucial for preserving a wholesome food supply and clean drinking water, can come from both natural and man-made sources. The WHO Guidelines for Drinking-Water Quality recommend a maximum value of 3 μg/L for Cd. The potential for Cd accumulation in plants to transfer to humans via the food chain, causing serious harm, is a nowadays a considerable concern [26,27]**.** Due to competition with calcium (Ca) and other nutrients, chronic Cd poisoning, also known as itai-itai disease and initially identified in Japan in the early 20th century, results in renal tubular dysfunction, osteomalacia, and osteoporosis [28–30]. According to Khan et al. 2017 [30], Cd exposure is also linked to problems with glucose metabolism, lung and breast cancer, myocardial infarction, and heart failure.

### *1.1.1 Effects of Cd in plants*

Crops, agricultural goods, and groundwater are significantly affected by Cd, [5] a trace element that is not necessary for plant growth, although it does accumulate in all sections of plants after absorption [2,31]. First signs of Cd toxic effects on plants include browning of the roots, a decrease in the number of lateral roots, and death of the tips of the roots due to inhibition of roots growth. Furthermore, accumulation of Cd could result in stem development retardation, terminal leaf chlorosis, and leaf curl [32,33].

By substituting the sulphydryl groups of proteins and enzymes, Cd replaces the essential elements of enzyme active sites needed in biological reactions. It also modifies macromolecule conformation, causes protein denaturation, and deteriorates cell membranes. The plant defence system reacts to the entry of Cd into plant cells by accumulating proline [34–36], variations in the synthesis and levels of phytohormones [37–39], and the initiation of several signaling pathways, including the Ca-calmodulin pathway as well as the activation of various antioxidant enzymes [40,41].

Cd significantly increases the production of reactive oxygen species (ROS) after binding with proteins and enzyme complexes which leads to oxidative stress [42,43]. Reactive nitrogen species (RNS) and ROS are byproducts of regular cellular metabolism, known to play two distinct roles in biological systems [44]. High ROS levels cause the cell to arrest and eventually become necrotic or apoptotic, whereas low ROS levels accelerate the cell cycle's progression [45]. The toxicity due to elevated ROS concentrations reflects the oxidation of proteins, DNA, and membrane lipids, as well as the breakdown of polyphenols, catecholamines, and thiols. Previous reports highlight ROS dual function in plant defence systems as a signalling molecule and as a source of toxicity [46,47]. According to multiple studies [48,49] these molecules are produced by the Fenton or Haber-Weiss reaction, respiratory burst oxidase homologs (also known as NADPH oxidases), and the inhibition of antioxidative enzymes, such as oxidases and peroxidases. The cell has evolved a sophisticated antioxidant system that may shield biological molecules from potentially hazardous, purely physiological, species-producing oxidative stress through both enzymatic and non-enzymatic methods. Proteins like catalase (CAT), glutathione peroxidase (GPx), ascorbic acid (Vitamin C), ϱ-tocopherol (Vitamin E), glutathione (GSH), carotenoids, flavonoids and others antioxidant agents are part of enzymatic defence system [50] (Figure 1).

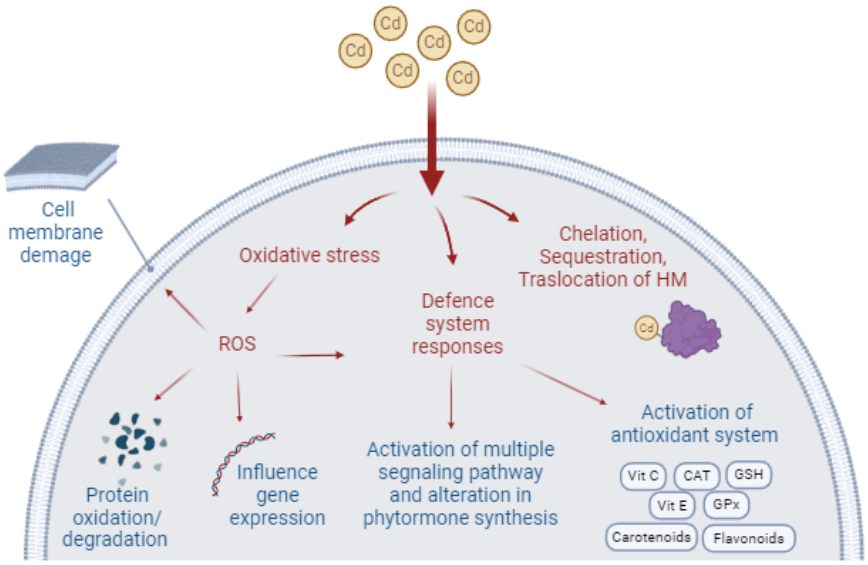


**Figure 1.** Toxic effects of Cd in plants. Induction of oxidative stress leading to ROS generation, resulting in cell membrane damage, protein oxidation, and degradation, with effects on gene expression. Cellular responses to Cd entry include activation of defence system, as well as chelation, sequestration, and translocation of the HM.

### 1.2 Molecular responses and mechanisms against heavy metal toxicity

Different plant species are affected by nutrient variance under Cd stress [15,51,52]. Certain molecular alterations control Cd mitigation, tolerance, and adaptation, including the overexpression of specific genes. It has been observed that the natural resistance and macrophage proteins (NRAMPs), the iron-regulated transporter-like proteins (IRTs), zinc-regulated transporter-like proteins (ZIPs), the zinc-regulated transporter-like proteins (HMAs), and the metal tolerance or transporter proteins (MTPs) play roles in the uptake, translocation, and sequestration of Cd within plants [53]. Jia et al. 2019 [54] revealed that a high concentration of Cd (6.5 μM Cd) increases the expression of genes (*SlQUA1* and *SlPME1*) associated with pectin synthesis in the cell walls of tomatoes, leading to an increase in pectin methyl esterase activity and ion binding sites, which counteracts Cd stress. Additionally, Song et al. 2017 [55] demonstrated that overexpression of *AtFC1* in *A. thaliana* enhances Cd accumulation and tolerance under Cd exposure. Conversely, genes like *HvIRT1* and *HvNramp5* in barley [56] downregulate Cd uptake, while lower expression of *HMA-A*, *HMA-B*, *IRT1*, and *ZIP1* in tobacco leads to reduced Cd accumulation [57]. Genes such as *ZIP2*, *ZIP3*, *IRT1*, *HMA2*, and *HMA4* and *CAX4*, *HMA3*, *MRP7*, *MTP3*, and *COPT5* are overexpressed in Pak choi (*B. rapa*) grown in sand artificially contaminated with 10 mg Cd $Kg^{-1}$ [58]. Other studies on the response to Cd stress have been conducted in rape, *A. thaliana*, maize, rice, and other crops [59,60]. *NcNramp1* was shown to be crucial for the process of plant absorption and accumulation of ionic form $Cd^{2+}$ when transcriptome technology was used to examine *N. caerulescens* under Cd stress in various genotypes [61].

As a result of the significant toxic impact on plant growth and development, plants have evolved a variety of tolerance and detoxification strategies to control the uptake, transportation, and accumulation of Cd and lessen its toxicity [62]. The plant root hairs, along with the cuticle and epidermis, produce protective tissue to keep Cd out [63]. They also release organic acids, including citric, malic, and lactic acids, which mix with Cd to form compounds that prevent Cd from passing through membranes. In order to reduce the quantity of Cd that migrates from the soil into the root, they also modify the pH and EH of the rhizosphere [64]. Furthermore, to reduce the toxicity of Cd to cell activity, Cd that does enter cells will be enriched in vacuoles. This enrichment occurs due to the ability of polysaccharides and proteins in the cell wall to bond with the metal and prevent it from entering the cell [65].

Plants, particularly the hyperaccumulator ones, react in different ways to the toxicity of HMs, including Cd. HM chelation utilizing peptide ligands called phytochelatins (PCn) is one of the

novel defence mechanisms [66]. These peptides are primarily composed of (c-Glu-Cys)n-Gly, with (2<n<11), although other PCn structures such as (c-Glu-Cys)n-Glu, (c-Glu-Cys)n-Ser, and (c-Glu-Cys)n-c-Ala have also been identified [67,68]. PCn are synthetized from GSH by the activation of the enzyme phytochelatin synthase (PCS), a γ-EC dipeptidyl (trans)peptidase that is constitutively expressed in the plant cytosol [69–71]. Synthesized PCn can form a complex with Cd, referred to as a chelator-Cd complex. Intracellular Cd promotes PCS activity, and the subsequent metal-induced production of PCn allows the intracellular Cd detoxification [72]. Indeed, the PCn complex aids in transporting Cd from the cytosol into the vacuole, where it becomes inactive [73,74] (Figure 2).

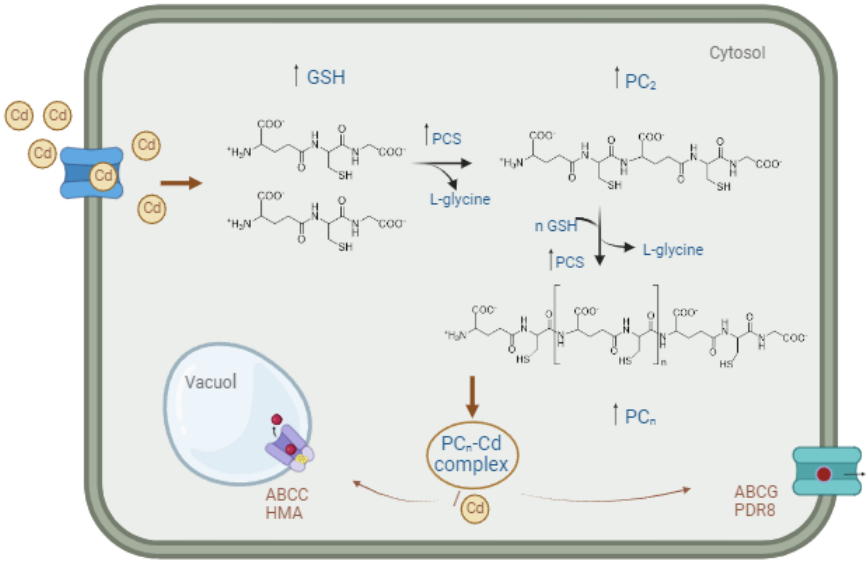


**Figure 2.** The Cd-PCn complex. Cd influx into cells induces overexpression of PCS and involves glutathione in PC2 formation, resulting in the synthesis of other PCn. This production of PCn leads to cadmium chelation, and the complex is transported to the vacuole for detoxification or removed from the cell via membrane transporters and efflux pumps.

A study reports the exogenous presence of GSH to reduce Cd translocation to shoots and enhance Cd accumulation in *B. campestris* roots treated with 20 mM of Cd [40]. According to the authors, exogenous GSH promotes the synthesis of PCn by increasing Cd chelation and facilitating its translocation into the root vacuoles. In fact, recent studies [72,75–77] confirm that the exposure to Cd raises GSH levels in addition to activating the constitutively expressed

enzyme PCS in *M. polymorpha* (*MpPCS*), which significantly increases the amount of PCn generated overall. Particularly, a detailed gene expression analysis confirmed the constitutive transcription of *MpPCS*, indeed Cd is able to induce the activity, but not the gene expression, of the enzyme [72]. As a result, PCn synthesis is essential for plant detoxification and tolerance to high Cd concentrations. Another notable instance is seen in rice plants, where PCn increase by 23% and 47%, respectively, in response to 1 and 2 mM Cd [78]. Similarly, *B. auriculata* treated with 125 mM of Cd showed similar outcomes [70]. In response to metallic micronutrients including Fe, Zn, Cu, and the hazardous element Cd, PCn activation has recently been found in tracheophytes (mostly in angiosperms), as well as bryophytes and charophytes [79–81]. Therefore, *M. polymorpha* may be a great model organism to study the cellular and molecular mechanisms involved in Cd detoxification. Studies examining how metal detoxifying mechanisms evolved from aquatic to terrestrial environments can benefit greatly from the study of bryophytes. Not to mention, these plants do not form strong hydrophobic barriers, have a very high surface/volume ratio, an elevated cation exchange capacity, and are hence more susceptible to unrestricted, seemingly uncontrolled metal absorption [18,82]. Consequently, bryophytes have been employed as a crucial biological monitoring system for metal environmental pollution because of their widespread distribution [82–84]. Additionally, a study conducted by Bellini et al. 2020 [85] examined the medium acidification of this liverwort and its thiol-peptide synthesis (GSH, PCn) following a 72 h exposure to Cd. The loss of selective permeability, a well-known property of biological membranes, can lead to swelling or shrinking of cell compartments due to HM-induced membrane damage or energy loss. Moreover, changes in chloroplast ultrastructure have been linked to HM concentrations in studies conducted both in field and *in vitro* on bryophytes [83,86]. *L. riparium* has been explored whether this moss could be suitable for biomonitoring in natural field conditions. Recent works showed that Cd exposure severely affected the amount of photosynthesis, PCn, GSH, and nitrogen metabolism in *L. riparium* plants. Nitrogen ($N_2$) and Cd metabolism are known to be closely correlated [87–90]. $N_2$ is typically associated with the abiotic stress response because it competes with essential reductants required for antioxidant responses, particularly in the presence of metals and metalloids [89,91]. High $N_2$ levels promote the uptake of Fe, Zn, Cu, Ca, Hg, and other cations in certain plants [90]. Instead, the activity of glutamate dehydrogenase, another important enzyme involved in abiotic stress, is reduced because it serves as a substitute route for assimilating N and detoxifies excess $NH_4$ that is produced under stressful circumstances [91,92]. On the other hand, several major crops such as rice, beans, peas, and corn exhibited reduced glutathione synthase (GS) activity in response to HM uptake

[93,94]. Research conducted by Maresca et al. 2022 [95] demonstrated that *L. riparium* has a natural tendency to increase the occurrence of GS2 proteins. Cd exposure causes the metal to be chelated in the roots and transferred to the shoots via GSH and PCn [90]. Maintaining this chelation mechanism, which controls the amount of GSH and non-protein thiols, as well as the expression of *PCS* and GSH synthase genes, requires a sufficient absorption of $N_2$ [90].

### *1.2.1 Role of GSH in mitigating Cd-induced abiotic stress*

Due to the implication of GSH in mitigating HM stress, which is linked to its involvement in PCn synthesis, it is relevant to deepen our understanding of GSH response during abiotic stress. Two ATP-dependent enzymes, glutamate-cysteine ligase (GSH1, previously known as γ-glutamylcysteine synthetase) and GSH synthase (GSH2), sequentially synthesize GSH from its three amino acid building blocks [96]. The first enzyme, GSH1, conjugates Cys and Glu to produce the dipeptide γ-glutamylcysteine. The second step is catalysed by GSH2, which joins Gly to γ-glutamylcysteine to generate GSH. Growth and viability are restored when cytosol-specific GSH2 is added to the seedling-lethal GSH2 mutant strains. Therefore, for normal plant growth, cytosolic production of GSH alone is sufficient [97]. Although both *GSH1* and *GSH2* are relatively widely expressed in plant tissues, biotic stressors such as methyl jasmonate and high light [98], as well as abiotic stresses like HM [99,100], but not $H_2O_2$ or oxidative agents [99], increase transcriptional levels of both *GSH1* and *GSH2*. Its homodimerization is therefore thought to increase enzyme stability by shielding sensitive regions [101]. Since the chloroplast is home to GSH1, the redox state of this organelle plays a crucial role in controlling the synthesis of GSH. Due to the inherent instability of oxygenic photosynthesis, chloroplasts are highly reactive to unfavourable environmental conditions, which subsequently provides quick responses to abiotic and biotic challenges [102]. The recognized function of GSH in maintaining intracellular redox homeostasis largely depends on the redox control of GSH biosynthesizing enzymes. Indeed, oxidative stress-induced metabolic circumstances create a demand for GSH and the production of its oxidated form GSSG, while also promoting GSH synthesis through the post-translational activation of GSH1. Consequently, elevated GSH levels establish a reducing environment, triggering a regulatory feedback loop to slow down GSH synthesis and decrease GSH1 activity. The activity of the sulphate assimilation pathway also influences GSH synthesis [103]. Cys serves as the initial organic product of sulphur assimilation in plants, and thus, its availability plays a crucial role in determining GSH

production [103,104]. Consequently, several regulatory mechanisms influence the GSH biosynthesis process. Various environmental conditions and stresses impact the coarse control of *GSH1* and *GSH2* expression. Additionally, precursor availability affects the system's activity, and a redox mechanism that considers feedback information finely regulates GSH1 activity. Currently, it remains uncertain whether a redox-coupling mechanism is necessary for the transformation of GSH1 from its oxidized to reduced form. The redox state of GSH, along with its cellular concentration, plays a critical role in mediating and finely regulating metabolism and stress responses. The flavoenzyme NADPH-dependent GSH reductase (GR) efficiently regenerates GSSG to GSH and permits recurrent redox cycling. In order to sustain fundamental functions in the cytosol, mitochondria, and chloroplast stroma in the light, GR contributes to the maintenance of a negative EGSH (i.e., high GSH/GSSG). Gill et al. 2013 [105] conducted a thorough literature analysis about *GR* genes and found evidence that a variety of abiotic stressors, including exposure to HMs, including Cd, salt, drought, UV radiation, and cold temperatures, boost GR activity in many plant species. Moreover, several stress-tolerant plants exhibit significant GR activity [106]. Because of its effective ROS scavenging capacity, transgenic techniques to control GR activity in plants also demonstrate that increased GR activity significantly improves tolerance to oxidative stress brought on by a range of abiotic stimuli [105]. Two nuclear genes, *GR1* (*At3g24170*) and *GR2* (*At3g54660*), which both code for differently localized isoforms, are responsible for encoding GRs in *A. thaliana*. *GR1* is more highly expressed in roots, while *GR2* expression is more pronounced in photosynthetic tissues [98]. *GR1* is localized in the cytoplasm, nucleus, and peroxisomes [107–110] while *GR2* targets mitochondria as well as chloroplasts [108].

### 1.3 Transporters involved in Cd detoxification

There are various forms of Cd in soil, but many of them are not absorbed by plants [111]. For Cd to be absorbed, it must be available for uptake, which depends on the plant species, the physicochemical conditions of the soil, and the speciation of the metal [112,113].

A number of technologies have been developed to lower soil Cd levels. Phytoremediation, used by plants to absorb Cd and store it in easily harvested aerial sections of the plant, is one of the approaches [114]. The choice of appropriate plants that can grow in Cd-polluted soils and accumulate Cd in aerial parts is crucial to the effectiveness of phytoremediation. Over the past ten years, Cd hyperaccumulating plants have received attention [114], however, only a few plant species that can withstand high amounts of Cd have been identified, including *A. halleri*, *N. caerulescens*, and *S. alfredii.*

Meighan et al. 2011 [115] found that herbaceous Cd hyperaccumulators had limited relevance for phytoremediation in Cd-polluted fields due to their slow development and low biomass output. The use of *Populus* species has been suggested as an alternative for phytoremediation because these woody species can be managed in short rotation coppicing plantations and are known for their fast growth and deep rooting systems [116–119].

Metal uptake is significantly influenced by root features such as surface area, size, and shape [113,120–124]. Furthermore, plants with thin, hairy roots have demonstrated high absorption and accumulation of metals [125]. In most cases, bivalent forms of trace elements are absorbed [126]. The same transporters that carry Ca, Fe, Mg, Cu, and Zn must carry Cd across root cell walls [15]. By passive transport (diffusion), Cd can move from the soil to plant roots through the cell walls [120,127]. Furthermore, studies have shown that Cd uses nonspecific membrane transport proteins (IRTs and ZIPs) and metal pumping ATPases to facilitate active transport across the plasma membrane of root cells [128,129]. Different transporters are used by plants to sequester metal ions inside organelles, whether in a free ionic state or as chelates. Plants can store extra metals in vacuoles when they are in neutral chelated forms. Long-distance transportation also makes use of chelated-metal forms. To lessen the harmful effects of metals, metal chelators can be proteins that bind to metals or other compounds such amino acids, their derivatives, or organic acids [130].

These metal chelators also exhibit antioxidant properties. By detoxifying metal ions, specific protein metal chelators like glutaredoxins (GRXs), metallothionins (MTs), and PCn, are essential in reducing the effects of metal stress-mediated oxidative damage [130]. Thereby, according to Kumar et al. 2020 [131], the overexpression of glutaredoxin *CaGRX* in chickpeas

decreases the absorption of metal ions and boosts the ROS scavenging mechanism, thus mitigating metal stress.

Transporters serve dual roles as receptors and transporters, known as transceptors, within the plant's sensory apparatus aimed at preserving metal homeostasis [132–135]. Transceptors have the capability to discern the availability of metal ions in soil and their scarcity within the cytosol, thereby orchestrating the regulation of metal ion uptake through low- or high-affinity transporters. This intricate process leads to a substantial decrease in metal ions, effectively maintaining metal homeostasis within plant cells through the expulsion and exclusion mechanisms facilitated by transporters.

Among these transporters, Cd, Co, Fe, Mn, and Zn divalent ions are transported by IRT1. Within root cells, IRT1 acts as a transceptor within sensing and signaling mechanisms, prioritizing the sensing of $Fe^{2+}$ above other ions. Additionally, IRT1 regulatory domain senses additional ions such as Co, Mn, and Zn, thereby inhibiting IRT1 function [132]. In a different study, CBL-interacting protein kinase 23 (CIPK23) phosphorylates the metal-bound IRT1, leading to ubiquitination by the IRT1 degradation factor 1 (IDF1) protein. This ubiquitination targets IRT1 for breakdown in the vacuole, effectively halting further metal absorption [136].

Wu et al. 2020 [137] discovered in their intriguing study on *A. thaliana* that the use of hydrogen-rich water accelerates the uptake of Cd. Elevated levels of Cd result in hydrogen production, which in turn triggers a cytosolic influx of Ca. Moreover, the activation of respiratory burst oxidase homolog protein D (RBOHD) by Ca elevation results in the production of ROS, primarily $H_2O_2$. In the end, the induced-$H_2O_2$ can inhibit IRT1 transcripts, which will lessen the absorption of more Cd [137].

Another instance in which Cd stress is mitigated is shown in apple where the kinase salt overly sensitive 2-like1 (SOS2L1) phosphorylates the malate transporter aluminum-activated malate transporter 14 (ALMT14), enhancing its functionality [49]. Otherwise, a rice natural resistance-associated macrophage protein 1 (OsNRAMP1) plasma-membrane localized Fe transporter which is involved in absorbing Cd is overexpressed, increasing the amount of Cd stored in leaves. Additionally, it was found that the expression of *OsNRAMP1* is correlated with the amount of Cd found across different rice cultivars. Compared to the hyperaccumulating cultivar Sasanishiki, it was expressed up to two times greater in the Cd hyperaccumulating rice cultivar Habataki [138]. According to Lang et al. 2011 [139], *B. juncea* exhibits Cd tolerance through the involvement of two cation efflux transporters, BjCET3 and BjCET4, whose overexpression results in increased Cd-accumulation in the shoot without lowering plant biomass.

Otherwise, in *A. thaliana* the gene *AtNRAMP6* confers Cd tolerance by locating at the Golgi apparatus. By transferring the Fe contained in Golgi vesicles into the cytosol during Fe-depletion, *AtNRAMP6* overexpression plays a critical role in preserving intracellular Fe equilibrium [140]. Consequently, by compartmentalizing and redistributing metals to specific organelles including vacuoles, the endoplasmic reticulum, chloroplasts, and mitochondria, Golgi apparatus-localized metal transporters are necessary to maintain metal homeostasis of Fe, Cd, and Mn.

Furthermore, plants utilize energy-dependent metal transport systems to expel or remove metals, primarily relying on HM ATPases (HMAs) and ABC (ATP-binding Cassettes) transporters. Typically, these transporters expel metals from root cells into the surrounding air or other sections of the plant, where they can accumulate harmlessly. The role of ABC transporters in the translocation and redistribution of metals has been extensively studied. Fu et al. 2019 [141] demonstrated that Cd treatment in rice promoted the expression of the G-type ABC transporter ABCG36. A loss-of-function mutant exhibited higher Cd concentration in its roots, suggesting that ABCG36 facilitates Cd translocation from roots to shoots. A interesting study revealed that *P. tomentosa ABCG36* gene can be overexpressed to improve Cd tolerance in *A. thaliana* plants, suggesting that this transporter serves as a Cd extrusion pump [142]. In accordance with a different study, the *A. thaliana* ABC transporter pleiotropic drug resistance 8 (AtPDR8) acts as a plasma membrane-localized Cd efflux pump, pushing Cd out of the cytosol and onto the cell's exterior, so providing HM stress tolerance [143]. In certain plants, only C-type ABC transporters (ABCCs) localize on tonoplasts and contribute to metal tolerance. According to Brunetti et al. 2015 [144] and Song et al. 2010 [145], tonoplast-localized ABCCs in *A. thaliana*, such as AtABCC1, AtABCC2, and AtABCC3, facilitate the transport of PCn and its complexes with As, Cd, Mn, and Zn into the vacuole, thus enhancing metal tolerance.

A recent study compared wild type (WT) *P. alba* clone Villafranca plants with trans-genic plants overexpressing an aquaporin (*aqua1*) in a hydroponic treatment with 10 μM Cd. *PaHMA2, PaNRAMP1.3, PaNRAMP2, PaNRAMP3.1, PaNRAMP3.2, PaABCC9,* and *PaABCC13* gene expressions were evaluated revealing that the majority of the genes analysed exhibited a prompt transcriptional response in WT plants at 1-day post-treatment and adaptation at 60 days. Conversely, *aqua1* plants showed a weaker transcriptional response along with a higher Cd content in the medial leaves. In conclusion, *aqua1* overexpression in poplar enhanced Cd translocation, indicating that *aqua1* plants are less sensitive to Cd. Given the significance of *PaNRAMP3* in Cd compartmentalization, a different transcription of this

gene in the WT line may account for this distinct response. Nevertheless, even after two months of treatment, Cd administration did not cause observable toxicity symptoms in WT and *aqua1* plants, demonstrating the remarkable resistance of this poplar species to Cd [146].

As part of a redistribution strategy, the HMA family of P1B-ATPases also serves as metal pumps, transporting metals into the xylem, phloem, and apoplast for transfer to other plant components including shoots and grains. Members of HMA family are essential for the mobilization of metal ions in a variety of plants, including Cu, Cd, and Zn. HvHMA1 is essential for scavenging Cu and Zn from the chloroplast to the cytosol in barley, facilitating their transport to areas of need [147]. To prevent their intracellular accumulation, HMA2 in *A. thaliana* expels excess cytosolic Zn, Cd, and other ions into the apoplast [148]. In response to Zn deficiency in the shoot, HMA2 and metal transporter protein 2 (MTP2) are stimulated to redistribute Zn from the root to the shoot [149]. Additionally, when cultivated in environments with high concentrations of metals, the HMA2 mutant exhibits raised intracellular Cd and Zn levels.

AtHMA3, localized in tonoplasts, plays a role in storing Cd, Zn, Co, and Pb. According to Morel et al. 2009 [150], overexpression of *AtHMA3* enhances resistance to metal stress and boosts Cd storage capacity. Furthermore, research by Sasaki et al. 2014 [151] observed that vacuolar sequestration of Cd in rice roots contributes to its accumulation. In a comparable way, *GmHMA3* in soybeans is essential for Zn and Cd tolerance. Moreover a study on rice showed how it has the capability to diminish the quantity of Cd present in its grains by adjusting the Zn-to-Cd ratio via the mutation of OsHMA2 [152].

Additionally, the endomembrane system includes the endoplasmic reticulum (ER), housing a spacious lumen utilized for the storage and utilization of metals for various purposes [153]. Within the ER membrane, there exist broad-specificity transporters for Cd, Cu, and Zn, which are occasionally observed to also localize on the plasma membrane. The endomembrane system's continuity as an element of the secretory way may be the cause of this shared location. For example, OsZIP1 in rice is situated at both the ER and plasma membrane, primarily in roots where Cd, Cu, and zinc levels are elevated. All the different aforementioned transporters are summarized in Table 1.

| Subfamily | Name | Subcellular localization | Substrate |
|---|---|---|---|
| IRT | IRT1 | Plasma membrane | Fe, Co, Mn, Zn, Cd |
| SOS | SOS2L1* | Plasma membrane | Malate and malic acid |
| ALMT | ALMT14* | Plasma membrane | Malate and malic acid |
| CET | BjCET3 | Plasma membrane | Zn, Co, Ni, Cd |
| | BjCET4 | | |
| RAMP | OsNRAMP1 | Plasma membrane | Fe, Cd |
| | AtNRAMP6 | Golgi | Fe, Mn, Cd |
| ABCG (PDR) | PtABCG36 | Plasma membrane | Pb, Cd |
| | AtPDR8 | | |
| ABCC | AtABCC1 | Tonoplast | PCn and its complexes with As, Mn, Zn, Cd |
| | AtABCC2 | | |
| | AtABCC3 | | |
| HMA | HvHMA1 | Chloroplast | Zn, Cd |
| | PaHMA2 | Plasma membrane | Zn, Cd |
| | AtHMA2 | | |
| | AtHMA3 | Tonoplast | Zn, Co, Pb, Cd |
| ZIP | OsZIP1 | Endoplasmic reticulum and plasma membrane | Zn, Cu, Cd |

**Table 1.** Main features of transporters implicated in Cd tolerance. **Not directly used for Cd transport. Cd presence enhances their functionality increasing Cd tolerance.*

## 1.4 *Populus* as a phytodecontaminating genus

Poplar trees belong to the family Salicaceae within the order Malpighiales. Although the family includes 10 genera, the majority of species come from the *Populus* and *Salix* genera.

The *Populus* gene pool is richest in the Sino-Japanese region and during the age of the middle Miocene, it migrated to the Himalayas. More than 100 approved names and 582 records of *Populus* species are available [154]. In their article, Naithani and Nautiyal 2012 [155] listed 44 species of *Populus* in five sections: Leucoides, Turanga, Black Poplars (Aigeiros), Balsam Poplars (Tacamahaca), and White Poplars (Leuce). Nonetheless, the genus *Populus* is split into six sections and twenty-nine species, which are spread throughout the Northern Hemisphere and tropical Africa, according to Eckenwalder's most widely accepted taxonomy [156,157]. Poplars are distributed across a wide range of latitudes, and the same species is found in different climatic regions. This broad geographic distribution suggests that poplar plants can withstand a wide variety of environmental conditions, making them good candidates for stress tolerance experiments [158]. In the case of unfavourable climatic conditions, such as low temperatures, poplars reproduce vegetatively, even when sexual reproduction is inhibited [158]. This trait allows for easy propagation of poplar plants, either through cuttings or by using *in vitro* micropropagation.

| Section | *Populus* species | Common name | Distribution |
|---|---|---|---|
| *Populus* (LeuceDuby) | *P. adenopoda* Maxim | Chinese Aspen | China |
| | *P. alba* L. | White Poplar | Europe, North Africa, Central Asia |
| | *P. gamblei* Haines | Himalayan Aspen | East Eurasia, India |
| | *P. grandidentata* Michx | Bigtooth Aspen, Largetooth Aspen | North America |
| | *P. guzmanantlensis* A. Vazquez & Cuevas | Manantlan White Poplar | Mexico |
| | *P. monticola* Brandegee | Baja White Poplar | Mexico |
| | *P. tremula* var. *sieboldii* (Miq.) H. Ohashi Synn. *P. sieboldii* Miq | Japanese Aspen | Japan |
| | *P. simaroa* Rzed | Balsas White Poplar | Mexico |
| | *P. tremula* L | Eurasian Aspen | Europe, North Africa, North East Asia |
| | *P. tremuloides* Michx | Quaking (trembling) Aspen | North America |
| Tacamahaca Spach | *P. angustifolia* E. James | Narrow Leaf Cottonwood Poplar | North America |
| | *P. balsamifera* L | Balsam Poplar | North America |
| | *P. ciliata* Wall. ex Royle | Himalayan Poplar | India, Pakistan, Bhutan, Nepal, Myanmar |
| | *P. laurifolia* Ledeb | Laurel Poplar | Eurasia |
| | *P. simonii* Carriere | Simon Poplar | Eastern Asia |
| | *P. suaveolens* Fisch. ex Loudon | Asian Poplar | North East China, Japan, Asia |
| | *P. szechuanica* C. K. Schneid | Szechuan Poplar | East Eurasia |
| | *P. trichocarpa* Torr. & A. Gray ex Hook | Black Cottonwood Poplar | North America |
| | *P. yunnanensis* Dode | Yunnan Poplar | Eurasia |
| Aigeiros Duby | *P. deltoides* Marshall | Eastern Cottonwood | North America |
| | *P. fremontii* S. Watson | Fremont's Cottonwood | USA |
| | *P. nigra* L | Black Poplar | Europe, Central Asia |
| Leucoides Spach | *P. jacquemontiana* Dode | Sichuan Poplar | China, USA, India |
| | *P. heterophylla* L | Swamp Cottonwood Poplar | China |
| | *P. lasiocarpa* Oliv | Chinese Necklace Poplar | China |
| Turanga Bunge | *P. euphratica* Oliv | Euphrates Poplar | North East Africa, Asia |
| | *P. ilicifolia* (Engl.) Rouleau | Tana River Poplar, Kenyan Poplar | East Africa |
| | *P. pruinosa* Schrenk | Desert Poplar | Asia |
| Abaso Eckenwalder | *P. mexicana* Wesm. ex DC | Mexico Poplar | Mexico |

**Table 2**. Populus species, their common name and distribution.

Table 2 displays the common name and distribution of all 29 *Populus* species, highlighting *Populus alba* species, taken as subject of this thesis work.

*Populus* includes forest tree species that are economically significant. It is cultivated worldwide as a dominant pioneer species in riparian habitats [159] and for controlling soil erosion on degraded lands [160]. It meets the demands of energy production, pulp and paper, fiber, and wood products. As a keystone species for various microbes, herbivores, and insects, *Populus* species also play an important role in supporting biodiversity [161,162]. Additionally, *Populus* species are used for carbon sequestration and bioenergy production, similar to other fast-growing trees like *Salix* and *Robinia pseudoacacia* [163]. Approximately 130 secondary metabolites have been isolated and identified from species in the genus *Populus*, which also has therapeutic uses. Several isolated compounds and plant extracts from *Populus* have demonstrated interesting biological activities, including antioxidant, anti-inflammatory, antimicrobial, neuroprotective, and anticancer properties [164–168]. Additionally, previous reviews have focused on the molecular aspects of *Populus* [169], biofuel production [170], and identified phytocompounds of *Populus*, highlighting their potential role in forest biorefineries and bioproducts.

Before delving into how *Populus* can participate in phytoremediation processes, it is important to clarify that phytoremediation refers to the use of green plants to extract, sequester, and detoxify pollutants. Phytoremediation utilizes many mechanisms including degradation (rhizo-degradation, phytodegradation), accumulation (phytoextraction, rhizofiltration), dissipation (phytovolatilization), and immobilization (hydraulic control and phytostabilization) to degrade, remove, or immobilize the pollutants [171]:

- Rhizodegradation: the breakdown of contaminants through the biological activity of organisms in the rhizosphere (bacteria and fungi). Microbial communities are supported and increased by the presence of roots. Contaminants that typically undergo rhizodegradation include total petroleum hydrocarbons, polycyclic aromatic hydrocarbons, pesticides, chlorinated solvents and polychlorinated biphenyls.
- Phytodegradation: absorption and transformation of contaminants through plant processes. Substances involved in this process include chlorinated solvents, benzene, toluene, ethylbenzene, xylene, pesticides, and phenols.
- Phytoextraction: some plant species can extract and accumulate contaminants, translocating them to the roots and/or aerial parts. HMs and radionuclides are involved in this phytoremediation process.

- Phytovolatilization: the contaminant is absorbed by the plant, potentially modified in its chemical form, and released from the leaves into the atmosphere through transpiration. The contaminants considered in this process include mercury, selenium, silver, arsenic, chlorinated solvents, and tert-butyl methyl ether.
- Evapotranspiration: precipitation is intercepted by the leaves, and water absorption and transpiration by the plant allow for hydraulic control in the site contaminated by all water-soluble pollutants.
- Phytostabilization: absorption and accumulation in the roots, precipitation, or immobilization in the root zone, particularly of substances such as HMs.

Plants exhibit varying degrees of tolerance to HMs, either by excluding them or by accumulating and storing them in specific organs, tissues, modified cells (trichomes), and subcellular compartments (vacuoles). Some species are classified as hyperaccumulators because they can accumulate large amounts of HMs. Despite herbaceous such as *A.halleri, N. caerulescens* and *S. alfredii* are able to tolerate high Cd concentrations [172,173] these Cd hyper-accumulators display slow growth and little biomass production, the applicability of these plants for phytoremediation in Cd-polluted fields is limited [174]. Alternatively, due to their rapid growth and high biomass poplar trees have been suggested as possible candidates for phytoremediation applications [158,175–177], and various cultivars have already been screened in metal tolerance trials [119,178–180]. According to previous research, poplar trees exhibit varying levels of Cd accumulation in their bark, roots, and leaves [181–184]. Typically, the Cd concentration in the aerial parts of poplar plants does not exceed 100 μg/ g, which is the threshold for Cd hyperaccumulators [185]. Nonetheless, in temperate zones, poplars can produce substantial aboveground biomass within a single growing season [119,186]. Consequently, compared to herbaceous hyperaccumulators, the total Cd accumulated in the aerial parts of poplar plants remains significantly higher [119,186]. These findings suggest that poplar trees hold potential for the phytoremediation of Cd.

Indeed, these Salicaceae species are known not only for their ability to accumulate HMs but also for their capacity to grow in contaminated areas [175]. Another beneficial aspect of phytoremediation to consider is the management of poplar plantations through short-rotation coppice systems [187]. Poplars are well-suited for short-rotation harvesting due to their ease of propagation, and their genome has been fully sequenced [188]. They are also easily used in genetic engineering and can be replicated *in vitro*. It has been shown that intraspecific genetic dissimilarity can lead to varied HM tolerance in different clones of the same poplar species

[189]. Tolerance to Cd among various poplar species is thought to vary greatly. However, little is known about this characteristic in many poplar species [190]. Physiological and molecular analyses of poplar plants' responses to Cd exposure have been conducted [182,190–194]. He. J et al 2013 [195] in one of their study examined Cd accumulation, translocation, and biological stress and defence responses as the basis for Cd tolerance in their study, using six *Populus* species with different growth traits and water-use efficiency [196]. Poplar plants were subjected to either 0 or 200 μM $CdSO_4$ for 20 days in pots filled with sand. The physiological mechanisms behind the differences in Cd tolerance among the six poplar species were examined. The hypothesis is that they differ in their levels of Cd tolerance, and that these high levels of tolerance are due to well-coordinated physiological adjustments and transport activities into different plant tissues. To investigate this hypothesis, the six poplar species were analysed for photosynthetic pigments, soluble sugars and starch, reactive oxygen species ($O_2^{\bullet-}$ and $H_2O_2$), free proline and soluble phenolics, Cd concentrations, Cd amount per plant, bio-concentration factors, and translocation factors. The assessment and selection of poplar plants for the phytoremediation of Cd-polluted soils are discussed in relation to Cd tolerance and the underlying physiological mechanism.

However, *Populus alba* L. clone Villafranca is considered tolerant to high concentrations of HMs. Di Lonardo et al. 2011 [119] testing in an *in vitro* experiment the response to Cd, Zn, As and Cu of four *Populus alba* clones found that the clone Villafranca was the most tolerant accumulating the higher amount of HMs.

For these reasons this project focused on *Populus alba* clone Villafranca.

**Figure 3.** White poplar (*Populus alba*) illustration adopted by © DEA PICTURE LIBRARY.

## 1.5 Analytical method for qualitative and quantitative characterization of thiol-peptides in plants

High-Performance Liquid Chromatography coupled with Tandem Mass Spectrometry (HPLC-MS/MS) is a highly effective analytical method used in chemistry, biology, laboratory medicine, and biochemistry for detailed analysis of compounds in complex mixtures. This technique combines a liquid chromatography system with a tandem mass spectrometer to achieve a precise separation, identification, and quantification of components. In HPLC, a high-pressure liquid mobile phase separates compounds based on their interactions with both the mobile phase and a stationary phase, typically within a chromatographic column. This interaction leads to the separation of different compounds.

### *1.5.1 High-Performance Liquid Chromatography*

HPLC is a liquid chromatography method performed under high operational pressures, which can reach up to thousands of bars in ultra-high performance liquid chromatography (UHPLC) systems.

In actual use, separation takes place in the stationary phase, the core component of the HPLC system, after analytes are dissolved in an appropriate liquid mobile phase and pushed through it. The stationary phase is housed in a chromatographic column densely packed with solid particles, which interact with the target molecules due to their size, surface coating, and porosity. Each compound has a unique retention time ($t_R$) based on its interactions with the eluent and the adsorbent material. Typically, a compound with a stronger affinity for the stationary phase (or lower affinity for the mobile phase) will elute later from the column. On the other hand, an analyte with a lower affinity for the stationary phase will elute with a shorter $t_R$. The compound's chemical structure, its physical-chemical characteristics, including polarity, and the features of both the stationary and mobile phases all influence the type of interactions that occur. As a result, choosing the right stationary phase and mobile phase are essential to attaining the best possible selectivity for separating the different components of a mixture [197]. Siloxane and different alkyl (C8 or C18) or aryl groups frequently used surface coating of the silica particles in reverse stationary phases (RP), contrasting with earlier methods that used silica or alumina as the stationary phase. The interaction between the analytes and the stationary phase is handled by the terminal section of the cross-linking group. Hydrophilic interaction liquid chromatography (HILIC) is another separation method that has been extensively utilized for polar profiling in metabolomics investigations .

An RP column was utilized in this work, precisely a Kinetex ® 2.6 µm XB-C18, 100Å, 100 x 3 mm column. The 2.6 µm particle size of this column uses core-shell technology, combining a solid core with a porous outer layer to enhance separation efficiency, reduce band broadening, and deliver sharper peaks with lower backpressure than fully porous particles. The XB-C18 stationary phase, modified with C18 alkyl chains and di-isobutyl side chains, offers excellent chemical stability and selectivity for both polar and non-polar analytes. Its low ligand density enhances hydrogen bonding, making it ideal for thiol-peptide separation. Additionally, the 100Å pore size is ideal for analyzing small to medium-sized molecules like thiol-peptides, while the 3 mm internal diameter strikes a perfect balance between sensitivity and solvent consumption.

*1.5.2 Mass spectrometer*

The general framework followed by all mass spectrometers includes an ion source, a mass analyser (or a series of mass analysers), and a detector. MS converts the analyte molecules to a charged (ionized) state, with subsequent analysis of ions and any fragment ions generated during the ionization process, obtaining a spectrum in which metabolites are represented according to their masses to charge ratio (m/z) [198,199]. Ionization techniques can be categorized into two main groups: hard and soft techniques. These groups differ from each other based on the amount of residual energy transferred to the molecules. Focusing on soft ionization, nowadays electrospray ionization (ESI), developed by John Fenn and his collaborators and published in 1985 [200] and optimized by Andries Bruins [201,202] , is one of the most widely used.

ESI is achieved by introducing the samples into a metallic capillary maintained at 3-5 kV, where a stream of nitrogen nebulizes the sample at the tip of the capillary, forming a homogeneous spray of charged droplets. The capillary is typically oriented orthogonally or off-axis relative to the mass spectrometer's entrance to minimize noise from neutral droplets. The droplets are rapidly evaporated through the application of heat and dry nitrogen, transferring their electrical charge to the analytes. In the ionization chamber, where the ion source is located, intact molecular ions are produced and then transferred to the mass analyser region via various ion optics, such as skimmers, focusing lenses, and multipoles. These components are designed to focus the ion stream and maintain a stable trajectory. The mass analyser sorts and separates the ions based on their mass-to-charge ratio (m/z). The separated ions are then directed to the detector systems, which measure their concentration and display the results on a chart called a

mass spectrum. Since ions in the gas phase are highly reactive and short-lived, their formation and manipulation occur under high vacuum conditions. Thus, the ion optics, analyser, and detectors are maintained at very high vacuum levels (typically between 10−3 and 10−6 torr). The ion source is kept at atmospheric pressure, and a continuous pressure and voltage gradient from the source to the detector aids in moving the ions through the analyser to the detector.

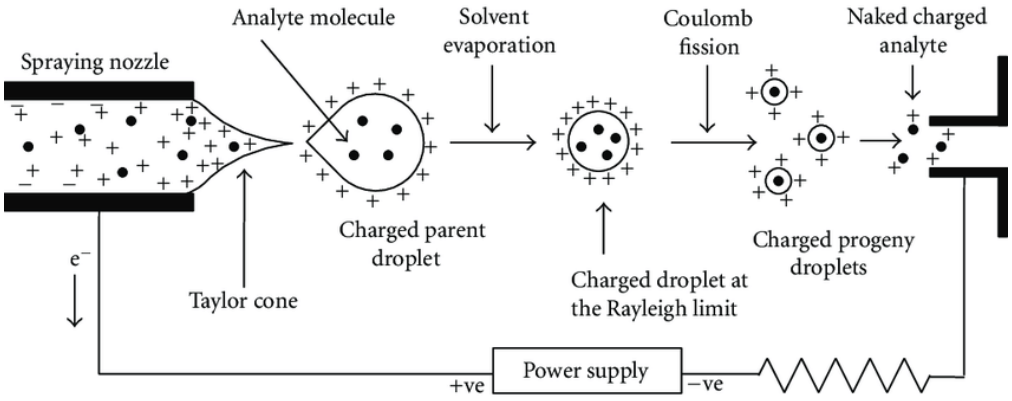


**Figure 4.** ESI mechanism (adapted from Banerjee S. and Mazumdar S., 2011 [203]).

There are two primary ionization modes: positive (POS) and negative (NEG). Positive ion mode (ESI+) is often favoured because it generally results in more compounds ionizing effectively. However, negative mode tends to produce lower background noise. Some metabolites are only detectable in negative mode, while others are only observed in positive ion mode. Consequently, employing both ionization modes provides more thorough coverage of the biological molecules.

A variety of ions can be produced by the source, such as mobile phase components, positive or negative charged molecules, adducts that result from combining with other molecules (mostly $Na^+$, $K^+$, and $NH_4^+$ adducts in positive ions, or $Cl^-$, $HCOO^-$, $CH_3COO^-$, and $OH^-$ adducts in negative mode), and fragment ions in the rare occurrence that in-source fragmentation takes place. Ion separation can be carried out using a variety of analysers, each of which uses a different technique depending on its m/z. These consist of the time-of-flight mass analyser, Fourier-transform ion cyclotron resonance and Orbitrap analysers, quadrupole mass analyser, and quadrupole and linear ion trap mass analysers [204,205].

The choice between a triple quadrupole mass spectrometer and a high-resolution mass spectrometer depends on the specific goals of the analysis. Targeted studies benefit from the sensitivity and specificity of triple quadrupole MS, while untargeted or exploratory studies

benefit from the comprehensive capabilities and accurate mass measurements provided by high-resolution MS. The quadrupole excels in quantifying known compounds with high sensitivity and specificity [204].

The quadrupole linear ion trap analyser consists of four parallel metal rods (Figure 5A); a combination of constant and varying (radio frequency) voltages allows the transmission of a narrow range of m/z values along the axis of the rods. By varying the voltages over time, it is possible to scan across a range of m/z values, resulting in a mass spectrum. Quadrupole analysers typically operate at unit mass resolution, meaning that the mass accuracy is usually within 0.1 m/z. Ions specifically selected by the quadrupole are called resonant and pass through the rods of the quadrupole following a sinusoidal pattern, ions not compatible with the selected voltages values are deflected and diverted from the ion path (Figure 5B). Additionally, introducing an inert gas into the ion trap can promote the fragmentation of ions. A notable feature of these ion trap analysers is their ability to repeatedly fragment and isolate ions before generating the final mass spectrum, which is known as MSn capabilities. Additionally, a quadrupole mass filter (QMF) can function as a trapping system, either alone or in combination with a linear ion trap (LIT). When QMF and LIT are integrated into a single device, it is called a QTrap mass analyser [30,31].

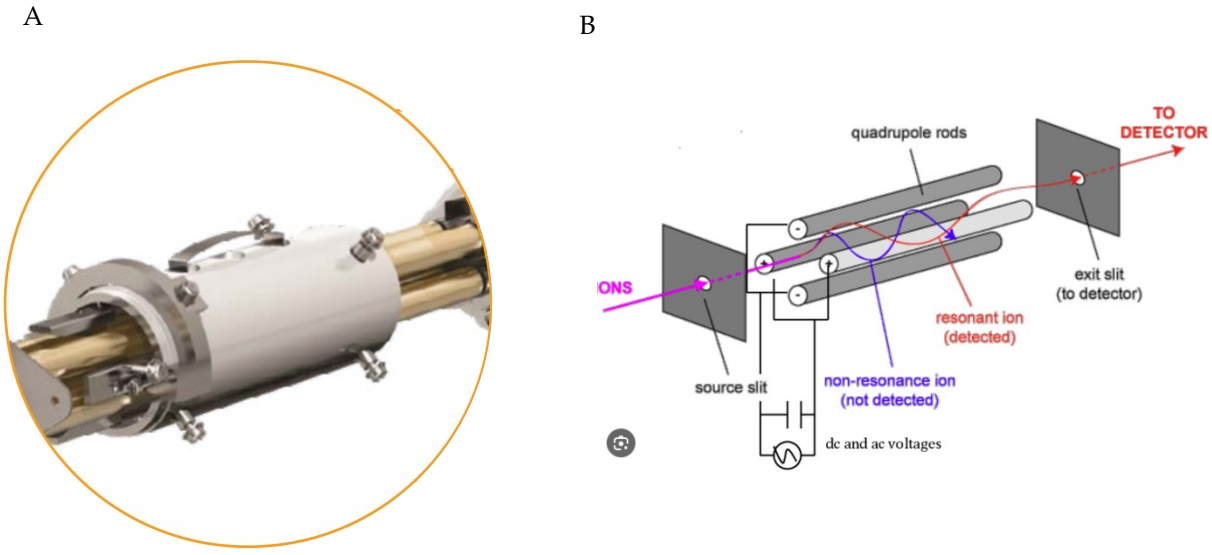


**Figure 5**. Quadrupole photo (A, reported by sciex.com content) and its schematic functioning representation (B, reported by Schmidt [206].

*1.5.3 Tandem Mass Spectrometry: bases and principles*

Tandem mass spectrometers incorporating various combinations of mass analysers have been developed and used in targeted metabolomic. A common combination is based on three quadrupoles in series (triple quadrupole mass spectrometer), the first of which (Q1) selects the precursor ion, the second (Q2), which basically is a collision cell, induces fragmentation, while the third (Q3) isolates and detects the specific product ions, allowing for precise quantification (Figure 6B). The advantage of tandem MS is the significantly increased specificity of the analysis compared to single-stage mass analysis. Fragmentation within the collision cell typically occurs using an inert gas such as Ar or $N_2$, a process known as collision-induced dissociation (CID). One of the possible operative modes, termed the "product ion scan," involves selecting an ion with a specific m/z value in Q1 and then fragmenting it in Q2. The quadrupole Q3 then scans and detects all the resulting fragment ions. A second operative mode, known as the "precursor ion scan", targets a specific fragment ion in Q2, while Q1 scans across a range of m/z values to identify the corresponding precursor ion. Another frequently used mode is the "neutral loss scan", in which both Q1 and Q3 scan ions within a selected m/z range, with a constant mass offset between the two quadrupoles. This mode identifies all fragmentations that result in the loss of a specific neutral fragment. Moreover, in tandem MS, the first and third quadrupoles can be simultaneously stepped to different m/z values, allowing for the creation of panels of precursor/product ion pairs. This enables the specific detection of a large number of targeted analytes. This process, known as multiple reaction monitoring (MRM), is commonly used in LC-MS assays [204]. In our experimental work, we specifically used a triple quadrupole mass spectrometer, particularly a Sciex API 4000 mass spectrometer (Figure 6A), which is capable of generating MS/MS experiments.

A B

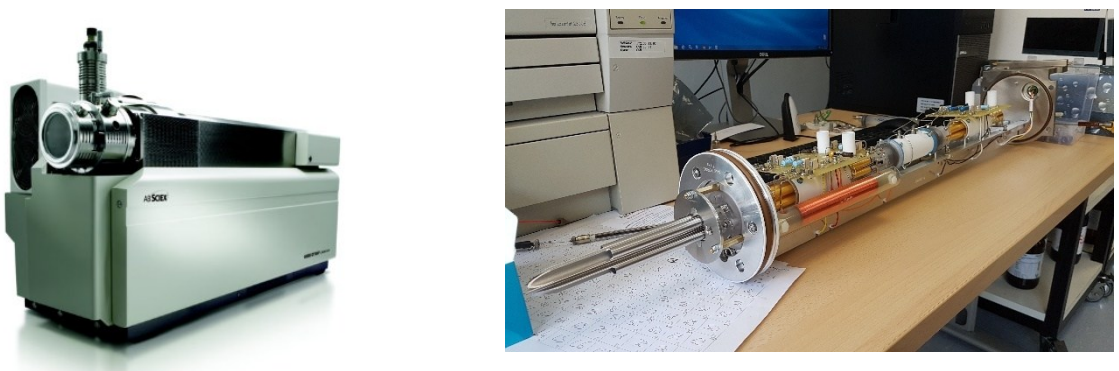

**Figure 6.** Sciex API 4000 mass spectrometer external (A, adapted by www.myco-instrumentation.com) and internal (B) representations of the ion pathway.

### *1.5.4 Analytical attempts to thiol-peptides characterization and relative issues*

Both GSH and PCn are highly susceptible to spontaneous oxidation, which can lead to erroneous analytical results in their quantification and characterization [207]. Furthermore, GSH, γ-glutamylcysteine (γ-EC), PCn, and their derivatives are amphoteric, highly polar, and lack strong chromophores. These properties make their quantification challenging using conventional analytical techniques [208]. Such techniques often involved RP HPLC, coupled with either pre-column derivatization using monobromobimane or post-column derivatization with 5,5-dithiobis(2-nitrobenzoic acid) (DTNB, Ellman's reagent) [209,210].

Although thiol-peptide derivatization is advantageous as it increases the stability of these compounds, the derivatizing reagents can react with any thiol group, making the process time-consuming and not specifically selective for PCn and related peptides. This lack of specificity often renders the method unsatisfactory for HPLC analysis [208,211]. Furthermore, some derivatization methods may overestimate thiol-peptides by detecting non-thiol compounds. Berlich et al. 2002 [212] in their study demonstrated that coumarins identified under the basic pH conditions of the Ellman test could produce false-positive post-column Ellman reactions.

To address these challenges, a previous study developed an isotope labelling combined with LC-ESI-MS/MS method using a derivatization strategy to detect PCn in plant samples without losing selectivity and sensibility [213]. However, derivatization complicates sample preparation, is time-consuming, and may compromise assay accuracy, making it preferable to avoid when not strictly necessary. Additionally, the choice of derivatizing agent can significantly affect outcomes.

For a more efficient and practical alternative, analysis without derivatization is often preferred. HPLC-ESI-MS/MS enables accurate quantification of multiple analytes with reduced risk of false positives; however, challenges remain due to variability in ionization efficiency and concentration across different sample matrices, even under consistent HPLC conditions [214]. ESI ionization may also cause matrix-dependent signal suppression that varies between samples [215]. To mitigate these effects, the use of stable isotope-labeled internal standards that coelute with the analytes is recommended. These standards improve quantification accuracy by compensating for ion suppression and matrix effects.

Notably, external standard methods are suboptimal for measuring PCn, because they fail to account for matrix effects and analyte loss during extraction [211,216,217]. Matrix composition significantly influences ESI efficiency, which impacts HPLC-MS/MS performance, particularly in complex matrices like plant samples.

Stable isotope-labeled internal standards have been employed in limited studies. For example, Liu et al. 2015 [213] developed a quantitative profiling method for PCn using ω-bromoacetonylquinolinium bromide (BQB) and BQB-$d_7$ as isotope-labeling reagents, while Simmons et al. 2009 [207] described a method using glycine-$^{13}C_2$-GSH as an internal standard. The critical biological roles of thiol-peptides in plants necessitate sensitive and accurate analytical techniques for their simultaneous detection and quantification. A recent study focusing on the plant model *A. thaliana* (Brassicaceae) introduced a robust HPLC-ESI-MS/MS method for measuring GSH, γ-EC, and PCn in roots and shoots. To enhance quantification accuracy, this method employs a rapid and straightforward extraction protocol using an appropriate reducing agent to prevent PCn oxidation, coupled with isotope-labeled internal standards for GSH and PCn [218].

## 2. PURPOSE OF THE PROJECT

The purpose of this project is to investigate the detoxification mechanisms in a Cd-tolerant plant, *Populus alba*, to gain a deeper understanding of its strategies for HM detoxification. Expanding knowledge in this field could have valuable applications for the remediation of soils contaminated by HMs, an issue of significant concern within European Union environmental policies.

Cd is a highly toxic trace element that is unnecessary for biological systems but widely present in the environment due to natural and industrial sources [14]. Consequently, it is regarded as a significant environmental pollutant [15,16]. Cd and its compounds are soluble, making them more mobile than other metals in environmental matrices. HMs, particularly Cd, represent significant dangers to plant health, causing toxicity, growth inhibition, and oxidative stress. According to numerous studies, dumps often contain Cd levels exceeding the permissible limit in soil [20–23] . With a global mean of 0.36 mg/kg, Cd usually occurs in soils at amounts ranging from 0.01 to 1 mg/kg [16] and soil water up to 5 µg/L [24] and groundwater up to 1 µg/L [25]. This research focuses on *Populus alba* as a potential solution for soil decontamination, given its ability to produce PCn, cysteine-rich peptides synthesized from GSH by the enzyme PCS. PCn plays a crucial role in detoxifying HMs by forming complexes that are sequestered in plant vacuoles.

To achieve this, the project aims to:

1. **Optimize the preanalytical extraction and analytical method**: improve the preanalytical step by performing an additional cleaning step to overcome matrix effect complications in MS. By HPLC-MS/MS method GSH and PCn were quantified in *Populus alba* (shoots, roots and growing media) under varying conditions of Cd stress. This involves assessing the impact of different $Cd^{2+}$ concentrations on PCn production and its accumulation in plant tissues.
2. **Evaluate the response to prolonged Cd stress in *Populus alba:*** testing resistance, consequences, and responses induced by high HM concentrations over extended exposure times.
3. **Investigate the role of intra and extracellular thiol-peptides in HM toxicity in *Populus alba* under short-term Cd conditions**: conduct experiments to determine *Populus alba* response mechanisms against $Cd^{2+}$ through PCn formation. This includes

analysing both intracellular and extracellular PCn levels at different exposure times and $Cd^{2+}$ concentrations, as well as monitoring the expulsion of GSH, PCn or PCn- $Cd^{2+}$ complexes from the roots into the growth medium.

4. **Investigation study of transporters involved in the secretion of thiol-peptides in *Populus alba* adult plants:** plant cells employ a variety of transporters to preserve metal homeostasis. Different transporters are used by plants to sequester metal ions inside organelles, whether in a free ionic state or as chelates. An inhibition study of hypothetical of (Cd) thiol-peptide transporter was performed. Sodium orthovanadate was selected as inhibitor due to its tetrahedral ion structure analogy to phosphorus ion. of both P-type ATPase and ABC transporters, glibenclamide has only been demonstrated to inhibit ABC transporter [219].

Overall, this project aims to explore the detoxification mechanisms of *Populus alba* under Cd stress, focusing on the role of thiol-peptides in HM detoxification. By integrating analytical and biological approaches, the study contributes to advancing phytoremediation strategies for Cd-contaminated environments.

# 3. MATERIALS AND METHODS

## 3.1 Plant material and growth conditions

*Populus alba* Villafranca clone plants were grown *in vitro* on Woody Plant Medium (WPM, Duchefa Biochemie, Haarlem, Netherlands) containing vitamins, 0.7 % agar and 20 g/L sucrose in water ($H_2O$, deionized using a Milli-Q system, Millipore Corp., USA). The WPM solid medium was adjust to 5.86 pH, autoclaved at 120°C for 20 min to obtain a sterile solution, and placed in plastic pots until solidification. The internodes were cut from an adult *Populus alba* plant, embedded in the solid soil, and the containers were closed with caps equipped with special filters that allow gas exchange with the external environment (Figure 7). The seedlings were propagated every two months using single internodes and then placed in growth chambers at a temperature of 25°C with a photoperiod of 16 hours light / 8 hours dark.

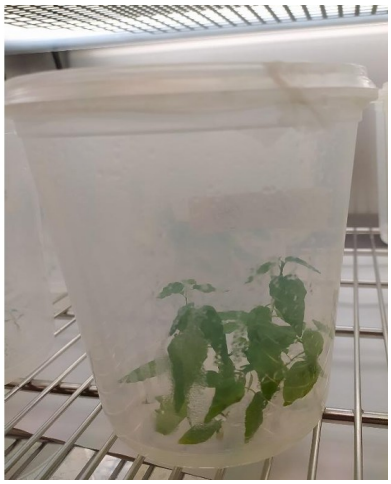

**Figure 7**. *In vitro Populus alba* plants on WPM growth medium.

*Populus alba* plants grown in control (CTRL) condition and in stressed condition as well. Before explaining the different treatments, the common shoots and roots extraction method was deepen.

After the treatment timing, leaves, stems and roots were separated, collected in 2 mL eppendorf tubes and stored at -80°C.

### 3.2 Extraction method of GSH and PCn from vegetal tissues

At the time of extraction, samples were frozen using liquid nitrogen ($N_2$) and homogenized (MM200, Retch, Haan, Germany), using two agate grinding balls (5 mm diameter) to facilitate mechanical cell lysis at a vibrational frequency of 30 Hz for 1 min.

The extraction of samples involved a specific extraction buffer containing diethylenetriaminepentaacetic acid (DTPA ≥ 99%) 6.3 mM, 5% p/p sulphosalicylic acid, tris(2-chloroethyl)phosphate (TCEP ≥ 99%) 2 mM , ethylenediaminetetraacetic acid (EDTA ≥ 99%) and analytes labelled internal standards (glycine-$^{13}C_2$-GSH and glycine-$^{13}C_2$,$^{15}N$-PC2, 200 ng/ mL for both). TCEP, EDTA, DTPA, were all supplied by Sigma-Aldrich, Saint Louis, MO, USA. GSH, PC2,PC3, PC4 and the internal standards glycine-$^{13}C_2$-GSH and glycine-$^{13}C_2$,$^{15}N$-PC2 were purchased from AnaSpec Inc., Fremont, CA, USA.

After the addition of the extraction buffer, samples were vortexed for 5 min and cooled down in ice, for three times. Then, the homogenates were centrifuged for 20 min at 4 °C at 10000 x g, the supernatants were removed and re-centrifuged under the same conditions. The extracts were filtered using a low thiols retention syringe filters (Minisart RC4 0.45 µm, Sartorius Italy S.r.l.) and the obtained filtrates were washed two times using 1.5x volume of normal butanol (n-BuOH, LC-MS grade). GSH and PCn quantification was performed by the injection of the extracted samples to HPLC-MS/MS system (Figure 8).

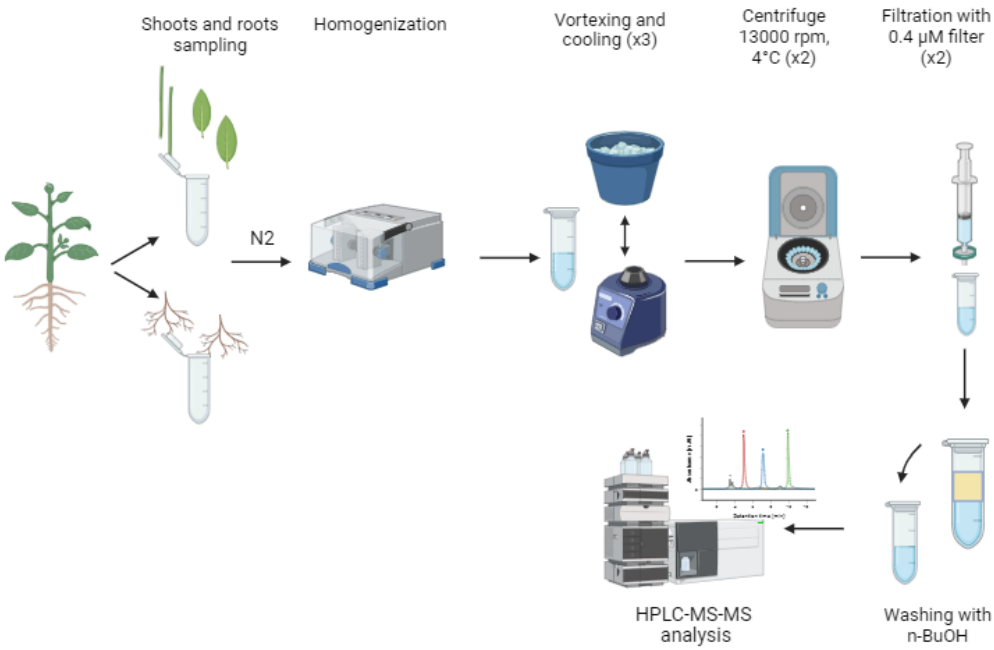


**Figure 8.** Extraction pathway to perform GSH and PCn analysis.

Before this final washing step, various additional biochemical methods were attempted to purify the sample, improve the accuracy of the analysis, reduce matrix effects, and keep the instrumentation cleaner. One of the tested approaches included solid-phase extraction cartridges (SPE), operating with weak anion exchange (WAX), weak cation exchange (WCX), or hydrophilic lipophilic balance (HLB, Bond Elute). HLB cartridges were supplied by Waters S.p.A. (MI, Italy); WCX, WAX and Bond Elute cartridges were sourced from Agilent Technologies (Santa Clara, CA, USA).The SPE process included:

1. Conditioning, where the solid phase was wetted with MeOH, $H_2O$, or sample buffer.
2. Sample loading.
3. Washing and elution, with solvent selection dependent on the cartridge and analyte properties.

Washing solvents tested included formic acid (FA), ammonium hydroxide ($NH_4OH$) solutions, and biological buffers like potassium phosphate ($K_2HPO_4$) or potassium acetate ($CH_3COOK$). These methods did not yield satisfactory results.

Other strategies, such as esterification of the target analytes and modification of the extraction buffers, were also attempted. Particularly, 50 µL of 1 ug/mL internal standards solution was added to 1 mL of MeOH and dried under nitrogen flux at room temperature. Subsequently, 100 µL of butanol in 3M HCl was added, and the solution was shaken for 1 hour. After drying, 200 µL of $H_2O$ and 200 µL of ethyl ether were added, vortexed and centrifuged at 14000 rpm for 30 sec. The organic phase was removed and the washing procedure repeated. Solvent was finally evaporated under nitrogen flux at room temperature and 50 µL of MeOH was added to evaluate derivatized thiol-peptides by MS injection.

Several buffer formulations were also tested to evaluate the most effective. These included 10 mM of DTPA and 200ng/mL of internal standards that were added to two biological common buffers TRIS-HCl or HEPES containing two different reducing agent such as β-mercaptoehanol and TCEP, both at 20 mM. These solutions were added to the vegetal materials, homogenized at 5500 RPM for 20 sec, centrifuged at 14000 rpm for 15 min at 4 °C, filtered with 0.45 µm filters, and analysed by HPLC-MS/MS. TCEP was identified as the optimal reducing agent, and further experiments were conducted to determine the ideal concentration (2, 5, 10, 20 mM) in a buffer containing TRIS-HCl (5 mM DTPA, 200 ng/mL labelled GSH and PC2). Results showed 2 mM TCEP as the most effective. The extraction buffer (TRIS-HCl vs aqueous buffer) and the sample-to-buffer ratio (1:3, 1:6, 1:10, 1:20) were

also compared starting from 50 mg of vegetal matrix and following the same extraction procedure.

Moreover, to enhance sample cleaning, washing steps using n-butanol (n-BuOH) were implemented. The solvent was selected due to its polarity, which removes water-soluble polar molecules while remaining separable from $H_2O$. n-BuOH was purchased from Sigma-Aldrich (Saint Louis, MO, USA). When mixed with $H_2O$, n-BuOH formed an upper phase that was removed. However, this step introduced the limitation of azeotropic mixture formation, which could alter the phase ratio. Washing volumes of 1.5x, 2x, and 3x of the extract volume were tested. The extracted matrices, washed once or twice, were injected into the HPLC-MS/MS system, and the GSH and PCn peak areas were compared.

Additional filtration techniques using I-Phree cartridges (obtained from Phenomenex ,Torrance, CA, USA) or Amicon filters (supplied by Sigma-Aldrich, Saint Louis, MO, USA), as well as precipitation attempts, were explored but were found to be ineffective compared to the liquid-liquid extraction technique.

Figure 9 summarizes all attempts to clean the vegetal matrices.

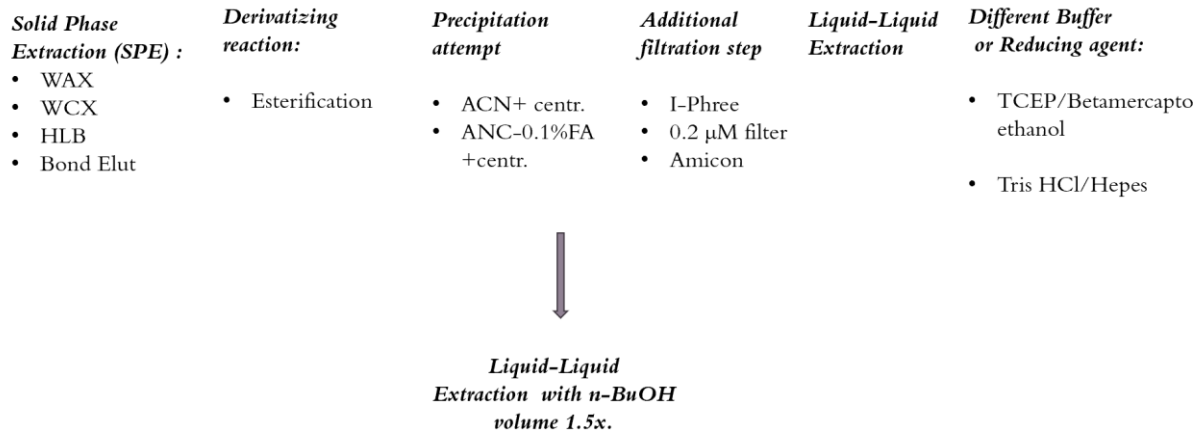


**Figure 9.** Attempts to purify the vegetal extract.

### 3.3 Quantification method of thiol-peptides by HPLC-MS/MS

Once extracted, 20 µL of each sample was injected into HPLC-MS/MS system: an Agilent 1290 Infinity UHPLC system (Santa Clara, CA, USA), including a thermostated autosampler, a binary pump, and a column oven, coupled to an AB Sciex API 4000 triple quadrupole mass spectrometer (Concord, ON, Canada), equipped with a Turbo-V ion spray. A ten-port switching valve (Valco Instruments Co. Inc., Huston, TX, USA) was used as a divert valve to discard both head and tail of the HPLC runs. The instrumentation also included an Agilent 1260 quaternary HPLC pump, which supplied the mass spectrometer when the eluent from the column was diverted to waste. Chromatographic separation was performed by a RP Phenomenex (Torrance, CA, USA) Kinetex 2.6 µm XB-C18 100 Å, 100×3 mm HPLC column, protected by a C18 3mm ID security guard ULTRA cartridge System control, data acquisition and processing were carried out by an AB Sciex Analyst® version 1.6.3 software [218].

Ten standard solutions ranging from 1 to 1000 ng/ mL (1, 2, 5, 10, 20, 50, 100, 200, 500, and 1000 ng/mL) containing GSH, PC2-3-4 were used each day to create calibration curves. The working solution was serially diluted with 2 mM TCEP to create each solution. Then, the appropriate concentrations of either glycine-$^{13}C_2$,$^{15}N$-GSH or glycine-$^{13}C_2$,$^{15}N$-PC2 were added, bringing the total concentration of both internal standards to 200 ng/mL.

The analytical method used was validated in the literature [218] and involves an HPLC method with a gradient run between the aqueous phase (solvent B), consisting of $H_2O$ + 0.1% FA, and the organic phase (solvent A), containing ACN + 0.1% FA (Table 3). The flow rate was set to 300 µL/min, with a quaternary pump operating at 100 µL/min of 50:50 MeOH: $H_2O$ for the entire 14-minute run (Table 3). Figure 10 represented the selected reaction monitoring (SRM) chromatogram of each analyte.

ACN (LC-MS grade), ultra-pure $H_2O$ (LC-MS grade), MeOH (LC-MS grade), FA (MS grade≈98%) were all supplied by Sigma-Aldrich (Saint Louis, MO, USA).

| Step | *HPLC Quaternary Pump* | | | | *HPLC Binary Pump* | | | |
|---|---|---|---|---|---|---|---|---|
| | Time (min) | Flow rate (µl min$^{-1}$) | Methanol (%) | Water (%) | Time (min) | Flow rate (µl min$^{-1}$) | Solvent A (%) | Solvent B (%) |
| 0 | 0.0 | 100 | 50 | 50 | 0.0 | 300 | 2 | 98 |
| 1 | 14.0 | 100 | 50 | 50 | 5.0 | 300 | 2 | 98 |
| 2 | | | | | 9.5 | 300 | 44 | 56 |
| 3 | | | | | 10.5 | 300 | 95 | 5 |
| 4 | | | | | 11.5 | 300 | 95 | 5 |
| 5 | | | | | 11.7 | 300 | 2 | 98 |
| 6 | | | | | 14.0 | 300 | 2 | 98 |

**Table 3.** HPLC run conditions [218].

SRM mode was used for MS/MS analysis. The SMR transitions, along with the corresponding operating parameters such as declustering potential (DP) collision energies (CEs),collision cell exit potential (CXP) , is provided in the table below (Table 4A). Further operative parameters include IonSpray voltage (IS), Gas Source 1 (GS1), Gas Source 2 (GS2), source Temperature (TE), Collision Gas (CAD) Nitrogen, Curtain Gas (CUR); Entrance Potential (EP), Prefilter (ST), and Focusing Lens 1 (IQ1), all listed in Table 4B.

A

| Analyte | SRM transition | Ion ratio | r.s.d. (%) | DP | CE | CXP |
|---|---|---|---|---|---|---|
| γ-EC | 251.1 → 83.8 (q) | 0.91 | 5.25 | 42 | 36 | 5.2 |
| | 251.1 → 121.8 (Q) | 1.0 | 0.00 | | 17 | 8.7 |
| | 251.1 → 129.9 (q) | 0.52 | 3.32 | | 23 | 10.2 |
| GSH | 308.1 → 75.9 (q) | 0.53 | 7.82 | 57 | 35 | 5.8 |
| | 308.1 → 162.0 (q) | 0.53 | 3.66 | | 25 | 12.4 |
| | 308.1 → 178.8 (Q) | 1.00 | 0.00 | | 18 | 16.1 |
| $^{13}C_2$,$^{15}N$-GSH | 311.1 → 75.9 (q) | 0.43 | 5.87 | 57 | 35 | 5.8 |
| | 311.1 → 165.0 (q) | 0.55 | 2.81 | | 25 | 12.4 |
| | 311.1 → 181.8 (Q) | 1.00 | 0.00 | | 18 | 16.1 |
| $PC_2$ | 540.1 → 308.0 (q) | 0.72 | 2.55 | 88 | 31 | 8.1 |
| | 540.1 → 336.1 (Q) | 1.00 | 0.00 | | 30 | 9.4 |
| | 540.1 → 411.3 (q) | 1.29 | 3.81 | | 25 | 12.3 |
| $^{13}C_2$,$^{15}N$-$PC_2$ | 543.1 → 311.0 (q) | 0.43 | 5.87 | 88 | 31 | 8.1 |
| | 543.1 → 337.1 (Q) | 0.55 | 2.81 | | 30 | 9.4 |
| | 543.1 → 414.3 (q) | 1.00 | 0.00 | | 25 | 12.3 |
| $PC_3$ | 772.2 → 232.9 (Q) | 1.00 | 0.00 | 121 | 52 | 19.3 |
| | 772.2 → 540.1 (q) | 0.53 | 7.75 | | 37 | 16.1 |
| | 772.2 → 643.3 (q) | 0.65 | 9.79 | | 34 | 9.7 |
| $PC_4$ | 1004.3 → 233.0 (Q) | 1.00 | 0.00 | 125 | 68 | 6.5 |
| | 1004.3 → 540.2 (q) | 0.54 | 6.73 | | 48 | 15.8 |
| | 1004.3 → 875.2 (q) | 0.33 | 8.85 | | 41 | 14.7 |

B

| *IS* | *5.5 kV* |
|---|---|
| *GS1* | 45 arbitrary units |
| *GS2* | 35 arbitrary units |
| *TE* | 600 °C |
| *CAD* | 6.3 mPa |
| *CUR* | 10 arbitrary units |
| *EP* | 10 V |
| *ST* | -15.4 V |
| *IQ1* | -10.6 V |

**Table 4.** Operating parameters of SRM method: mass transitions and relative conditions (A) imported by Bellini et al 2019 [218].

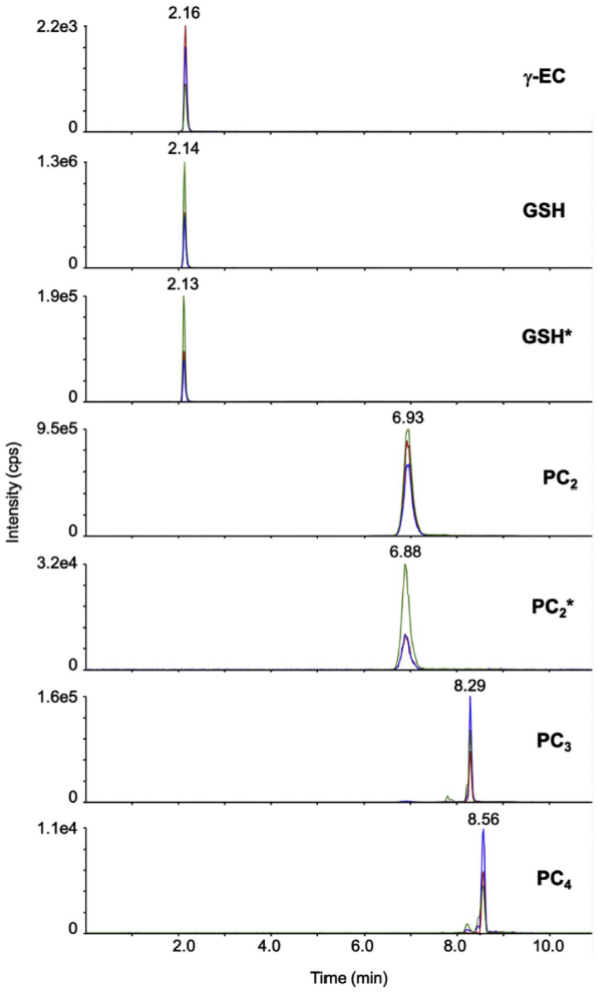


**Figure 10.** SRM chromatograms of a representative shoot extract of *A. thaliana* in the time-range of 0–10 min [218].

## 3.4 Experimental setup for the evaluation of *Populus alba* response under $Cd^{2+}$ hight stressed conditions

The experimental setup included two-month-old *P. alba* plants grown under solid WPM control conditions (0 µM $CdSO_4$) and in $Cd^{2+}$ contaminated WPM media (50 and 100 µM $CdSO_4$). As described in section 3.1, the plants were grown in plastic containers with caps equipped with special filters and then placed in growth chambers at a temperature of 25°C, with a photoperiod of 16 hours light / 8 hours dark.

Cd is typically found in soil at concentrations ranging from 0.01 to 1 mg/kg, with a global average of 0.36 mg/kg. Through weathering processes, Cd levels can increase to as much as 5 µg/L in soil water and up to 1 µg/L in groundwater. In aqueous solutions, Cd predominantly exists as the divalent ion $Cd^{2+}$, which becomes more mobile under oxic and acidic conditions [220]. However, less than 2% of Cd in the environment is usually in a bioavailable form [221]. Consequently, Cd treatments exceeding 20 µM represent severe contamination, far exceeding natural background levels.

For each treatment, three biological replicates were prepared, with each replicate represented by a single container holding five *P. alba* plants.

At the end of the experimental period, approximately 100 mg of roots, stems, and leaves from each condition were sampled and stored at -80°C for thiol-peptides quantitative analysis (section 3.4.3). Some *P.alba* control and stressed plants were used for biometric analysis (section 3.4.1) and for the evaluation of fluorescence and photosynthetic efficiency (section 3.4.2).

### *3.4.1 Biometric analysis*

Photos of control and treated plants were obtained and processed with ImageJ software (National Institutes of Health, Bethesda, MD, USA). The biometric data for *P. alba* were evaluated by analysing stem length, primary root length, and leaf area. The same plants were then weighed to consider their fresh weight (FW) and subsequently dried overnight in an oven at 60 °C to determine the dry weight (DW). The dry matter percentage was then calculated using the formula (FW · 100) / DW.

### *3.4.2 Fluorescence and Photosynthetic efficiency*

Photosynthetic efficiency was evaluated by analysing the transient stages of chlorophyll fluorescence (OJIP transients) by JIP test [222]. This technique calculates a large number of

parameters, providing detailed information on the structure and functionality of Photosystem II (PSII) and the efficiency of photosynthetic electron transport. Operating on the principle of continuous excitation, a Handy PEA fluorimeter (Hansatech Instruments Ltd, Norfolk, UK) was used to perform *in vivo* fluorescence analyses on *P. alba* leaves.

The instrument's photometric sensor measures only photons re-emitted as fluorescence by chlorophylls, thanks to a filter that excludes wavelengths below 700 nm. For each treatment, three replicates were used, with each replicate consisting of two seedlings, and measurements were taken on two leaves per seedling. Treated plants and controls were placed on Petri dishes (Ø 90 mm). Subsequently, the leaves were darkened with leaf clips for 30 minutes (Figure 11) by closing the central shutter, to ensure that the major non-photochemical de-excitation processes were deactivated. After the acclimatation at the darkness the leaves surface were illuminated for one second with an LED light source that irradiated the plant with saturating light levels (up to 3000 μmol · $m^{-2}$ · $s^{-1}$) at 650 nm. The calculated parameters (JIP test) provide an accurate overview of the photochemical process.

**Figure 11.** *P.alba* leaves acclimated at the darkness using leaf clips.

*3.4.3 Extraction and quantification of intracellular thiol-peptides*

For each treatment (0, 50, 100 μM $Cd^{2+}$) 100 mg of roots, stems and leaves were extracted as described in 3.2 chapter. Particularly 300 μL (1:3 weight (mg): volume (μL)) of extraction buffer were used. After the vortex/cooling steps the homogenates were centrifuged for 20 min at 4 °C at 10000 x g, the supernatants were removed and re-centrifuged under the same conditions. The extracts were filtered using a low thiols retention filters (Minisart RC4 0.45 μm, Sartorius Italy S.r.l.) and 20 μL were injected and analysed by HPLC-MS/MS method as explained in 3.3 section.

## 3.5 Experimental setup for evaluating responses to short-term and low-concentration $Cd^{2+}$ exposure

To replicate a reliable simulation of real plant stress conditions in the environment, a lower Cd concentration was chosen for plant treatments. HMs are more bioavailable to plants in liquid media compared to solid media. Therefore, working with liquid media, it was possible to reduce the treatment time to 24, 48, and 72 h of exposure. A hydroponic experimental setup was initially considered, but due to laboratory constraints this, could not be implemented. However, for the brief treatment durations, the setup described below was deemed acceptable. Additionally, the liquid form of the medium and the absence of sucrose allowed for the HPLC-MS/MS analysis of extracellular analytes released from the root system.

### *3.5.1 Extraction and quantification of intracellular and extracellular thiol-peptides*

*Populus alba* Villafranca plants were grown for one month in WPM medium containing vitamins, 0.7 % agar, and 20 g/L sucrose (pH 5.86). The growth chamber was set to 25 °C with a photoperiod of 16 hours light and 8 hours dark. Plastic pots with caps equipped with special filters were used to allow gas exchange with the external environment. Each container accommodated five *Populus alba* internodes. After the growth period, each plant was gently removed from the solid medium, ensuring the roots were not damaged, and transferred to a single tube containing 3 mL of Gamborg's B-5 Basal Medium with vitamins (pH 5.86, adjusted with HCl and KOH) as shown in Figure 12. These steps required sterile conditions and a great deal of precision in placing the plant in a single tube: no leaves or stems should come into contact with the liquid; only the roots needed to be submerged in the medium. In this way, any thiol derivatives found in the extracellular environment originated solely from the root system. Eight single sterile tubes were located in the plastic pots with caps equipped with the filters, and left in the growth chamber for the time of the treatments (24-48-72 h). Cd stressed conditions provide the addition of $CdSO_4$ solution at the medium to achieve 5-10-20-36 μM $Cd^{2+}$ concentrations.

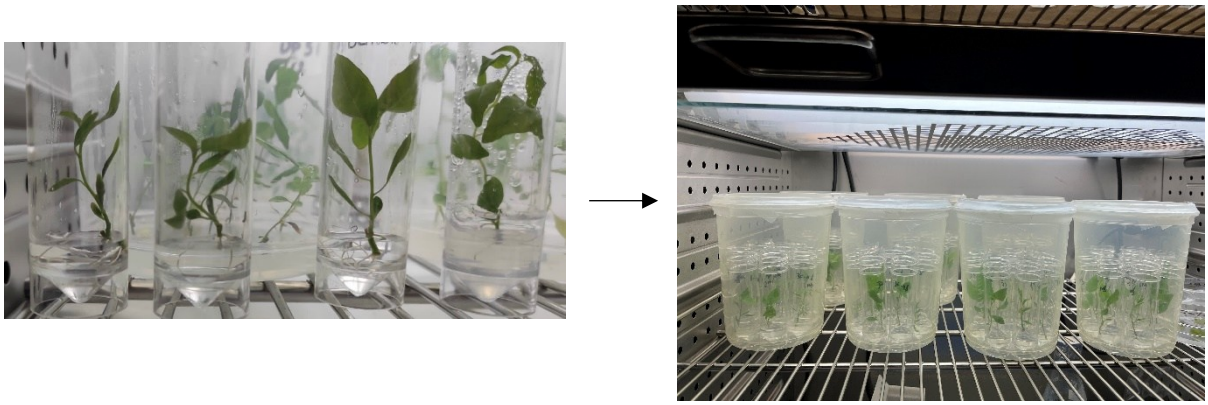

**Figure 12.** *P.alba* one month old plants treated with or without $Cd^{2+}$ , in B5 liquid medium, located in a grown chamber for 24-48-72 h.

For sampling, shoots from every 2-3 plants were pooled, to obtain a weight of 50-100 mg for each sample, and roots were similarly pooled, creating 3 biological replicates for each experimental condition, stored at -80°C until the extraction. At the same time, the media from 2-3 plants were pooled and filtered using a 0.45 µm filter, and each pool provided one biological replicate of 1 mL, resulting in 3 replicates for each treatment (Figure 13), stored in 1.5 mL tube at -80°C as well.

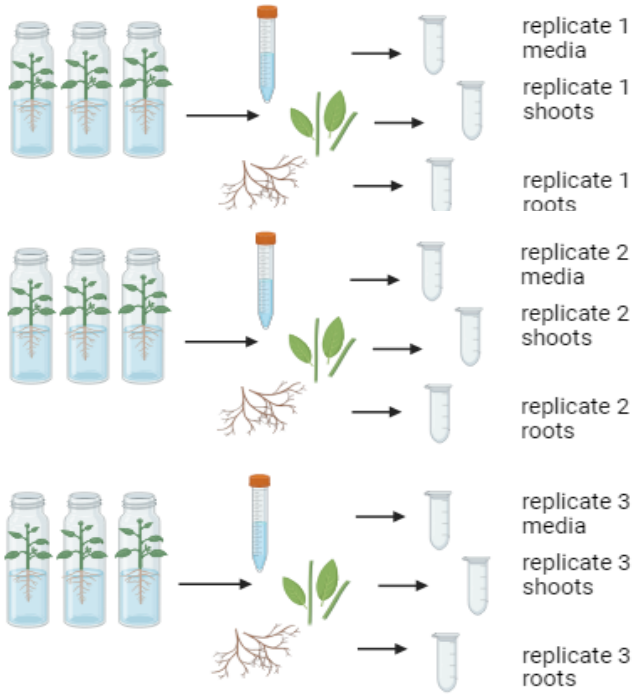


**Figure 13.** Sampling scheme to obtain 3 biological replicates of shoots, roots, and media for each experimental conditions.

Shoots and roots were extracted as described in section 3.2, and 20 µL of extracted were injected to HPLC-MS/MS with the method described in 3.3 section. Meantime, the liquid media were lyophilized using a freeze dryer and 20 µL were injected after reconstitution in 62.5 µL of $H_2O$, with glycine-$^{13}C_2$-GSH and glycine-$^{13}C_2$,$^{15}N$-PC2 used as internal standards. This volume ensured a 16-fold concentration of the sample, which was necessary to obtain visible chromatographic peaks corresponding to GSH, PC2, PC3, and PC4. For the quantitative analysis, a calibration curve was prepared with 10 different dilution levels in the extraction buffer for the solid matrices, and another curve in B5 solvent for media quantification. Notably, PC3 and PC4 originate from PC2 and are typically difficult to detect due to their low concentrations. Figure 14 summed up the experimental design.

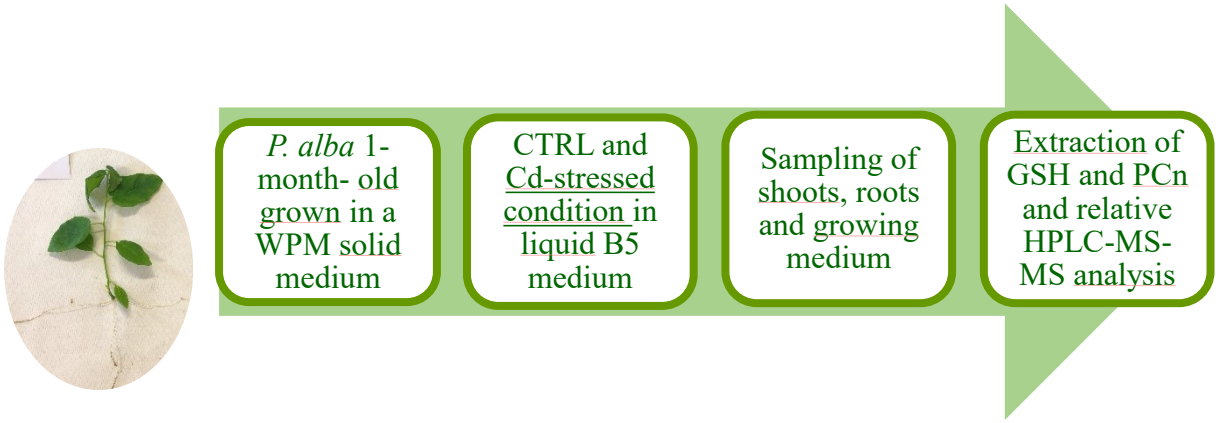


**Figure 14.** Workflow from control *P. alba* plants to $Cd^{2+}$ stressed treatments and subsequent thiol-peptide analysis.

### *3.5.2 Fluorescence and photosynthetic efficiency*

A preliminary evaluation of photosynthetic efficiency on control and $Cd^{2+}$ stressed plants treated in liquid media was performed. Only three plant as control and three plants under 36 µM $Cd^{2+}$ stressed condition were selected. For the measurements each plant was gently transferred into a petri disk containing its treatment medium to maintain the conditions. Two leaves per plant were subjected to the analysis of fluorescence transients. As described in 3.4.2 section, the measurement data were then subjected to the JIP test [222], providing detailed information on the structure and functionality of PSII and the efficiency of photosynthetic electron transport. To perform *in vivo* fluorescence analyses *P.alba* leaves were acclimated to the darkness and then were illuminated for one second with an LED light source that irradiated the plant with saturating light levels at 650 nm by a Handy PEA fluorimeter.

### 3.6 Experimental setup for the inhibition study of thiol-peptides transporters

To further investigate the mechanisms behind GSH and PCn release, potentially mediated by the plasma membrane of poplar root cells, an inhibition study targeting hypothetical (Cd-) thiol-peptide complex transporters was conducted.

The *Populus alba* plants were grown for one month in WPM medium, as described in sections 3.1 and 3.5. Similarly, the plants were gently removed from the solid medium to be treated in the liquid medium. For this study, the selected conditions included a control (0 µM), 20 µM, and 36 µM $Cd^{2+}$, with exposure times of 48 and 72 h. To perform the inhibition study, the same experimental design was repeated, with the addition of an inhibitor molecule to the treatment medium. Specifically, sodium orthovanadate ($Na_3VO_4$, purchased from Sigma-Aldrich, Saint Louis, MO, USA) was selected as the inhibitor due to its tetrahedral ion structure, which is analogous to the phosphorus ion. Indeed, enzymes involved in phosphotransferase or phosphohydrolase reactions could accept vanadate ion as an analog of inorganic phosphate. While vanadate inhibits both P-type ATPases and ABC transporters, glibenclamide has only been demonstrated to inhibit ABC transporters [219,223,224]. Initially, a first inhibition attempt was made using 500 µM of $Na_3VO_4$ according with the literature [219], later extending the study to include 250 µM and 125 µM concentrations. For glibenclamide, a concentration of 100 µM was selected as the inhibition condition based on its use in previous studies reported in the literature [219]. Before distributing the medium into individual tubes, it was important to check the pH to avoid introducing an additional variable to the experiment. The acidity of B5 medium should be adjusted with HCl to reach a pH of approximately 5.86. Figure 15 summarizes all tested conditions: thiol-peptides were evaluated at extracellular and intracellular levels, in CTRL and $Cd^{2+}$ stressed conditions for 48 and 72 h as exposure times.


**Figure 15.** Experimental setup of the inhibition study involving sodium orthovanadate and glibenclamide as inhibitors at different concentrations, and subsequently intracellular and extracellular evaluation of thiol-peptides at several $Cd^{2+}$ stressed condition.

Sample were collected following the Figure 13 procedure to obtain 3 biological replicates for each condition. The extraction of intracellular thiol-peptides was performed as described in section 3.2 and the obtained extracts were injected into HPLC-MS/MS system with 3.3 section methodology. At the same time treatments media were filtered with 0.45 µm filters, lyophilized, 16-fold concentrated, added with glycine-$^{13}C_2$-GSH and glycine-$^{13}C_2$,$^{15}N$-PC2 as internal standards and injected into the HPLC-MS/MS system as well as the tissue extracts.

The quantification of GSH, PC2, PC3 and PC4 was performed by AB Sciex Analyst® version 1.6.3 software.

### 3.7 Experimental setup for cell culture

To better study thiol-peptide release as a defence mechanism against HM stress, immortalized *Arabidopsis thaliana* cells (a model organism) were implicated, under $Cd^{2+}$ stressed and control conditions.

*Arabidopsis thaliana* cells were grown in a sterile suspension culture in 50 mL of Murashige & Skoog Medium (MS, Duchefa, Haarlem, BH, Netherlands) including micro- and macro-nutrients, vitamins, 0.8% agar, and 3% sucrose. Medium pH was measured and adjusted to 5.5, then the medium was autoclaved for 20 min at 120 °C. Before use, alpha-naphthaleneacetic acid (NAA) 0.5 mg/L and kinetin 0.05 mg/L were added to the medium. The suspension culture was weekly split into fresh MS medium. A suspension volume of 5 mL was transferred into a sterile tube and treated with 0, 10, 20 µM $CdSO_4$, as in Figure 16, and incubated in constant shaking for 48h and 72h at 25°C with a photoperiod of 16 hours light / 8 hours dark.

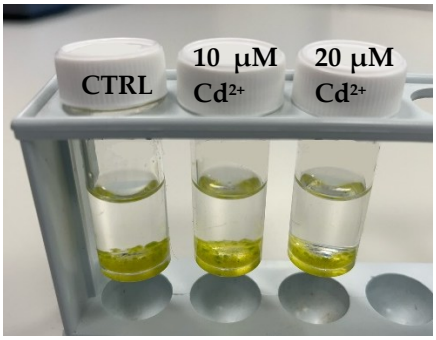


**Figure 16**. *A.thaliana* cell cultures in CTRL condition and under $Cd^{2+}$ stressed conditions.

After the exposure period, each treatment was transferred to a falcon tube and centrifuged for 5 minutes at 1000 rpm. The supernatant was filtered using a 0.20 µm filter, and 700 µL of the medium was lyophilized and resuspended in 28 µL of $H_2O$ containing $^{13}C_2$,$^{15}N$-GSH (final concentration of 200 ng/mL) to achieve a dilution factor of 25. For the evaluation of extracellular release of thiol-peptides, 20 µL of the sample was injected into the HPLC-MS/MS system using the analytical method described in chapter 3.3.

The resulting pellet was weighed, transferred to a 1.5 mL Eppendorf tube, and stored at -80°C for 1 hour to induce a thermal shock. To analyse intracellular thiol-peptides, the extraction buffer (as described in section 3.2) containing GSH as an internal standard (final concentration of 200 ng/mL) was added to resuspend the pellet. The sample was then vortexed and homogenized at 5500 rpm for 20 seconds. The homogenate was centrifuged for 10 min at 14000 rpm at 4 °C and filtered using a 0.45 µm filter to minimize thiol retention.

Various volumes of extraction buffer were tested to identify the optimal ratio for analysis, and a 1:10 ratio (mg of fresh sample weight per mL of extraction buffer) was found to be the most effective. The resulting cell lysate was analysed using HPLC-MS/MS.

### 3.8 Statistical analysis

The data obtained from thiol-peptide quantifications and reported in sections 3.4.3, 3.5, and 3.6 as well as the biometric analysis in subsection 3.4.1 and results of fluorescence and photosynthetic efficiency parameters in subsection 3.4.2 were all subjected to a statistical analysis.

The data analysis was performed using the commercial software GraphPad Prism 9.0.2 (GraphPad Software Inc., San Diego, CA, USA). Specifically, a one-way ANOVA followed by Tukey's multiple comparisons test was applied to analyse significant differences in biometric and photosynthetic efficiency data. Similarly, the comparison of the percentage distribution of shoots, roots, and growth media across the treatments in the inhibition study also utilized one-way ANOVA followed by Tukey's multiple comparisons test. For the evaluation of intracellular and extracellular thiol-peptides, as well as all absolute quantified data from the inhibition study, a two-way ANOVA followed by Tukey's multiple comparisons test was performed, too. Differences were considered significant at $p < 0.05$.

## 4. DISCUSSION AND RESULTS

### 4.1 Pre-analytical extraction method improvement

Several attempts were made to improve extraction efficiency of thiol-peptides, reduce the matrix effect, increase the method accuracy, and prevent the dust deposition inside the instrumentation, which can progressively reduce the instrument sensitivity.
The results confirmed that the use of SPE procedures with WCX, HPL, WAX, and Bond Elute cartridges did not improve the extraction method, also due to the low solid-phase extraction recovery rates of the target analytes that were below 10%, with a significant loss of HPLC-MS/MS signals.

An esterification attempt was made to render the target analytes less polar and thus more easily extractable from the aqueous plant matrix. However, the derivatization reaction involving ethyl ether presented several challenges, primarily regarding reaction completeness, and consequently yield. Specifically, the reaction resulted in the formation of three distinct products, visible in MS: monoesterified, diesterified, and triesterified forms. This limitation led to the exclusion of this approach, since it increased both extraction time and costs, without significant advantages.

Other approaches were explored to improve either selectivity or analyte' extraction efficiency, aimed by a reduction in analytical background noise and potential increase in signal intensity. To this end, various buffer combinations were tested and compared. Table 5 shows the peak areas obtained for each test using HPLC-MS/MS. From these results, it was evident that TCEP performed better than β-mercaptoethanol as a reducing agent for our extraction system. The use of TRIS-HCl or HEPES buffers did not seem to produce significant differences.

To determine the optimal concentration of the reducing agent and prevent rapid oxidation of thiol-peptides, different concentrations of TCEP were tested, as shown in Table 6. Once again, the reported peak areas confirmed that 2 mM, already used in the method described in the literature [218]was the optimal concentration. No significant differences were observed with higher TCEP concentrations, and increasing the amount would only lead to unnecessary material consumption.

| | GSH peak area (counts) | PC2 peak area (counts) | PC3 peak area (counts) | PC4 peak area (counts) |
|---|---|---|---|---|
| TRIS-HCL (10 mM)+ β-mercaptoethanol (20 mM) | 1.42E+07 | 1.66E+05 | 1.39E+04 | NA |
| HEPES (10 mM)+ β-mercaptoethanol (20 mM) | 1.61E+07 | 1.9E+05 | 2.27E+04 | NA |
| TRIS-HCL (10 mM)+ TCEP (20 mM) | 3.85E+07 | 7.94E+05 | 5.29E+04 | 3.26E+04 |
| TRIS-HCL (10 mM)+ TCEP (20 mM) | 3.36E+07 | 6.39E+05 | 3.39E+04 | 2.29E+04 |

**Table 5.** Attempts to modify the extraction buffer: involvement of β-mercaptoethanol or TCEP in TRIS HCl or HEPES solution: comparison between peak areas obtained by HPLC-MS/MS analysis and quantification. (NA = not available peak area).

| | GSH peak area (counts) | PC2 peak area (counts) | PC3 peak area (counts) | PC4 peak area (counts) |
|---|---|---|---|---|
| TRIS-HCL (10mM)+ TCEP (2 mM) | 2.49E+07 | 6.77E+05 | 2.58E+04 | 1.58E+04 |
| TRIS-HCL (10mM)+ TCEP (5 mM) | 1.78E+07 | 6.76E+05 | 2.80E+04 | 1.15E+04 |
| TRIS-HCL (10 mM)+ TCEP (10 mM) | 1.19E+07 | 5.71E+05 | 2.43E+04 | 1.23E+05 |
| TRIS-HCL (10 mM)+ TCEP (20 mM) | 8.27E+06 | 6.26E+05 | 2.31E+04 | 1.04E+04 |

**Table 6.** Attempts to modify the extraction buffer: the comprehension of right TCEP concentration.

To determine whether the use of TRIS HCl provided any advantages over the initial buffer and to understand the differences in using varying amounts of buffer, several trials derived from the same matrix pool were compared: four trials of 50 mg (A, B, C, D) were extracted using the standard aqueous buffer and four (E, F, G, H) using TRIS HCl. All buffers were

supplemented with TCEP (2 mM) and DTPA (6.3 mM). The results showed that while both buffer systems produced signals of similar magnitude, the trials using the standard buffer (A, B, C, D) yielded slightly more intense peaks. Therefore, the classic buffer described in the literature [218] proved to be the better choice.

Regarding the amount of buffer, different ratios of sample fresh weight (mg FW) to buffer volume (µL) were tested: 1:3 (A), 1:6 (B), 1:10 (C), and 1:20 (D). Additionally, the effect of one versus two washing steps was evaluated. As shown in Table 7, using a larger buffer volume resulted in an increased signal, likely due to better extraction of thiol-peptides or, at the very least, a reduction in matrix effects because of the greater dilution. At the same time, in terms of quantification, the addition of an extra washing step did not significantly enhance the signal but visibly improved the sample's clarity and transparency. This allowed for the injection of cleaner samples, thereby optimizing the performance and maintenance of the HPLC-MS/MS system.

| | **GSH (nmol/gFW)** | **PC2 (nmol/gFW)** | **PC3 (nmol/gFW)** | **PC4 (nmol/gFW)** |
|---|---|---|---|---|
| D 2 washing steps | 15.06 | 19.96 | 13.96 | 3.92 |
| C 2 washing steps | 9.19 | 9.65 | 6.75 | 1.52 |
| B 2 washing steps | 5.41 | 6.47 | 4.52 | 0.99 |
| A 2 washing steps | 2.41 | 6.72 | 4.50 | 1.11 |
| D 1 washing step | 15.77 | 19 | 13.29 | 3.17 |
| C 1 washing step | 9.67 | 9.96 | 6.97 | 1.8 |
| B 1 washing step | 5.39 | 6.69 | 4.68 | 1.13 |
| A 1 washing step | 2.45 | 4.78 | 3.34 | 0.59 |
| D | 9.48 | 15.55 | 10.88 | 2.83 |
| C | 5.84 | 5.87 | 4.11 | 1.03 |
| B | 4.54 | 5.55 | 3.89 | 1.02 |
| A | 2.8 | 4.49 | 3.14 | 0.67 |

**Table 7.** Comparison of peak areas obtained from the extraction of *P.alba* pool matrix using different ratios of sample fresh weight (mg FW) to buffer volume, along with the effect of 0, 1, or 2 washing steps.

To establish the importance of washing steps as a confirmed part of the extraction procedure, it was necessary to evaluate their impact on analytical recovery. The analytical procedure applied prior to the washing steps had already been assessed by Bellini et al. 2019 [218], who compared the peak areas of internal standards spiked before and after extraction. In shoot extracts, the recovery rates were 91.02% for glycine-$^{13}C_2$,$^{15}N$-labelled GSH and 83.90% for glycine-$^{13}C_2$,$^{15}N$-labelled PC2. In root extracts, recovery rates were 73.78% for glycine-$^{13}C_2$,$^{15}N$-labelled GSH and 88.96% for glycine-$^{13}C_2$,$^{15}N$-labelled PC2.

To further evaluate the washing steps, analytical results for treatments A, B, C, and D (described in Table 7) were compared using a pooled matrix of shoot and root extracts of *P.alba* plants spiked with 200 ng/mL of labeled internal standards. The samples were subjected to either no washing, one washing step, or two washing steps. The ratio between the peak areas of washed and unwashed samples is shown in Table 8. The results showed that recovery of thiol-peptides was approximately 80% after one washing step. With an additional washing step, the clarity of the extract noticeably improved, and recovery remained around 60–70%, confirming that these additional cleaning steps can be safely incorporated into the extraction procedure without significant loss of analyte.

| | **GSH-IS peak area** | **washed sample/not washed ratio %** | **PC2-IS peak area** | **washed sample/not washed ratio %** |
|---|---|---|---|---|
| D | 1.26E+06 | | 1.17E+05 | |
| D 1 washing step | 9.66E+05 | 76.67 | 8.81E+04 | 75.30 |
| D 2 washing steps | 7.60E+05 | 60.32 | 7.45E+04 | 63.68 |
| C | 1.43E+06 | | 1.27E+05 | |
| C 1 washing step | 1.22E+06 | 85.31 | 7.59E+04 | 59.76 |
| C 2 washing steps | 1.00E+06 | 69.93 | 7.70E+04 | 60.63 |
| B | 1.94E+06 | | 9.22E+04 | |
| B 1 washing step | 1.65E+06 | 85.05 | 9.85E+04 | 106.83 |
| B 2 washing steps | 1.30E+06 | 67.01 | 5.40E+04 | 58.57 |
| A | 1.72E+06 | | 4.69E+04 | |
| A 1 washing step | 1.39E+06 | 80.81 | 4.42E+04 | 94.24 |
| A 2 washing steps | 1.06E+06 | 61.63 | 3.22E+04 | 68.66 |

**Table 8.** Labeled-Internal standards Peak area obtained from HPLC-MS/MS analysis of pool-matrix *P.alba* extracts subjected to either no washing, one washing step, or two washing steps. Percentage of peak area ratio between not washed or washed samples were reported.

## 4.2 *Populus alba* response under $Cd^{2+}$ high stressed condition

### *4.2.1 Biometric analysis*

*Populus alba* seedlings were harvested two months after the start of the Cd treatment in order to measure biometric parameters. The effects of exposure to 50 µM and 100 µM $Cd^{2+}$ on seedling growth were examined using a number of growth indicators, such as leaf area, stem length, root length, leaf number, and dry weight percentage.

No significant differences were observed across treatments for any of the measured parameters. plants exposed to 50 µM $Cd^{2+}$ showed a slightly larger leaf area of 2.1 $cm^2$ (Figure 17A), while plants exposed to both concentrations of Cd showed a stem length of 5.8 cm in control plants and decreased to 5 cm in plants exposed to both concentrations of Cd (Figure 17B). At both Cd concentrations, the treated plants' root length rose marginally to 5.2 cm from the control plants' 4.6 cm (Figure 17C). The number of leaves dropped from 10 in the control group to 8 in both Cd-treated groups (Figure 17D). Lastly, the percentage of dry matter was 15% in controls, remained nearly constant at 16% in plants treated with 50 µM $Cd^{2+}$, but dropped to 11% in those treated with 100 µM $Cd^{2+}$ (Figure 17E).

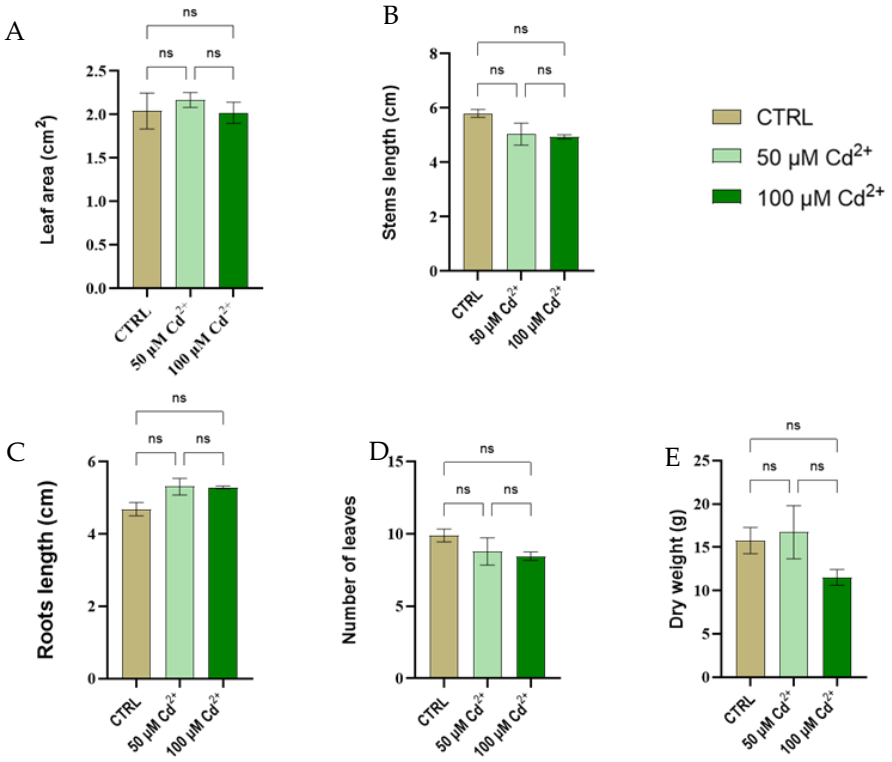


**Figure 17.** Leaf area (A), stems length (B), roots length (C), number of leaves per plant (D), and dry matter (E) measured in *P. alba* samples treated with 0 (CTRL), 50, and 100 µM $Cd^{2+}$. Values are presented as mean ± SE. The abbreviation "ns" indicates no significant differences between different concentrations and organs (one-way ANOVA followed by Tukey's test, $p < 0.05$).

In conclusion, the exposure to 50 µM and 100 µM $Cd^{2+}$ did not result in significant alterations to growth parameters under the experimental conditions. However, slight changes in specific indicators, such as a reduction in root length and dry matter content, may suggest early-stage physiological responses to Cd stress that do not yet impact overall growth. This indicates that *P. alba* exhibits a certain level of tolerance to moderate Cd exposure over the time as reported in previous studies [119,183]. The absence of toxic effects could be attributed to the plant's ability to detoxify Cd. As reported by Di Lonardo et al. 2011 [119], the concentration of Cd in the shoots exceeded levels generally considered toxic for plants. Based on the lack of significant effects from our treatments, the results suggest that poplars may tolerate and accumulate high levels of HMs without adverse effects.

### *4.2.2 Fluorescence and photosynthetic efficiency*

In order to observe the photochemical efficiency variation in relation to physical conditions, the *in vivo* analysis of fluorescence is conducted after treatment with Cd. The analysis of transient fluorescence stages (OJIP transients) is commonly used to evaluate the efficiency of photosynthesis. Following results were obtained following the JIP test [222], a method that allows the calculation of numerous parameters and provides detailed insights into the composition and functionality of PSII, as well as the efficiency of the photosynthetic electron transport chain.

The Handy-PEA fluorimeter recorded parameters categorized into fluorescence technical parameters, energy flux parameters, and specific energy flux parameters related to each reaction center, summarized in Table 9.

| **Fluorescence Technical Parameters** | |
|---|---|
| **Parameter** | **Meaning** |
| FV = FM – FO | Maximum variable fluorescence |
| Vt = (Ft – FO) / FV | Relative variable fluorescence |
| M0 = (ΔV/Δt)0 ≈ 4(F0.3ms – F0.05ms) / FV | Initial slope (in $ms^{-1}$) of the fluorescence rise in the O-J phase |
| **Specific Energy Fluxes (per active PSII)** | |
| **Parameter** | **Meaning** |
| ABS/RC = (M0/VJ)/φP0 | Apparent antenna size per active PSII |

| | |
|---|---|
| TR0/RC = M0/VJ | Maximum exciton flux captured per active PSII |
| ET0/RC = (M0/VJ)/φE0 | Electron flux transferred from $QA^-$ to PQ per active PSII |
| RE0/RC = (M0/VJ)/φR0 | Electron flux transferred from $QA^-$ to the final acceptors of PSI per active PSII |
| DI0/RC = ABS/RC – TR0/RC | Energy flux dissipated in processes other than electron capture per active PSII |
| **Phenomenological Energy Fluxes (per CS - cross-section)** | |
| **Parameter** | **Meaning** |
| ABS/CS0 ≈ FO and ABS/CSM ≈ FM | Photon flux absorbed (CS) per leaf analysed |
| TR0/CS = (TR0/ABS) × (ABS/CS) | Maximum exciton flux captured per leaf analysed |
| ET0/CS = (ET0/ABS) × (ABS/CS) | Electron flux from $QA^-$ to PQ per leaf analysed |
| RE0/CS = (RE0/ABS) × (ABS/CS) | Electron flux from $QA^-$ to the final acceptors of PSI per leaf analysed |
| RC/CS = (RC/ABS) × (ABS/CS) | Number of active PSII reaction centers per leaf analysed |
| ABS/CS0 ≈ FO and ABS/CSM ≈ FM | Photon flux absorbed (CS) per leaf analysed |

**Table 9.** Specific energy and phenomenological energy fluxes parameters and fluorescence technical parameters, evaluated for the fluorescence and photosynthetic efficiency.

The data obtained did not reveal any significant statistical differences across the experimental conditions as shown in Figure 18.

Once again the plant's capacity to store and detoxify Cd may be the reason for the lack of harmful consequences. Previous studies on poplar plants exposed to Cd have demonstrated that proteins involved in the Calvin cycle and light-dependent photosynthetic reactions were significantly affected by short-term Cd treatment (≤14 days). However, the impact of Cd on photosynthesis and the abundance of Calvin cycle proteins was less pronounced under long-term exposure (up to 56 days) [192]. These findings suggest that poplars may have the ability to adapt to Cd over extended periods, mitigating the negative effects on growth and photosynthesis.

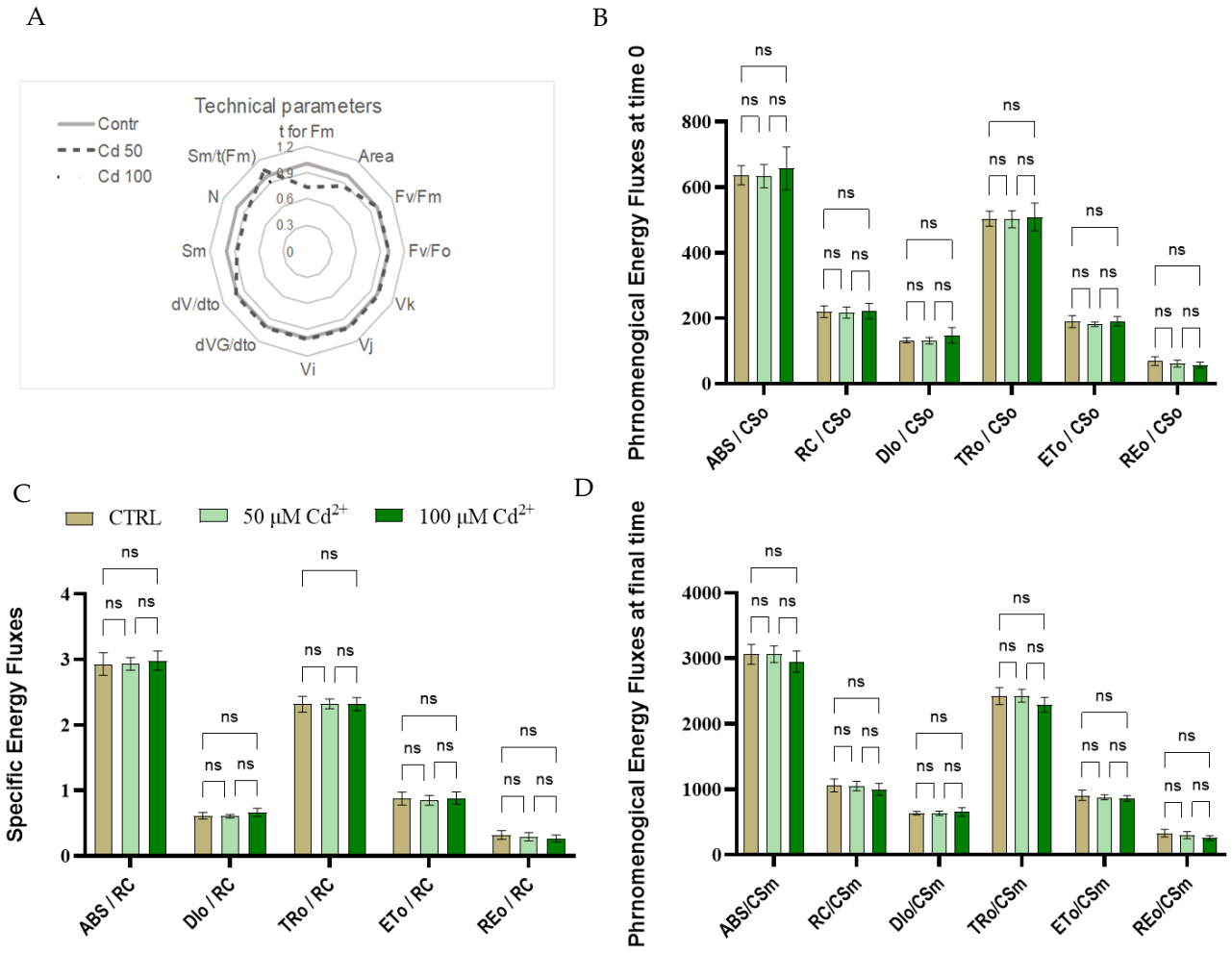


**Figure 18.** JIP-test parameters performed on *P. alba* samples treated with 0 (CTRL), 50, and 100 µM $Cd^{2+}$: technical parameters (A), phenomenological energy fluxes at time 0 (B), specific energy fluxes (C), and phenomenological energy fluxes at the final time (D). Values are presented as mean ± SE. The abbreviation "ns" indicates no significant differences between different concentrations and organs (one-way ANOVA followed by Tukey's test, $p < 0.05$).

### *4.2.3 Intracellular thiol-peptides quantification*

Upon entering the cytosol, $Cd^{2+}$ ions are chelated by thiol-peptides, such as PCn, to mitigate their toxic effects [225]. To explore the role of the PCS enzyme and the PCn it generates in Cd detoxification, the qualitative and quantitative levels of PCn and GSH were assessed. To perform this thiol-peptides analysis, samples from the three organs (leaves, stems, and roots) of *Populus alba* were extracted and analysed by HPLC-ESI-MS/MS method explained in 3.3 section. Figure 19 shows the reference chromatographic run of analytes solution concentrated 500 ng/mL.

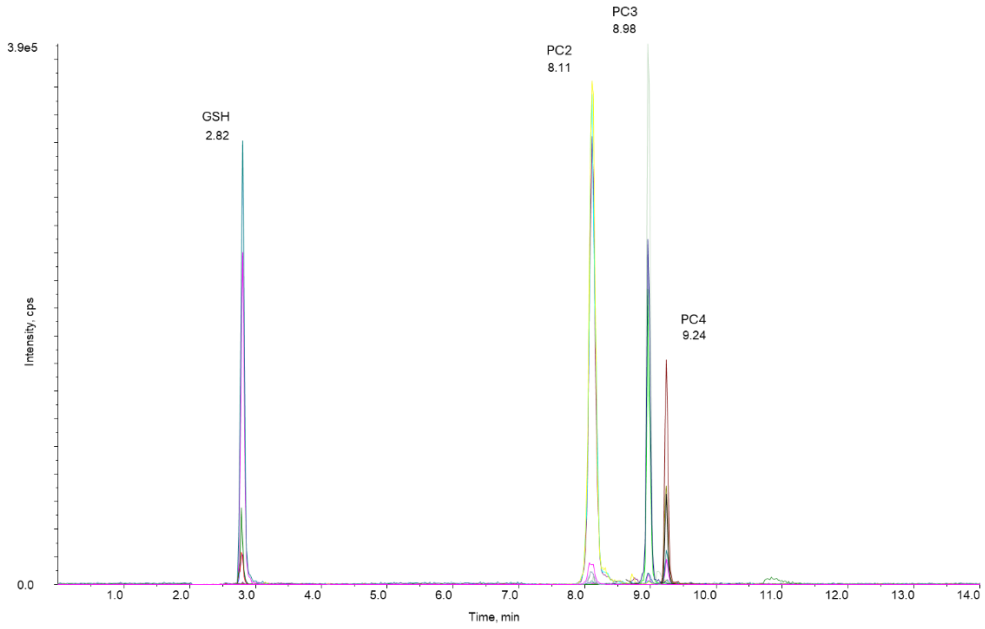


**Figure 19.** Chromatogram of standard mixture (500 ng/mL) of GSH, PC2, PC3, PC4 analytes in extraction buffer.

Referring to intracellular GSH (Figure 20), in both leaves and stems, its concentration was around 5 nmol/g FW without significant differences among the various conditions. However, in roots, a significant increase in intracellular GSH was observed with increasing Cd concentrations. The GSH concentration rose from 5 nmol/g FW in the controls to a maximum of approximately 12 nmol/g FW in samples treated with 100 µM $Cd^{2+}$.

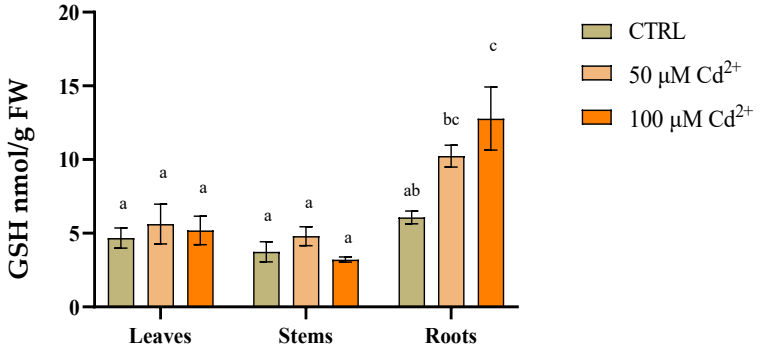


**Figure 20.** Intracellular GSH content in the three organs (leaves, stems, and roots) of *P. alba* samples treated with 0 (CTRL), 50, and 100 µM $Cd^{2+}$, expressed as nmol/g FW. Values are presented as mean ± SE. Different letters indicate significant differences between different concentrations and organs (two-way ANOVA followed by Tukey's test, $p < 0.05$).

The data obtained from the analysis of total intracellular PCn (Figure 21) showed no significant differences in the leaves among control samples, which had a concentration of 1 nmol/g FW, samples treated with 50 µM $Cd^{2+}$ (5 nmol/g FW), and those treated with 100 µM $Cd^{2+}$ (13 nmol/g FW). In the stems, there were no differences between the control samples and those treated with 50 µM $Cd^{2+}$, which reached concentrations of 2 nmol/g FW and 12 nmol/g FW, respectively. However, a significant increase was observed in samples treated with 100 µM $Cd^{2+}$, reaching a concentration of 25 nmol/g FW. Finally, roots did not showed significant differences in terms of total PCn between control samples and those treated with 50 µM $Cd^{2+}$, which reached concentrations of 3 nmol/g FW and 14 nmol/g FW, respectively. A notable increase was observed in samples exposed to 100 µM $Cd^{2+}$, with concentrations rising to 90 nmol/g FW.

It is noteworthy that the increase in total intracellular PCn was primarily attributed to the production of PC2 across all Cd treatments, while PC3 and PC4 contributed only marginally. Specifically, PC2 was the only PCn detected in the controls, with concentrations of 0.5 nmol/g FW in leaves, 1 nmol/g FW in stems, and 2 nmol/g FW in roots. Samples treated with 50 µM $Cd^{2+}$ reached concentrations of approximately 4 nmol/g FW in leaves and 10 nmol/g FW in stems and roots. The concentration of PC2 significantly increased in all three organs in samples treated with 100 µM $Cd^{2+}$, reaching approximately 15 nmol/g FW in leaves, 17 nmol/g FW in stems, and 34 nmol/g FW in roots. PC3 and PC4 generally exhibited lower concentrations than PC2, and were absent in the controls of all three organs. With 50 µM $Cd^{2+}$, PC3 and PC4 levels were low, ranging from 0.5 to 2.5 nmol/g FW across tissues. At 100 µM $Cd^{2+}$, PC3 rose to 2, 7, and 18 nmol/g FW in leaves, stems, and roots, respectively, while PC4 reached 2 and 6 nmol/g FW in leaves and stems, and 38 nmol/g FW in roots.

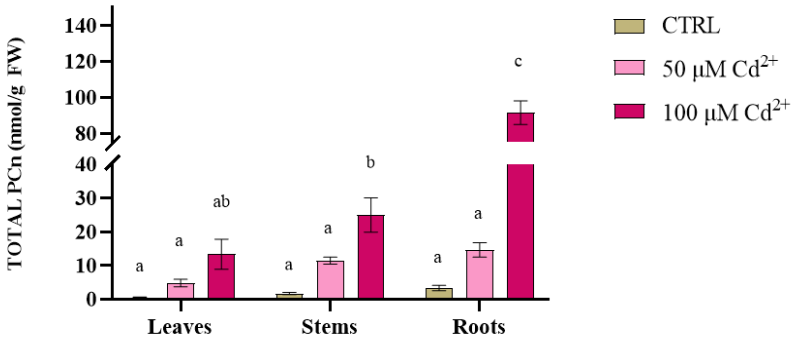


**Figure 21.**Total intracellular PCn content in the three organs (leaves, stems, and roots) of *P. alba* samples treated with 0 (CTRL), 50, and 100 µM $Cd^{2+}$, expressed as nmol/g FW. Values are reported as mean ± SE. Different letters indicate significant differences between different concentrations and organs (two-way ANOVA followed by Tukey's test, $p < 0.05$).

The results reveal an increase in total PCn production in stems and roots treated with 100 µM $Cd^{2+}$, with PC2 being the most prevalent, alongside lower levels of PC3 and PC4. Notably, even under control conditions, PC2 was synthesized, suggesting a constitutive role for PCS as previously proposed by Degola et al. 2014 [80]. In contrast, PC3 and PC4 were absent in controls but increased under higher Cd stress, likely reflecting their enhanced chelating efficiency due to more thiol groups, as reported by Kneer and Zenk 1997 [226]. In studies conducted on the model organism *A. thaliana*, data suggest that PCn overproduction may provide an advantage in tolerating high Cd concentrations, especially when the initial levels of PCn are insufficient to sequester all the available Cd. Consistently, we also observe in *P.alba* an increase in PCn levels with higher Cd exposure in our experiments. This upward trend in PCn synthesis in roots is further supported by a study conducted by Di Lonardo et al. 2011 [119], which investigated three clones of *P. alba*. The findings revealed that roots were significantly more affected by metal toxicity than shoots highlighting the critical role of PCn in root tissues under Cd stress. An increase in PCn levels in the roots suggests a correspondingly higher concentration of Cd in these tissues. This indicates that *P. alba* may employ a metal exclusion or non-translocation strategy, retaining Cd within the roots to prevent its movement to stems and reproductive tissues. In conclusion, the findings highlight the adaptability of *Populus alba* to Cd stress, with differential PCn production reflecting the plant's strategic response to varying levels of HM toxicity. This underscores the importance of PCn diversity in enhancing the plant's tolerance to Cd.

## 4.3 *Populus alba* under $Cd^{2+}$ short-term and lower stressed condition: role of thiol-peptides

An experimental setup was designed to explore the potential role of thiol-peptides under Cd-lower stressed conditions. In detail, based on our previous research conducted on different plant species (Appendix), this study aims to investigate whether thiol-peptides could contribute to extracellular detoxification as well as in the intracellular one.

### *4.3.1 Intracellular content and extracellular release of thiol- peptides in* Populus alba

Shoots showed an increased content of GSH as the increasing concentration of Cd, at least after 24 and 48 h. On the contrary, after 72 h of treatment the presence of GSH did not exhibit any significant increment with the increasing of Cd concentration. The GSH levels in shoots showed a significant increase when comparing treatments with $Cd^{2+}$ at 24 h versus 48 h particularly regarding 36 µM $Cd^{2+}$ and 10 µM $Cd^{2+}$ ($p< 0.001$) concentrations and at significant decrease at 24h and 48 h versus 72 h, specifically at higher concentrations of 20-36 µM $Cd^{2+}$ (Figure 22A). These results are reminiscent of trends in other species studied and cited by Bellini et al. [85,227] suggesting the usage of GSH as a direct ligand for Cd sequestration, in addition to as a precursor for PCn synthesis.

In roots, intracellular GSH levels demonstrated a moderate increase with higher Cd concentrations and prolonged exposure times, as shown in Figure 22B. The most notable differences were observed when comparing 24 h and 72 h exposures: under 36 µM $Cd^{2+}$, a more pronounced increase was recorded, from 19.02 to 37.40 nmol/g FW.

Regarding the extracellular response, a progressive upward trend in GSH levels was observed over time. Specifically, the 36 µM $Cd^{2+}$ treatment showed a significant difference between 24 h versus 48–72 h of exposure, with GSH levels increasing from 13.3 nmol/g FW to 29.8 nmol/g FW, reaching 33.58 nmol/g FW over time (Figure 22C). The FW considered for the extracellular evaluation is the fresh weight of the corresponding root system inside each medium.

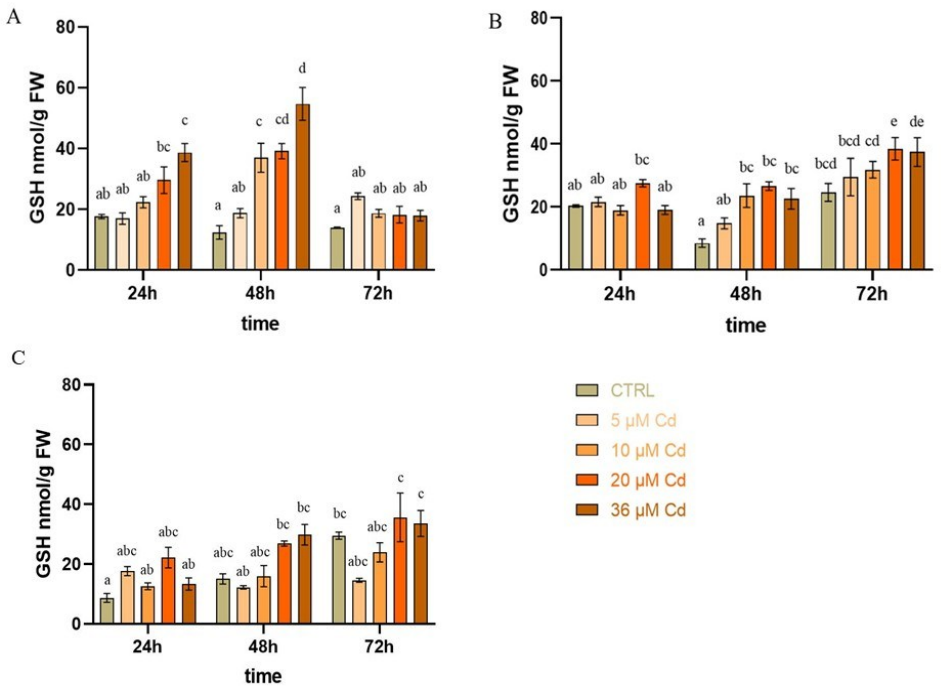


**Figure 22.** Intracellular content in shoots (A) and roots (B) and extracellular presence (C) of GSH at 0 (CTRL), 5,10, 20, 36 µM $Cd^{2+}$ after 24-48-72 h as exposure times. Values are means ± SE (n = 3). Different letters indicate significant differences (two-way ANOVA followed by Tukey's test, $p < 0.05$).

The intracellular/extracellular ratio was assessed to analyse the relationship between the synthesis and release of GSH under varying $Cd^{2+}$ concentrations over time. The ratio suggests that the magnitude of intracellular and extracellular levels remains consistent, indicating that the quantity released extracellularly is substantial and noteworthy (Table 10).

| | ***CTRL*** | ***5uM $Cd^{2+}$*** | ***10 uM $Cd^{2+}$*** | ***20 uM $Cd^{2+}$*** | ***36uM $Cd^{2+}$*** |
|---|---|---|---|---|---|
| ***24h*** | 2.32 | 1.27 | 1.42 | 1.24 | 1.42 |
| ***48h*** | 0.59 | 1.30 | 1.61 | 0.98 | 0.75 |
| ***72h*** | 0.83 | 2.72 | 1.53 | 1.19 | 1.11 |

**Table 10.** Intracellular/extracellular GSH ratio calculated for each treatment.

Concerning the analytical evaluation of intracellular PCn, Figure 23 A shows a general increase in nmol/g FW in shoots associated with 20 and 36 µM $Cd^{2+}$ concentrations over time. Focusing on a single time point, after 72 hours, exposure to 36 µM $Cd^{2+}$ results in a significant PCn content, reaching up to 5.7 nmol/g FW. Regarding PCn in roots and specifically PC2, an augmented presence was underlined at 20 and 36 µM $Cd^{2+}$ stressed conditions comparing 24 h vs 48 h and 72 h treatments. The 20 µM $Cd^{2+}$ treatment caused a time-dependent increase in PCn levels, rising from 12.6 nmol/g FW at 24 h to 23.5 nmol/g FW at 48 h, and ultimately reaching 34.0 nmol/g FW at 72 h. Similarly, the 36 µM $Cd^{2+}$ treatment led to significant increases, starting from 18.6 nmol/g FW at 24 h, climbing to 38.8 nmol/g FW at 48h, and reaching a peak of 65.6 nmol/g FW at 72 h. Results also spotlighted in roots a significant increase of PCn between 20-36 µM $Cd^{2+}$ groups, both at 48 h and 72 h timepoints ($p < 0.0001$). Comparing the effects of different Cd concentrations within the same time point, it was observed that after 24 h, only the treatments with the highest Cd concentrations showed significant differences compared to the control. In contrast, after 48 and 72 h , more significant differences emerged—not only between the controls and the treatments but also among the different $Cd^{2+}$ concentrations (Figure 23B).

At the extracellular level, the extrusion of PCn became significant when comparing 24 h or 48h treatments to the 72 h treatment. After 72 h, the increase in PCn was clear, with significant differences observed among the treatments under varying $Cd^{2+}$ stress levels (Figure 23 C).PCn level after 72 hours starts at approximately 2 nmol/g FW in the CTRL and 5 µM Cd treatments, reaching 4.26 nmol/g FW in the 20 µM Cd treatment and 6.25 nmol/g FW at the highest Cd concentration of 36 µM."

It is important to highlight that the total PCn values were calculated as the sum of PC2, PC3, and PC4, with PC2 having the greatest weight in the calculation. PCn with a higher degree of polymerization may be more efficient under high-intensity Cd stress due to the greater number of thiol groups in their structure, which provides these peptides with a stronger metal-chelating capacity [226]. Indeed, as demonstrated by our results, higher Cd concentrations led to an increase in PC3 and PC4 levels, which were absent in the control. In our experiments, PC3 and PC4 are absent not only in the CTRL treatments but also in shoots $Cd^{2+}$ treated, confirming a higher synthesis of these oligomers in roots than in shoots. Figure 24 shows the roots intracellular PC2-3-4 distribution and the relative extracellular medium concentration.

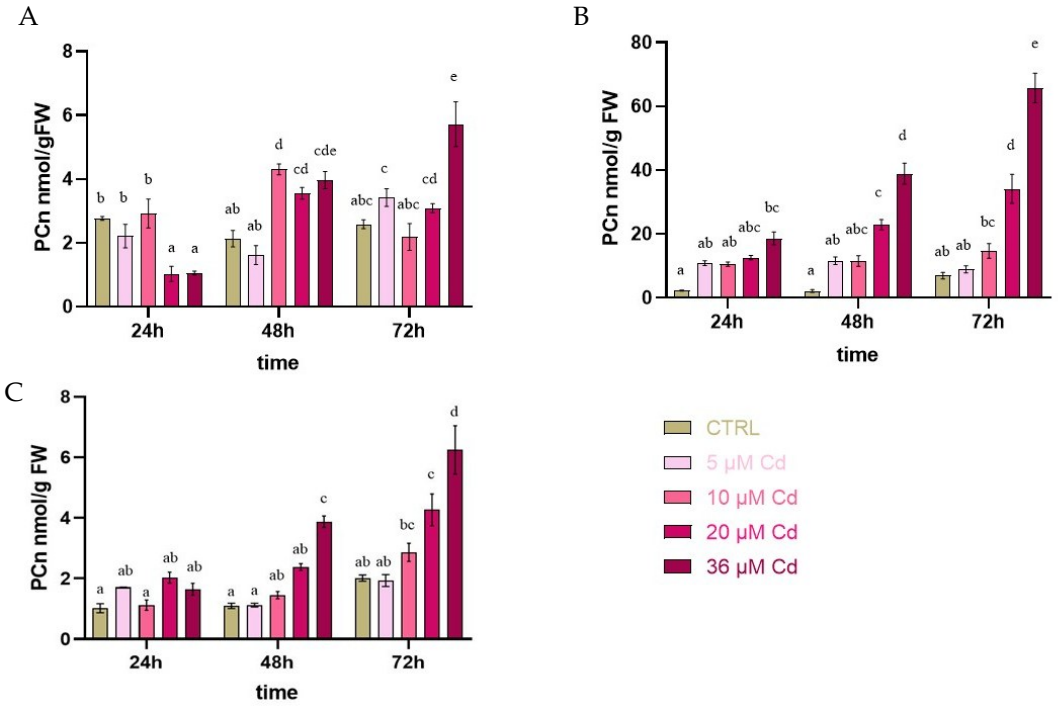


**Figure 23.** Intracellular content in shoots (A) and roots (B) and extracellular presence (C) of PCn at 0 (CTRL), 5,10, 20, 36 µM $Cd^{2+}$ after 24-48-72 h as exposure times. Values are means ± SE (n = 3). Different letters indicate significant differences (two-way ANOVA followed by Tukey's test, $p < 0.05$).

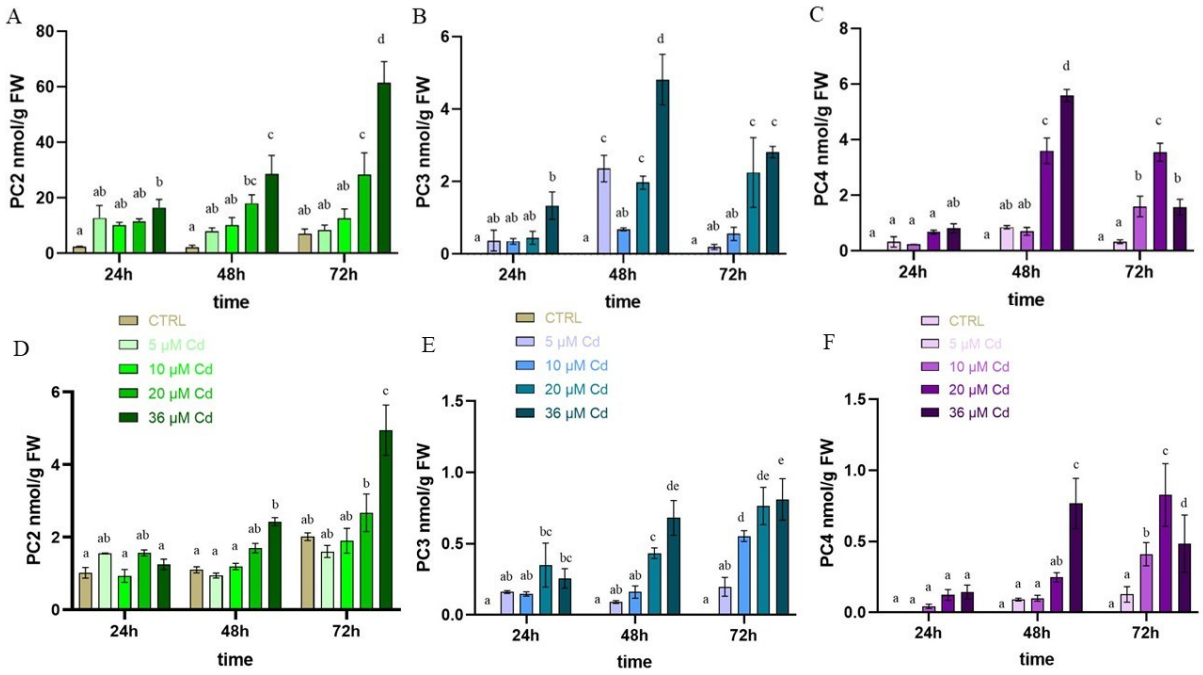


**Figure 24**. Intracellular (in roots, A, B, C) and extracellular (D, E, F) phytochelatin oligomers PC2-3-4 (nmol/g FW) at 0 (CTRL), 5,10, 20, 36 µM $Cd^{2+}$ stressed condition, after 24-48-72 h as exposure times. Values are reported as mean ± SE (n = 3). Different letters indicate significant differences (two-way ANOVA followed by Tukey's test, $p < 0.05$).

The intracellular/extracellular ratio was analysed for PCn amount as well. The results indicate that the proportion between intracellular and extracellular levels remains quite stable, highlighting that the amount released into the extracellular space is significant and relevant for further investigation.

| | ***CTRL*** | ***5uM $Cd^{2+}$*** | ***10 uM $Cd^{2+}$*** | ***20 uM $Cd^{2+}$*** | ***36uM $Cd^{2+}$*** |
|---|---|---|---|---|---|
| ***24h*** | 2.23 | 7.82 | 9.49 | 6.21 | 11.32 |
| ***48h*** | 1.97 | 10.39 | 7.96 | 9.90 | 10.04 |
| ***72h*** | 3.43 | 4.62 | 5.12 | 8.00 | 10.50 |

**Table 11.** Intracellular/extracellular PCn ratio calculated for each treatment.

The results obtained in this study align closely with existing literature, highlighting the correlation between increased Cd concentration in the treatment medium and a corresponding rise in intracellular Cd levels. For instance, Dai et al. 2013 [228] investigated the effects of Cd exposure on growth and GSH content in *Populus* × *canescens* plants treated with 0, 10, 30, and 70 μM $CdSO_4$. Their findings revealed that Cd accumulation increased proportionally with external Cd concentrations, with roots showing significantly higher Cd levels compared to bark, wood, and leaves. Notably, Cd exposure led to a marked decline in GSH content across tissues, alongside a proportional increase in PCn synthesis. This trend was particularly pronounced in roots, where PCn production was consistently higher than in other tissues. These data collectively suggest that Cd in *Populus* × *canescens* roots predominantly exists in the form of Cd-PCn complexes. Similarly, studies on hydroponically grown *Populus* × *euramericana cv. 'Neva'* and *Populus nigra* × *Populus ussuriensis* under Cd stress conditions demonstrated significant increases in Cd content in roots, shoots, bark, and wood with rising Cd concentrations [229]. This trend mirrors our findings in *P. alba*, although the low Cd transfer from roots to shoots observed in these studies—and in our experiments—may be attributed to the short duration of the metal exposure [230]. Likewise, in our *P. alba* liquid treatment experiments, a limited exposure time appeared insufficient to enable substantial metal accumulation in aerial plant parts. This interpretation aligns with our observation of lower PCn accumulation in shoots, further supporting the hypothesis of restricted Cd translocation to aboveground tissues.

This observation in *P. alba* parallels findings in other plants with high Cd tolerance. For instance, in Indian mustard (*Brassica juncea L. Czern*.), Cd exposure significantly increased GSH content, likely replenishing the pool used for PCn synthesis. GSH levels rose markedly in both roots and shoots under Cd stress, while $Cd^{2+}$-stressed tissues contained PC2, PC3, and PC4 oligomers. However, the relative amounts of these oligomers differed between organs. Similarly to our findings in *P. alba*, Cd exposure in *B. juncea* led to a generalized increase in all PCn oligomers, corroborating previously reported trends for GSH and total PCn production [231]. Bellini et al. 2023 [72] further demonstrated that Cd exposure activates the constitutively expressed PCS enzyme, driving a significant increase in PCn synthesis and concurrently enhancing GSH levels. This suggests that GSH synthesis exceeds its consumption for PCn production, allowing it to support additional detoxification pathways [72,232,233]. These findings underline the dual functionality of GSH in maintaining cellular homeostasis while contributing to Cd detoxification.

Concerning the extracellular release of thiol-peptides, our findings align with studies on the liverwort *M. polymorpha*. In this model, both GSH and PCn have been shown to chelate Cd in the cytosol, enabling its detoxification through vacuolar sequestration, likely mediated by tonoplast transporters of the type-C ABC subfamily. Notably, Cd, GSH, and PCn were also detected extracellularly, pointing to a potential novel role for these molecules in Cd detoxification via a pH-dependent mechanism. This dual role—facilitating intracellular detoxification while also contributing to extracellular metal handling—broadens our understanding of the multifaceted functions of GSH and PCn in metal stress responses [72].

The present study builds on this foundation, proposing a new hypothesis regarding thiol-peptides as both intracellular and extracellular detoxifying agents. Extensive studies on GSH-$Cd^{2+}$ complexes have illustrated the highly dynamic coordination chemistry of GSH and PCn [234–236]. Supporting this hypothesis, research on white lupin (*Lupinus albus*) revealed a diverse array of PCn variants enriched in the exudates of arsenic-treated plants, suggesting the deployment of detoxification metabolites directly into the rhizosphere. Intracellularly, arsenic detoxification in plants primarily involves the formation of As(III)-PC complexes [237]. Furthermore, there is evidence that As(III)-$(PC_2)_2$ complexes are released from roots, providing a mechanism for arsenic exclusion akin to vacuolar sequestration.

Together, these findings strongly support the hypothesis that thiol-peptides serve as dual-function detoxifying agents, mediating both intracellular compartmentalization and

extracellular expulsion of metal complexes. This dual role highlights the versatility of thiol-peptides in enabling plants to tolerate and adapt to HM stress in diverse environmental contexts. Thus, both in bryophytes and in tracheophytes, an intriguing new role played by thiol-peptides as intracellular and extracellular Cd-detoxifying agents, might now be assumed. Future studies will concentrate on the complex path through the plasma membrane, particularly on metal-thiol transporter inhibition mechanisms. Overall, these studies could help us understand the main mechanisms underpinning various phytomonitoring technique, and accordingly help improve them from an applied standpoint as well.

An analytical consideration must be highlighted among the obtained results. The HPLC-MS/MS analysis is influenced by the sample matrix, which explains the differences observed between intracellular and extracellular evaluations, even at the methodological level. Specifically, one key factor to keep in mind during the identification of analyte peaks and their corresponding areas under the curve is the retention time shift observed when comparing HPLC-MS/MS injections of shoot-root extracts with those of the treatment medium. Particularly, GSH shows a $t_R$ of 2.81 minutes related to the injected buffer for the intracellular evaluation, which shifts to 2.36 minutes when analysing the medium. Similarly, the PCn also exhibit retention time shifts: PC2 $t_R$ changed from 8.11 to 7.72 minutes.

Furthermore, a preliminary experiment to study the photosynthetic efficiency and fluorescence was also perform on a few group of CTRL and 36 µM $Cd^{2+}$ under 72h exposure time. These preliminary data suggests that low concentrations of $Cd^{2+}$ may have positive effects on poplar plantlets. A treatment with 36 µM $Cd^{2+}$ for 72 h positively influenced the light reactions of photosynthesis, as shown by the analysis of fast fluorescence transients (OJIP) in dark-acclimated leaves. The elaboration of the data by the JIP test [222] yielded the results that are summarized in Figure 25 reporting the parameters that were significant different between treated and control plants. Apparently, the treated plants exhibited a higher content of the primary quinone acceptor QA (as suggested by the greater Area and FM values). The parameters that are referred to CS (both $CS_O$ and $CS_M$) are the phenomenological energy fluxes and provide information on the energy fluxes per excited cross section of PSII. Their overall increase in treated plants demonstrated that $Cd^{2+}$ enhanced the flow of energy through the whole photosynthetic electron transport chain. This may be the reason of the higher value of $PI_{ABS}$, a parameter that expresses the potential for energy conservation from exciton to the reduction of intersystem electron acceptors. Positive effects of a low $Cd^{2+}$ concentration on the light reactions of photosynthesis were not unexpected, because they had been already

demonstrated in multiple species [238,239] our results are only preliminary evidence, but they deserve further investigation.

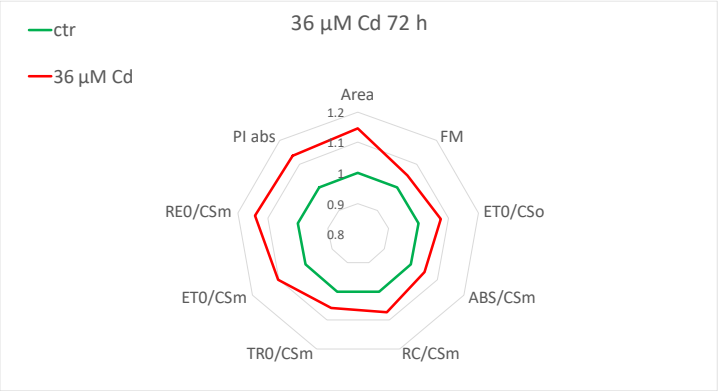


**Figure 25.** JIP-test technical parameters performed on *P. alba* samples treated with 0 (CTRL), and 36 µM $Cd^{2+}$, both under 72 h of treatment.

### *4.3.2 Response in* A.thaliana *colture cells*

After treating immortalized *Arabidopsis thaliana* cells with 0 (CTRL), 10, and 20 µM $Cd^{2+}$, cell lysates were extracted as described in 3.7 section to evaluate intracellular thiol-peptides. Additionally, the growth media were analysed using HPLC-MS/MS to assess extracellular thiol-peptides. In this experiment, no calibration curve was used for absolute quantification; instead, the ratio between the analyte of interest and its isotopically labeled internal standard was employed to ensure accurate data interpretation. It is important to note that the matrix in this case differs from those analysed previously, potentially influencing results. Therefore, spiking the internal standard prior to the extraction process—both intracellular and extracellular—is fundamental. Any loss or anomalous behaviour of the unlabeled analytes would similarly affect the internal standard. Using the analyte-to-internal standard ratio related to the grams of treated cells helps to mitigate errors or variability among replicates. The experiment, conducted in triplicate, confirmed the presence of thiol-peptides both intracellularly and extracellularly. Notably, the intracellular content and release of thiol-peptides into the growth medium increased in the presence of $Cd^{2+}$ compared to controls. Table 12 highlights GSH data, which were particularly relevant for preliminary studies investigating thiol-peptide transporter proteins. From the data, it is evident that 10 µM $Cd^{2+}$ is sufficient to

induce an increase in thiol-peptides. However, at higher $Cd^{2+}$ concentrations, a decrease in GSH levels was observed, consistent with findings from other studies on different plant species [77,85].

| | | Treatment | I | II | III |
|---|---|---|---|---|---|
| **Cell Lysates** | 48 h | CTRL | 9.52 | 12.08 | 25.47 |
| | | 10 µM $Cd^{2+}$ | 110.14 | 65.79 | 136.73 |
| | | 20 µM $Cd^{2+}$ | 12.77 | 27.64 | 24.07 |
| | 72h | CTRL | 97.68 | NA | NA |
| | | 10 µM $Cd^{2+}$ | 12.78 | 86.78 | 60.10 |
| | | 20 µM $Cd^{2+}$ | 14.45 | 9.72 | 14.43 |
| **Media** | 48h | CTRL | 81.45 | 29.22 | 101.12 |
| | | 10 µM $Cd^{2+}$ | 16.54 | 28.66 | 183.30 |
| | | 20 µM $Cd^{2+}$ | 83.86 | 23.10 | 74.98 |
| | 72h | CTRL | 30.18 | 9.49 | NA |
| | | 10 µM $Cd^{2+}$ | 62.01 | 16.40 | 14.74 |
| | | 20 µM $Cd^{2+}$ | 5.34 | 6.01 | 8.92 |

**Table 12**. Values of (GSH/IS-GSH) per gram of pelleted *A. thaliana* immortalized cells, corresponding to 48- and 72-hour treatments with 0 (CTRL), 10, and 20 µM $Cd^{2+}$ concentrations in both cell lysates and the respective treatment media. NA = values not available due to detection issues.

Given the experimental conditions, where $Cd^{2+}$ is more bioavailable and the cells—unlike a more complex organism such as a whole plant—are more directly exposed to metal absorption, prolonged exposure times (up to 72 hours) did not visibly damage the cells but did lead to alterations in their metabolism. These metabolic changes were associated with reduced GSH levels, possibly due to the formation of interfering molecules that also exacerbate the existing matrix effect, thereby influencing the analytical process. The aim of this attempts was to

demonstrate that even in cell cultures, mechanisms of synthesis and, importantly, extrusion of thiol-peptides similar to those observed in *Populus alba* plants are employed under comparable conditions. Building on these results, future research could focus on identifying plasma membrane transporters involved in the transport of GSH or thiol-peptides more broadly. Immunoprecipitation studies on cells treated for 48 h with 0 and 10 µM $Cd^{2+}$ would provide valuable insights. MS analysis of gel bands containing the proteins of interest could further enrich this study and answer key biological questions.

## 4.4 Inhibition study of thiol-peptides transporters: intracellular and extracellular evaluation of GSH and PCn in response to Glibenclamide and Sodium orthovanadate inhibition ability.

An inhibition study targeting putative (Cd-) thiol-peptide complex transporters was conducted to better understand the mechanisms underlying the release of GSH and PCn, which may be mediated by the plasma membrane of poplar root cells.

As known from the literature, the major class involved in the transport of HMs and their potential complexes are ABC transporters. For example, members of the ABCC family are localized in the tonoplast and are therefore implicated in the vacuolar compartmentalization of metals and other substances. The vacuolar import of PCn–Cd complexes is mediated by ATP-binding cassette (ABC)-type transporters [240], transmembrane proteins that utilize ATP to translocate various substrates across membranes.

ABC-type proteins have a characteristic modular structure consisting of two basic components: a hydrophobic transmembrane domain (TMD), typically composed of six membrane-spanning α-helices, and a cytosolic nucleotide-binding domain (NBD) responsible for ATP binding. The two TMDs dimerize to form the substrate-binding cavity [241,242].

Additionally, the G-type ABC transporter PDR8 from *A. thaliana* has been implicated in the extrusion of $Cd^{2+}$ ions or Cd conjugates across the plasma membrane of root epidermal cells [143]. Numerous studies have investigated the role of ABC transporters in the translocation and redistribution of metals. In rice, Cd treatment was shown to increase the expression of the G-type ABC transporter ABCG36, as reported by Fu et al. 2019 [141]. Higher Cd concentrations were observed in the roots of a loss-of-function mutant, indicating that ABCG36 facilitates the translocation of Cd from roots to shoots. Interestingly, an intriguing study [142] demonstrated that overexpression of the *ABCG36* gene from *P. tomentosa* in *A. thaliana* enhanced Cd tolerance. This suggests that the transporter functions as a Cd extrusion pump.

To inhibit ABC transporters, and more broadly, possible ATPase-driven plasma membrane transporters, the literature identifies potential molecules such as glibenclamide and sodium orthovanadate. Orthovanadate, in particular, is effective due to its ability to mimic phosphate groups, allowing it to be easily recognized by the transporter.

Different treatments with or without inhibitors, in control and $Cd^{2+}$ stressed conditions, were performed in *P.alba* plants and an HPLC-MS/MS analysis was performed on both the media and the plant extracts from shoots and roots, enabling quantification of the nmol/g FW of thiol-

peptides. What was expected from this study was a reduction in extracellular thiol-peptide content in the presence of inhibitory molecules.

Regarding glibenclamide, no inhibition was observed, even after 72 h of treatment. Furthermore, when analysing the absolute values of GSH and phytochelatins (PC2, PC3, PC4), an unexpected pattern was noted: a lower-than-expected content of PC2, accompanied by increased levels of higher oligomers such as PC3 and PC4. These findings suggest that glibenclamide does not selectively inhibit plasmalemma transporters and could have some implication in the synthesis and metabolism of intracellular PCn. Consequently, the investigation proceeded with the second inhibitor, sodium orthovanadate.

As a first observation, it is important to note the significant toxicity associated with the inhibitor at a concentration of 0.500 mM. While shoots showed no visible or organoleptic damage, the roots appeared to suffer, with root hairs progressively blackening over time. This condition worsened noticeably after 48 h and became severe after 72 h of treatment. Consequently, the experiment was adjusted to focus on lower inhibitor concentrations, specifically 0.250 mM and 0.125 mM, for both shoots and roots. Additionally, the extracellular thiol-peptide presence in the treatment media was evaluated.

In terms of absolute extracellular values, expressed in nmol/g FW for the root system, the higher presence of thiol-peptides under Cd stressed conditions compared to the control, as detailed in chapter 4.3, was confirmed. In the presence of sodium orthovanadate and Cd, GSH exhibited a decrease at 0.125 mM inhibitor concentration. Specifically in controls, after 72 h, GSH levels dropped from approximately 16.1 to 3.9 nmol/g FW under 0.125 mM of inhibitor and to 9.1 nmol/g FW under 0.250 mM (Figure 26 A,B).

In Cd-treated samples, GSH levels decreased from 11.03 to 8.3 nmol/g FW after 48 h and from 26.4 to 9.3 nmol/g FW after 72 h (Figure 26A). Also at higher inhibitor concentrations (0.250 mM), there was a decrease of GSH levels that rose to 6.7 nmol/g FW after 48 h and 7.8 nmol/g FW after 72 h (Figure 26B).

Regarding absolute values of PCn, particularly in samples treated with $Cd^{2+}$ in combination with sodium orthovanadate, an inhibition effect was observed after 72 h at both inhibitor concentrations (Figure 26 C,D). However, unlike GSH, this inhibition did not follow a clear trend. The data suggest that this inhibitor demonstrates a certain degree of selectivity toward GSH, while the inhibition of PCn appears more random.

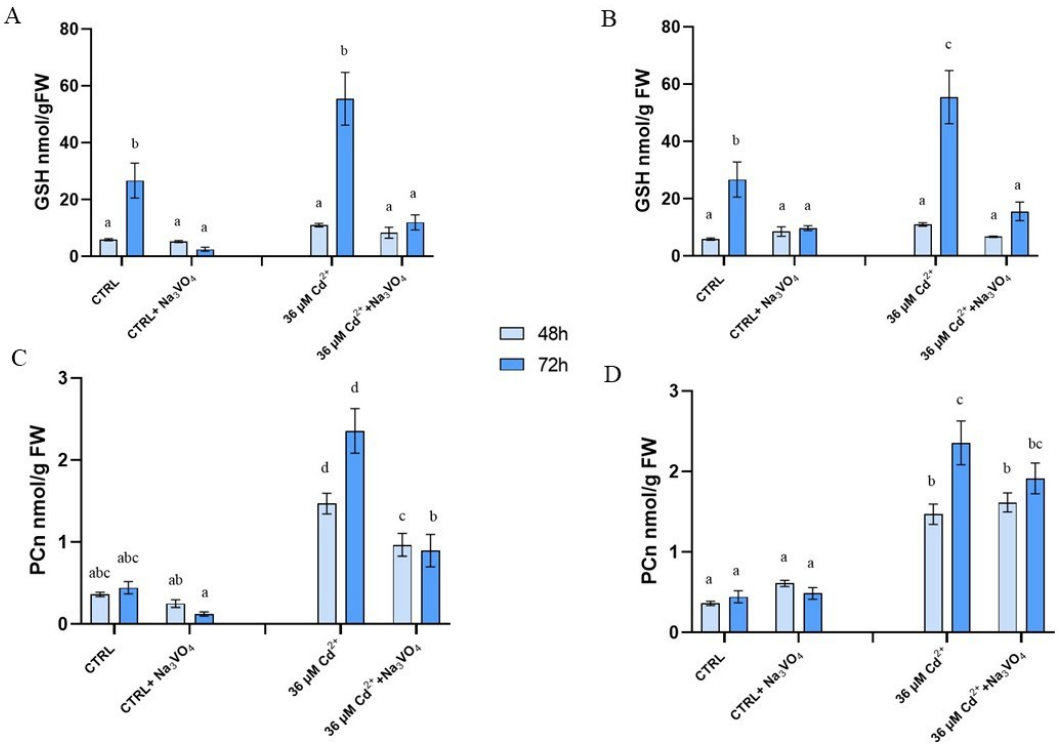


**Figure 26:** Inhibition study on *P.alba* plasmalemma transporters: GSH values (nmol/g FW of root system) obtained by HPLC-MS/MS analysis of extracellular thiol-peptides at 0 (CTRL) and 36 µM $Cd^{2+}$ without inhibitor and with sodium orthovanadate 0.125mM (A) or 0.250 mM (B). PCn values (nmol/g FW of root system) obtained by HPLC-MS/MS analysis of extracellular thiol-peptides at 0 (CTRL) and 36 µM $Cd^{2+}$ without inhibitor and with sodium orthovanadate 0.125mM (C) or 0.250 mM (D). Values are reported as mean ± SE (n = 3). Different letters indicate significant differences (two-way ANOVA followed by Tukey's test, $p < 0.05$).

Given that the presence of Cd induces higher thiol-peptide synthesis and extracellular efflux, a comparative analysis was performed to assess their distribution across shoots, roots, and the extracellular media. In Figure 27, the relative percentages of GSH in shoots, roots, and media are shown, with 100% representing the total sum of these three compartments.

From Figure 27A, it is evident that after both 48 and 72 h of treatment, the percentage of GSH in the media decreases in the presence of the inhibitor. Simultaneously, GSH levels in shoots increase more than in roots, suggesting the possibility of thiol-peptide translocation within the plant.

The inhibition percentages, summarized in Table 13, further clarify the observed trends: the percentage of inhibition does not appear to be concentration-dependent, as no significant increase in inhibition is observed between 0.125 mM and 0.250 mM of the inhibitor. On the contrary, longer exposure times seem to have a greater influence on the % inhibition of GSH:

after 72 h, the inhibition effect became more pronounced, with up to 70% inhibition observed, compared to the 40% after 48 h.

The inhibition percentages were calculated as:

$$\%\text{Inhibition} = 100 - \frac{\text{Absolute GSH or PCn values (inhibited treatment)}}{\text{Absolute GSH or PCn values(not inhibited treatment)}}$$

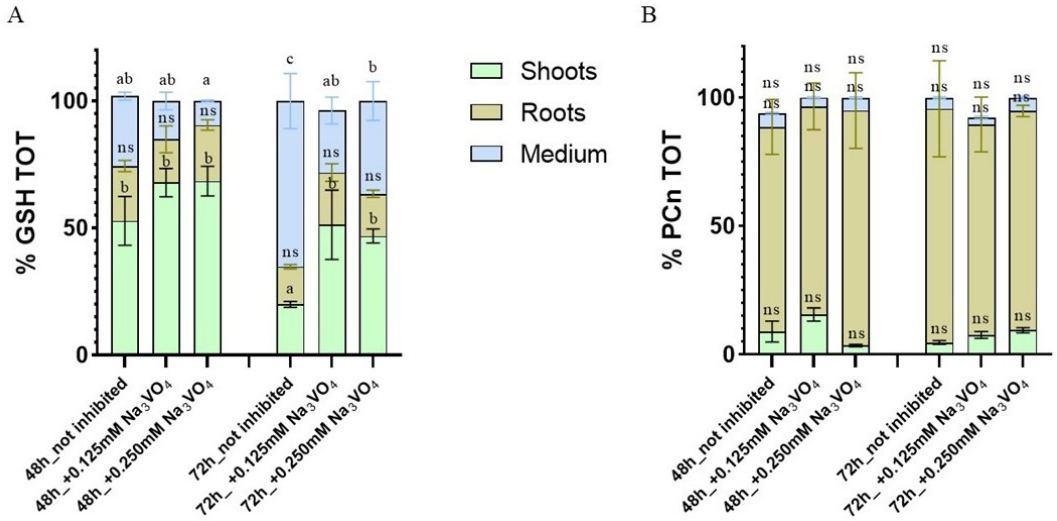


**Figure 27.** Relative percentages of GSH (A) and PCn (B) in shoots, roots, and media, with 100% representing the total sum of these three compartments, under 36 µM $Cd^{2+}$ stressed condition maintained for 48 and 72 h, with or without sodium orthovanadate (0.125-0.250 mM). Values are reported as mean ± SE (n = 3). The comparison of the percentage distribution of shoots, roots, and growth medium across different conditions was performed. Different letters indicate significant differences and the abbreviation "ns" indicates no significant differences (one-way ANOVA followed by Tukey's test, $p < 0.05$).

| Exposure time | Inhibitor concentration | GSH % of inhibition | PCn % of inhibition |
|---|---|---|---|
| **48h** | 0.250 mM | 38.85 ± 3.2 | 0.00 ± 0.0 |
| | 0.125 mM | 40.3 ± 5.5 | 34.00 ± 4.3 |
| **72h** | 0.250 mM | 71.89 ± 7.5 | 24.80 ± 8.0 |
| | 0.125 mM | 78.34 ± 5.9 | 45.50 ± 8.8 |

**Table 13.** GSH and PCn inhibition % calculated as $\%\text{Inhibition} = 100 - \frac{\text{Absolute GSH or PCn values (inhibited treatment)}}{\text{Absolute GSH or PCn values(not inhibited treatment)}}$ for each treatment condition (± percentage error): 48-72h as exposure time, 0.125 -0.250 mM as sodium orthovanadate concentration.

These results highlight sodium orthovanadate's impact as an inhibitor, with a pronounced selectivity for GSH. The observed decrease in extracellular GSH levels in the presence of the inhibitor, alongside increased levels in shoots, suggests a disruption in GSH efflux and a potential redirection of thiol-peptides within the plant system. Moreover, based on our results, it seems that GSH and PCn/Cd-PCn complexes may not utilize the same plasma membrane transporters for extrusion. Further investigation is needed to clarify the mechanisms involved, particularly in relation to PCn transport. These findings pave the way for future studies exploring the biological pathways and molecular targets affected by this inhibitor.

Alternatively, $Cd^{2+}$ may utilize other efflux mechanisms, with the metal potentially being released either as a complex with PCn via specific transporters or in its free form. PCn, whether chelated with the metal or not, could also be transported through alternative efflux pathways involving other protein transporters. One hypothesis is that aquaporins might play a role in this transportation process [243].

## 5. CONCLUSION

The results of this study highlight significant advancements and insights into pre-analytical extraction methods, thiol-peptide quantification, and plant responses to $Cd^{2+}$ stress. The optimization of the extraction protocol demonstrated that while methods such as SPE and derivatization were ineffective, adjustments in buffer systems, reducing agents, and washing steps significantly improved sample clarity and analytical accuracy without compromising recovery rates. The addition of washing steps notably enhanced sample quality, making the extraction procedure more reliable and compatible with HPLC-MS/MS analysis.

Exploring long-term effects of Cd exposure, biometric analysis of *Populus alba* seedlings revealed limited alterations in growth parameters under Cd stress, suggesting a degree of physiological resilience. Minor changes, such as increased root length and decreased dry matter at higher Cd concentrations, indicate early responses to Cd exposure. This tolerance, coupled with findings from *in vivo* fluorescence analyses, further supports the hypothesis that *P. alba* can accumulate Cd without showing significant photosynthetic or growth impairments in the short term. These results align with prior studies, highlighting a potential metal exclusion strategy that sequesters Cd within roots to mitigate systemic toxicity.

Overall, this research not only refines the analytical methodology for thiol-peptide detection but also contributes to understanding the physiological and biochemical mechanisms underlying Cd stress tolerance in *P. alba*. The results of this study demonstrate the pivotal role of intracellular thiol-peptides, particularly PCn and GSH, in the detoxification of Cd in *Populus alba*. While GSH levels remained stable in leaves and stems, a significant increase in roots under higher Cd concentrations suggests its crucial role in early defence mechanisms. PCn production, predominantly driven by PC2, was significantly elevated in stems and roots at 100 µM $Cd^{2+}$, indicating a dose-dependent response to HM stress. These findings underscore *P. alba*'s capacity to deploy differential and organ-specific responses to mitigate Cd toxicity, affirming the importance of thiol-peptide diversity in HM tolerance.

The presented findings concerning a short-term $Cd^{2+}$ stress highlight the critical role of thiol-peptides, particularly GSH and PCn, in managing HM stress across diverse plant systems. In *Populus alba*, both intracellular content and extracellular release of GSH and PCn were enhanced under Cd stress, demonstrating their importance in Cd detoxification and homeostasis. Similar trends were observed in *Marchantia polymorpha*, where thiol-peptides responded dynamically to excess Zn, Cu, and Fe, further supporting their dual role as intracellular and extracellular detoxifying agents[227]. These mechanisms appear conserved across bryophytes and tracheophytes, emphasizing their evolutionary significance. In

*Arabidopsis thaliana* cell cultures, Cd exposure also induced thiol-peptide synthesis and release, reinforcing their general role in HM tolerance. Collectively, these findings contribute to understanding the physiological and molecular strategies plants use to cope with HM stress, with implications for phytomonitoring applications.

This study provides important insights into the extracellular transport of thiol-peptides and the effects of transport inhibitors on their synthesis and release under $Cd^{2+}$ stress. Evidence suggests that ABC transporters, particularly those localized in the plasma membrane and tonoplast, mediate the transport of GSH, PCn, and their respective metal complexes. Inhibition studies identified sodium orthovanadate as a putative inhibitor of thiol-peptide transporters, specifically targeting GSH transport. The significant decrease in extracellular GSH levels and its accumulation in shoots in the presence of sodium orthovanadate suggests a disruption in GSH efflux and potential redirection within the plant system. However, PCn inhibition appeared less pronounced and lacked a consistent trend, highlighting possible differences in the transport mechanisms or selectivity of the inhibitor.

The study further underscores the complexity of thiol-peptide transport and the potential involvement of other pathways, including aquaporins or alternative transporter proteins, in managing $Cd^{2+}$ stress. The findings also emphasize the need for further exploration of the molecular targets and pathways involved in thiol-peptide transport and metal detoxification. Understanding these processes will enhance our knowledge of plant detoxification strategies and inform future applications in phytoremediation and stress tolerance improvement.

## APPENDIX

*Intracellular and extracellular presence of thiol-peptides in response to Cd stress in* Marcantia polimorpha

Given the critical role of PCn and GSH in detoxification, I participated in the investigation of PCn in *Marchantia polymorpha*—a liverwort considered a key species in the phylogeny of land plants. The study focused on *M. polymorpha* gametophytes grown under physiological levels, deprivation, and excess of three essential metal micronutrients: Zn, Cu, and Fe. Specifically, gametophytes were exposed to 80 μM or 200 μM Zn, 80 μM or 200 μM Cu, and 200 μM or 300 μM Fe for 24 and 72 hours.

This research provided valuable biological insights, which guided the direction of this PhD project. It paved the way for addressing the same questions initially posed for *M. polymorpha* in the context of *P. alba*, transitioning from a study on bryophytes to one on a tracheophyte model.

Concerning the result obtained from our recent study on *M. polymorpha* at both tested concentrations and throughout the experiment, *in vivo* treatments with excess Zn markedly increased PCn production. PCn levels peaked at 24 and 120 h at a concentration of 80 μM. In samples treated with 200 μM Zn, PCn biosynthesis was lower at 24 h but higher at 14 and 72 h compared to those treated with 80 μM Zn (Figure 28A). Analysis of the various PCn oligomers produced in response to both Zn concentrations revealed that PC2 was the most prevalent oligomer small amounts (~0.05 nmol/g FW) of higher-order PCn oligomers were detected, with synthesis observed as early as 6 h after treatment initiation (Figure 29 A,B).

Figure 28B shows *in vivo* PCn concentrations in response to excess Cu, along with corresponding control levels. Similar to Zn treatments, PC2 was the most abundant oligomer produced in response to Cu exposure, while PC3 and PC4 were present in lower amounts (between ~0.05 and 2 nmol/g FW) (Figure 29 C,D). Higher-degree oligomers were found in smaller quantities, with PCn synthesis detectable as early as 6 h post-treatment. PCn levels in samples treated with 80 μM Cu diverged from control only after 24 h of metal exposure, decreasing thereafter and approaching control values. In contrast, 200 μM Cu caused a significant rise in PCn levels as early as 6 h after treatment onset, with concentrations consistently remaining above control at approximately 20 nmol/g FW.

In contrast, after 14 h of exposure to 300 μM Fe, the first discernible rise in PCn was noted. After that, the PCn levels were continuously greater than the control's, fluctuating around 12

nmol/g FW before reaching a final peak at 120 h, when they were roughly 28.5 ± 1.8 nmol/g FW (Figure 28C). Similar to Zn and Cu treatments, a rise in PC2 concentration was the main cause of the increase in total PCn after exposure to Fe. Additionally, PC3 and PC4 were synthesised, but at very low amounts (less than 0.9 nmol/g FW) (Figure 29 E,F).

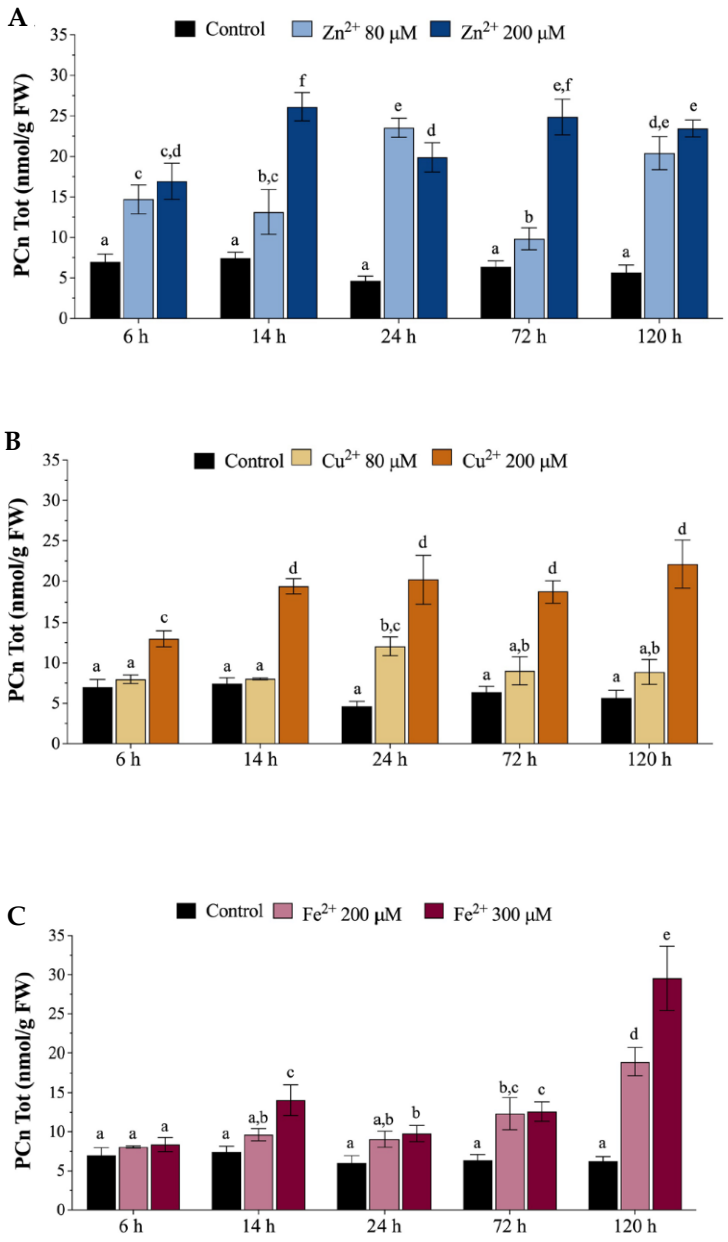


**Figure 28.** *In vivo* concentrations of phytochelatins (PCn, nmol/g FW) in *Marchantia polymorpha* gametophytes exposed for 6, 14, 24, 72, and 120 h to 80 µM (light blue bars) or 200 µM (blue bars) Zn (A) and to 80 µM (beige bars) or 200 µM (orange bars) Cu (B) and to 200 µM (pink bars) or 300 µM (amaranth bars) Fe (C). Values are reported as mean ± SE. Different letters indicate significant differences between different concentrations and organs (two-way ANOVA followed by Tukey's test, $p < 0.05$) [227].

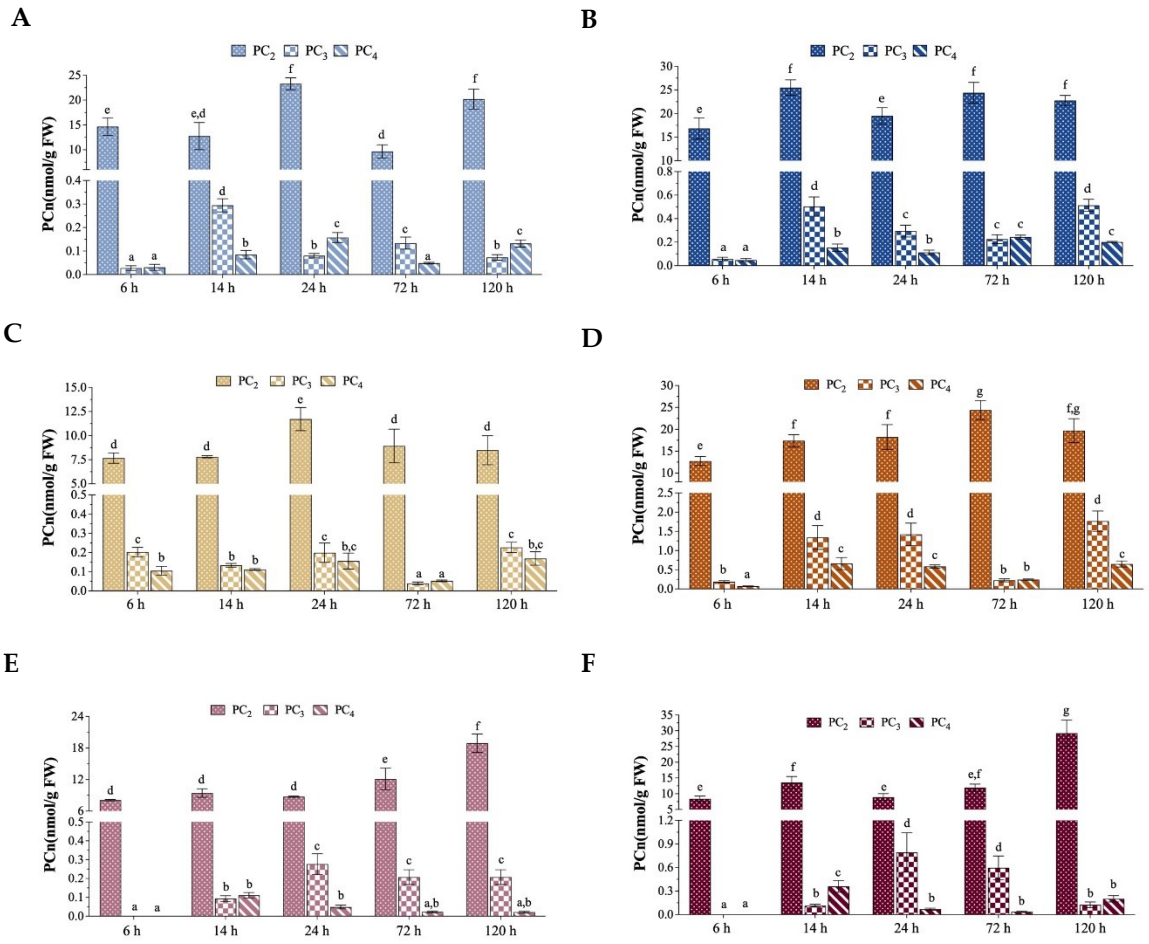


**Figure 29**. *In vivo* phytochelatin oligomers PC2-3-4 (nmol/g FW) in *Marchantia polymorpha* gametophytes exposed for 6, 14, 24, 72, and 120 h and to 80 µM (light blue bars, A) or 200 µM (blue bars, B) Zn and to 80 µM (beige bars, C) or 200 µM (orange bars, D) Cu and to 200 µM (pink bars, E) or 300 µM (amaranth bars, F) Fe.Values are reported as mean ± SE. Different letters indicate significant differences between different concentrations and organs (two-way ANOVA followed by Tukey's test, $p < 0.05$) [227].

In conclusion, Excess Zn, Cu, and Fe raised the concentrations of PCn in gametophytes, while starvation lowered them. However, PCn were detected also when plants were supplied with physiological levels of these micronutrients, thus proving their constitutive presence. This observation essentially confirms what has been previously demonstrated in other photoautotrophic species [77,80,81,85].

Excess Zn in *in vivo* treatments caused extracellular release of PCn, following a pattern similar to that observed with Fe (Figure 30 A,E). However, for Zn, only the highest concentration (200 µM) had a significant effect. In contrast, both Cu doses triggered a relatively rapid extracellular release of PCn, which was prominent 24 h after treatment initiation and appeared to plateau by

72 h (Figure 30C). The extracellular release of PCn was also observed under exposure to 200 and 300 µM Fe, though it became noticeable only after 72 h (Figure 30E). Additionally, extracellular GSH release exhibited a pattern similar to that of PCn across all treatments (Figure 30). However, the quantities of thiol-peptide released varied significantly, especially for Zn and Fe (Figure 30 A,B,E,F), where GSH levels in the growth medium were an order of magnitude higher than those of PCn. In contrast, for Cu, the extracellular levels of GSH and PCn were comparable.

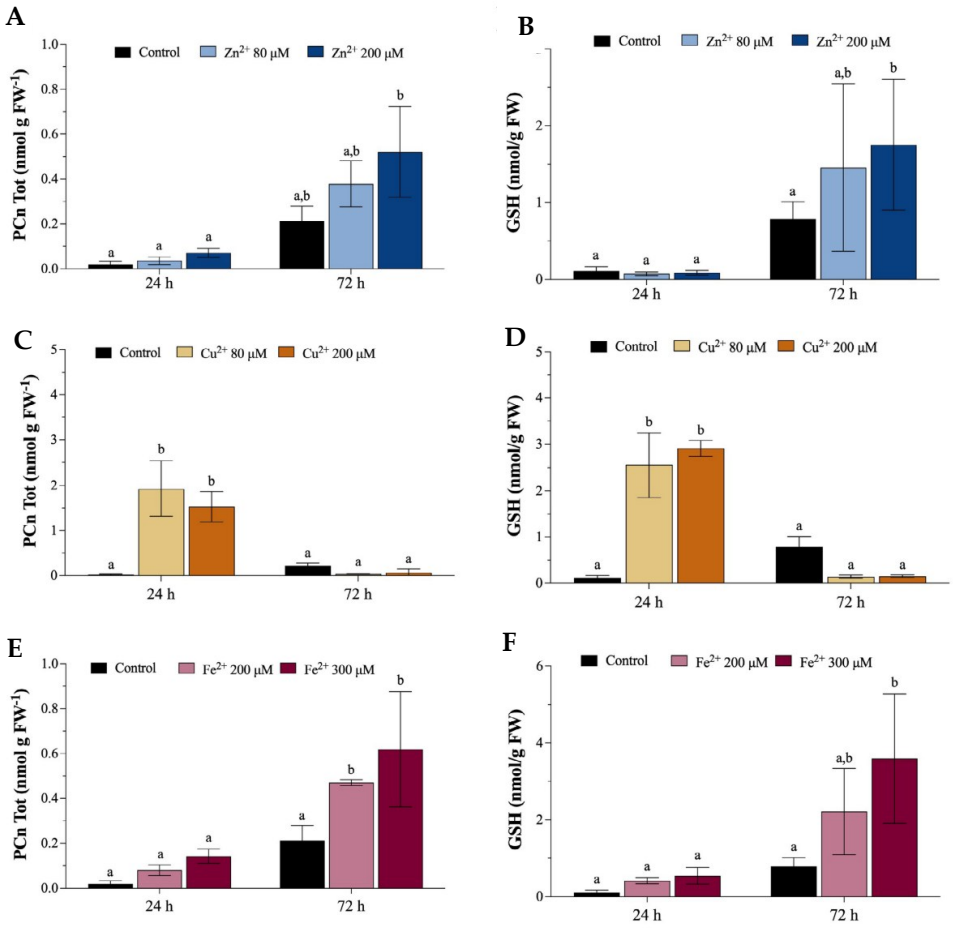


**Figure 30.** Extracellular concentrations of phytochelatins (PCn, nmol/g FW) in the ms ½ growth medium, where *Marchantia polymorpha* gametophytes were exposed for 24 and 72 h to 80 µM (light blue bars) or 200 µM (blue bars) Zn (A); 80 µM (beige bars) or 200 µM (orange bars) Cu (C); 200 µM (pink bars) or 300 µM (amaranth bars) Fe (E). Extracellular concentrations of GSH (nmol/g FW) in the MS ½ growth medium, where *M. polymorpha* gametophytes were exposed for 24 and 72 h to 80 µM (light blue bars) or 200 µM (blue bars) Zn (B); 80 µM (beige bars) or 200 µM (orange bars) Cu (D); 200 µM (pink bars) or 300 µM (amaranth bars) Fe (F). Values are means ± SE (n = 3). Different letters indicate significant differences (two-way ANOVA followed by Tukey's test, $p < 0.05$) [227].

Lastly this study showed that excess Cu, Fe, and Zn triggered the release of PCn and GSH into the growth medium, supporting the idea that these thiol-peptides function as extracellular detoxifying agents [72]. The presence of PCn and GSH in the growth media of plants treated with metal(loid)s has been widely reported, further suggesting their role in extracellular detoxification [72,243]. For instance, exudates from *Lupinus albus* (white lupin) plants exposed to As contained significant levels of PCn and GSH derivatives, which may either prevent As uptake into the root system or facilitate the exudation of As complexed with thiol-peptides from the root symplasm into the surrounding environment [243]. Similarly, *Oryza sativa* (rice) was found to have an As efflux system at the plasma membrane, based on the activity of certain ABC transporters [244].

This study's findings do not allow for a definitive conclusion on whether complexation of excess Zn, Cu, and Fe by GSH and PCn occurred extracellularly, preventing entry into cells, or intracellularly before their release into the growth medium. However, based on current data and previous studies using Cd [72], we believe the first hypothesis is more plausible: metal elements may be complexed intracellularly and sequestered in the vacuole, with excess metal-bound thiol-peptides released extracellularly.

Interestingly, gametophytes exposed to Cu quickly released PCn and GSH into the growth medium, with PCn concentrations exceeding those observed following Zn and Fe treatments and nearing GSH concentrations. This rapid release aligns with reports that thiol-peptides are potent Cu chelators [245,246]. The faster release of GSH compared to PCn could reflect an effective mechanism for binding and neutralizing Cu toxicity.

Given all results obtained on *M. polymorpha*, it was decided to extend our research to *in vitro P. alba* plants, which were also subjected to HM stress, particularly Cd. Our study aims to investigate the hypothesis of a dual role of thiol-peptides in both intra and extracellular detoxification in *P. alba*.

## REFERENCES


1. Jiang, Y.; Jiang, S.; Li, Z.; Yan, X.; Qin, Z.; Huang, R. Field Scale Remediation of Cd and Pb Contaminated Paddy Soil Using Three Mulberry (Morus Alba L.) Cultivars. *Ecol Eng* **2019**, *129*, 38–44, doi:10.1016/j.ecoleng.2019.01.009.
2. Bhattacharya, S. Protective Role of the Essential Trace Elements in the Obviation of Cadmium Toxicity: Glimpses of Mechanisms. *Biol Trace Elem Res* **2022**, *200*, 2239–2246, doi:10.1007/s12011-021-02827-7.
3. Yadav, M.; Gupta, R.; Sharma, R.K. Chapter 14 - Green and Sustainable Pathways for Wastewater Purification. In; Ahuja, S.B.T.-A. in W.P.T., Ed.; Elsevier, 2019; pp. 355–383 ISBN 978-0-12-814790-0.
4. Lin, X.; Li, S.; Wei, Z.; Chen, Y.; Hei, L.; Wu, Q.-T. Indirect Application of Sludge for Recycling in Agriculture to Minimize Heavy Metal Contamination of Soil. *Resour Conserv Recycl* **2021**, *166*, 105358, doi:10.1016/j.resconrec.2020.105358.
5. Qin, X.; Xia, Y.; Hu, C.; Yu, M.; Shabala, S.; Wu, S.; Tan, Q.; Xu, S.; Sun, X. Ionomics Analysis Provides New Insights into the Co-Enrichment of Cadmium and Zinc in Wheat Grains. *Ecotoxicol Environ Saf* **2021**, *223*, 112623, doi:10.1016/j.ecoenv.2021.112623.
6. Gu, Y.-G.; Li, Q.; Fang, J.; He, B.; Fu, H.; Tong, Z. Identification of Heavy Metal Sources in the Reclaimed Farmland Soils of the Pearl River Estuary in China Using a Multivariate Geostatistical Approach. *Ecotoxicol Environ Saf* **2014**, *105C*, 7–12, doi:10.1016/j.ecoenv.2014.04.003.
7. Ministry of Ecology and Environment of the People's Republic of China 2021 China Ecology and Environment Statement. **2022**.
8. Kim, E.; Hopke, P.; Edgerton, E. Improving Source Identification of Atlanta Aerosol Using Temperature Resolved Carbon Fractions in Positive Matrix Factorization. *Atmos Environ* **2004**, *38*, 3349–3362, doi:10.1016/j.atmosenv.2004.03.012.
9. Fei, X.; Lou, Z.; Xiao, R.; Ren, Z.; Lv, X. Source Analysis and Source-Oriented Risk Assessment of Heavy Metal Pollution in Agricultural Soils of Different Cultivated Land Qualities. *J Clean Prod* **2022**, *341*, 130942, doi:10.1016/j.jclepro.2022.130942.
10. Xiao, R.; Ali, A.; Wang, P.; li, R.; Tian, X.; Zhang, Z. Comparison of the Feasibility of Different Washing Solutions for Combined Soil Washing and Phytoremediation for the Detoxification of Cadmium (Cd) and Zinc (Zn) in Contaminated Soil. *Chemosphere* **2019**, *230*, doi:10.1016/j.chemosphere.2019.05.121.
11. Ekrami, E.; Pouresmaieli, M.; Hashemiyoon, E.; Noorbakhsh, N.; Mahmoudifard, M. Nanotechnology: A Sustainable Solution for Heavy Metals Remediation. *Environ Nanotechnol Monit Manag* **2022**, *18*, 100718, doi:10.1016/j.enmm.2022.100718.
12. Chen, L.; Beiyuan, J.; Hu, W.; Zhang, Z.; Duan, C.; Cui, Q.; Zhu, X.; He, H.; Huang, X. Phytoremediation of Potentially Toxic Elements (PTEs) Contaminated Soils Using Alfalfa (Medicago Sativa L.): A Comprehensive Review. *Chemosphere* **2022**, *293*, 133577, doi:10.1016/j.chemosphere.2022.133577.
13. Chaoua, S.; Boussaa, S.; Gharmali, A.; Boumezzough, A. Impact of Irrigation with Wastewater on Accumulation of Heavy Metals in Soil and Crops in the Region of Marrakech in Morocco. *Journal of the Saudi Society of Agricultural Sciences* **2018**, *18*, doi:10.1016/j.jssas.2018.02.003.
14. Sanita' di Toppi, L.; Gabbrielli, R. Response to Cadmium in Higher Plants. *Environ Exp Bot* **1999**, *41*, doi:10.1016/S0098-8472(98)00058-6.
15. Ismael, M.A.; Elyamine, A.M.; Moussa, M.G.; Cai, M.; Zhao, X.; Hu, C. Cadmium in Plants: Uptake, Toxicity, and Its Interactions with Selenium Fertilizers. *Metallomics* **2019**, *11*, 255–277, doi:10.1039/c8mt00247a.
16. Kubier, A.; Wilkin, R.T.; Pichler, T. Cadmium in Soils and Groundwater: A Review. *Appl Geochem* **2019**, *108*, 1–16, doi:10.1016/j.apgeochem.2019.104388.

17. Clemens, S.; Aarts, M.; Thomine, S.; Verbruggen, N. Plant Science: The Key to Preventing Slow Cadmium Poisoning. *Trends Plant Sci* **2012**, *18*, 92, doi:10.1016/j.tplants.2012.08.003.
18. Stankovic, J.; Sabovljevic, A.; Sabovljevic, M. Bryophytes and Heavy Metals: A Review. *Acta Bot Croat* **2018**, doi:10.2478/botcro-2018-0014.
19. Zhao, H.; Li, P.; He, X. Remediation of Cadmium Contaminated Soil by Modified Gangue Material: Characterization, Performance and Mechanisms. *Chemosphere* **2021**, *290*, 133347, doi:10.1016/j.chemosphere.2021.133347.
20. Alimba, C.G.; Gandhi, D.; Sivanesan, S.; Bhanarkar, M.D.; Naoghare, P.K.; Bakare, A.A.; Krishnamurthi, K. Chemical Characterization of Simulated Landfill Soil Leachates from Nigeria and India and Their Cytotoxicity and DNA Damage Inductions on Three Human Cell Lines. *Chemosphere* **2016**, *164*, 469–479, doi:https://doi.org/10.1016/j.chemosphere.2016.08.093.
21. Wang, R.; Lin, K.; Chen, H.; Qi, Z.; Liu, B.; Cao, F.; Chen, H.; Wu, F. Metabolome Analysis Revealed the Mechanism of Exogenous Glutathione to Alleviate Cadmium Stress in Maize (Zea Mays l.) Seedlings. *Plants* **2021**, *10*, 1–12, doi:10.3390/plants10010105.
22. Wang, Y.; Hu, Y.; Xue, C.; Khan, A.; Zheng, X.; Cai, L. Risk Assessment of Lead and Cadmium Leaching from Solidified/Stabilized MSWI Fly Ash under Long-Term Landfill Simulation Test. *Science of The Total Environment* **2022**, *816*, 151555, doi:https://doi.org/10.1016/j.scitotenv.2021.151555.
23. Hölzle, I.; Somani, M.; Ramana, G. V; Datta, M. Heavy Metals in Soil-like Material from Landfills – Resource or Contaminants? *J Clean Prod* **2022**, *369*, 133136, doi:https://doi.org/10.1016/j.jclepro.2022.133136.
24. Alloway, B. *Heavy Metals in Soils: Trace Metals and Metalloids in Soils and Their Bioavailability*; 2013; ISBN 978-94-007-4469-1.
25. Naseem, S.; Hamza; Nawaz-Ul-Huda, S.; Erum, B.; ul-Haq, Q. Geochemistry of Cd in Groundwater of Winder, Balochistan and Suspected Health Problems. *Environ Earth Sci* **2013**, *71*, doi:10.1007/s12665-013-2572-z.
26. Alengebawy, A.; Abdelkhalek, S.; Qureshi, S.; Wang, M.-Q. Heavy Metals and Pesticides Toxicity in Agricultural Soil and Plants: Ecological Risks and Human Health Implications. *Toxics* **2021**, *9*, 42, doi:10.3390/toxics9030042.
27. Rehman, A.; Nazir, S.; Irshad, R.; Tahir, K.; Rehman, K.; Islam, R.; Wahab, Z. Toxicity of Heavy Metals in Plants and Animals and Their Uptake by Magnetic Iron Oxide Nanoparticles. *J Mol Liq* **2020**, *321*, 114455, doi:10.1016/j.molliq.2020.114455.
28. Aoshima, K. Itai-Itai Disease: Renal Tubular Osteomalacia Induced by Environmental Exposure to Cadmium—Historical Review and Perspectives. *Soil Sci Plant Nutr* **2016**, *62*, 319–326, doi:10.1080/00380768.2016.1159116.
29. Arain, M.B.; Kazi, T.G.; Baig, J.A.; Afridi, H.I.; Sarajuddin; Brehman, K.D.; Panhwar, H.; Arain, S.S. Co-Exposure of Arsenic and Cadmium through Drinking Water and Tobacco Smoking: Risk Assessment on Kidney Dysfunction. *Environ Sci Pollut Res Int* **2015**, *22*, 350–357, doi:10.1007/s11356-014-3339-0.
30. Khan, M.A.; Khan, S.; Khan, A.; Alam, M. Soil Contamination with Cadmium, Consequences and Remediation Using Organic Amendments. *Sci Total Environ* **2017**, *601–602*, 1591–1605, doi:10.1016/j.scitotenv.2017.06.030.
31. Meysam Hoseini, S.; Zargari, F. Cadmium in Plants: A Review. *International Journal of Farming and Allied Sciences* **2013**, *2*, 579–581.
32. Li, Y.; Sun, M.; He, W.; Wang, H.; Pan, H.; Yang, Q.; Lou, Y.; Zhuge, Y. Effect of Phosphorus Supplementation on Growth, Nutrient Uptake, Physiological Responses, and Cadmium Absorption by Tall Fescue (Festuca Arundinacea Schreb.) Exposed to Cadmium. *Ecotoxicol Environ Saf* **2021**, *213*, 112021, doi:10.1016/j.ecoenv.2021.112021.
33. Meng, Y.; Jing, H.; Huang, J.; Shen, R.; Zhu, X. The Role of Nitric Oxide Signaling in Plant Responses to Cadmium Stress. *Int J Mol Sci* **2022**, *23*, doi:10.3390/ijms23136901.

34. Rady, M.; Elrys, A.; Aboelmaati, M.; Desoky, E.-S. Interplaying Roles of Silicon and Proline Effectively Improve Salt and Cadmium Stress Tolerance in Phaseolus Vulgaris Plant. *Plant Physiology and Biochemistry* **2019**, *139*, doi:10.1016/j.plaphy.2019.04.025.
35. Semida, W.; Hemida, K.; Rady, M. Sequenced Ascorbate-Proline-Glutathione Seed Treatment Elevates Cadmium Tolerance in Cucumber Transplants. *Ecotoxicol Environ Saf* **2018**, *154*, doi:10.1016/j.ecoenv.2018.02.036.
36. Zouari, M.; Ben Ahmed, C.; Zorrig, W.; Elloumi, N.; Rabhi, M.; Delmail, D.; Ben Rouina, B.; Labrousse, P.; Ben Abdallah, F. Exogenous Proline Mediates Alleviation of Cadmium Stress by Promoting Photosynthetic Activity, Water Status and Antioxidative Enzymes Activities of Young Date Palm (Phoenix Dactylifera L.). *Ecotoxicol Environ Saf* **2016**, *128*, 100–108, doi:10.1016/j.ecoenv.2016.02.015.
37. Shahid, M.; Javed, M.T.; Mushtaq, A.; Akram, M.S.; Mahmood, F.; Ahmed, T.; Noman, M.; Azeem, M. Microbe-Mediated Mitigation of Cadmium Toxicity in Plants. In; 2019; pp. 427–449 ISBN 9780128148648.
38. Sidhu, G.P.S.; Bali, A.; Kumar, V.; Bhardwaj, R. Mitigating Cadmium Toxicity in Plants by Phytohormones. In; 2019; pp. 375–396 ISBN 978-0-12-814864-8.
39. Hameed, A.; Rasool, S.; Azooz, M.M.; Hossain, M.A.; Ahanger, M.A.; Ahmad, P. Chapter 24 - Heavy Metal Stress: Plant Responses and Signaling. In; Ahmad, P.B.T.-P.M.I., Ed.; Elsevier, 2016; pp. 557–583 ISBN 978-0-12-803158-2.
40. Huang, Y.; Zhu, Z.; Wu, X.; Liu, Z.; Zou, J.; Chen, Y.; Su, N.; Cui, J. Lower Cadmium Accumulation and Higher Antioxidative Capacity in Edible Parts of Brassica Campestris L. Seedlings Applied with Glutathione under Cadmium Toxicity. *Environmental Science and Pollution Research* **2019**, *26*, 13235–13245, doi:10.1007/s11356-019-04745-7.
41. Meng, Y.; Zhang, L.; Wang, L.; Zhou, C.; Shangguan, Y.; Yang, Y. Antioxidative Enzymes Activity and Thiol Metabolism in Three Leafy Vegetables under Cd Stress. *Ecotoxicol Environ Saf* **2019**, *173*, 214–224, doi:10.1016/j.ecoenv.2019.02.026.
42. Shahid, M.; Dumat, C.; Khalid, S.; Schreck, E.; Xiong, T.; Niazi, N.K. Foliar Heavy Metal Uptake, Toxicity and Detoxification in Plants: A Comparison of Foliar and Root Metal Uptake. *J Hazard Mater* **2017**, *325*, 36–58, doi:https://doi.org/10.1016/j.jhazmat.2016.11.063.
43. Faizan, M.; Alam, P.; Rajput, V.; Faraz, A.; Afzal, S.; Ahmed, S.; Yu, F.-Y.; Minkina, T.; Hayat, S. Nanoparticle Mediated Plant Tolerance to Heavy Metal Stress: What We Know? *Sustainability* **2023**, *15*, doi:10.3390/su15021446.
44. Valko, M.; Rhodes, C.; Izakovic, M.; Mazur, M. Valko M, Rhodes CJ, Moncol J, Izakovic M, Mazur MFree Radicals, Metals and Antioxidants in Oxidative Stress-Induced Cancer. Chem Biol Interact 160: 1-40. *Chem Biol Interact* **2006**, *160*, 1–40, doi:10.1016/j.cbi.2005.12.009.
45. Boonstra, J.; Post, J. Molecular Events Associated with Reactive Oxygen Species and Cell Cycle Progression in Mammalian Cells. *Gene* **2004**, *337*, 1–13, doi:10.1016/j.gene.2004.04.032.
46. Kumar, A.; Majeti, P. Plant-Lead Interactions: Transport, Toxicity, Tolerance, and Detoxification Mechanisms. *Ecotoxicol Environ Saf* **2018**, *166*, 401–418, doi:10.1016/j.ecoenv.2018.09.
47. Liu, Y.; Liu, L.; Qi, J.; Dang, P.; Xia, T. Cadmium Activates ZmMPK3-1 and ZmMPK6-1 via Induction of Reactive Oxygen Species in Maize Roots. *Biochem Biophys Res Commun* **2019**, *516*, doi:10.1016/j.bbrc.2019.06.116.
48. Berni, R.; Luyckx, M.; Xu, X.; Legay, S.; Sergeant, K.; Hausman, J.-F.; Lutts, S.; Cai, G.; Guerriero, G. Reactive Oxygen Species and Heavy Metal Stress in Plants: Impact on the Cell Wall and Secondary Metabolism. *Environ Exp Bot* **2019**, *161*, 98–106, doi:https://doi.org/10.1016/j.envexpbot.2018.10.017.
49. Ma, Q.-J.; Sun, M.-H.; Lu, J.; Hu, D.-G.; Kang, H.; You, C.-X.; Hao, Y.-J. Phosphorylation of a Malate Transporter Promotes Malate Excretion and Reduces Cadmium Uptake in Apple. *J Exp Bot* **2020**, *71*, 3437–3449, doi:10.1093/jxb/eraa121.
50. Sharma, S.K.; Singh, D.; Pandey, H.; Jatav, R.B.; Singh, V.; Pandey, D. An Overview of Roles of Enzymatic and Nonenzymatic Antioxidants in Plant BT - Antioxidant Defense in Plants:

Molecular Basis of Regulation. In; Aftab, T., Hakeem, K.R., Eds.; Springer Nature Singapore: Singapore, 2022; pp. 1–13 ISBN 978-981-16-7981-0.
51. Metwally, A.; Safronova, V.I.; Belimov, A.A.; Dietz, K.-J. Genotypic Variation of the Response to Cadmium Toxicity in Pisum Sativum L. *J Exp Bot* **2005**, *56*, 167–178, doi:10.1093/jxb/eri017.
52. Nada, E.; Ferjani, B.A.; Ali, R.; Bechir, B.R.; Imed, M.; Makki, B. Cadmium-Induced Growth Inhibition and Alteration of Biochemical Parameters in Almond Seedlings Grown in Solution Culture. *Acta Physiol Plant* **2007**, *29*, 57–62, doi:10.1007/s11738-006-0009-y.
53. Fan, W.; Liu, C.; Cao, B.; Qin, M.; Long, D.; Xiang, Z.; Zhao, A. Genome-Wide Identification and Characterization of Four Gene Families Putatively Involved in Cadmium Uptake, Translocation and Sequestration in Mulberry. *Front Plant Sci* **2018**, *9*.
54. Jia, H.; Wang, X.; Wei, T.; Zhou, R.; Muhammad, H.; Hua, L.; Ren, X.; Guo, J.; Ding, Y. Accumulation and Fixation of Cd by Tomato Cell Wall Pectin under Cd Stress. *Environ Exp Bot* **2019**, *167*, 103829, doi:https://doi.org/10.1016/j.envexpbot.2019.103829.
55. Song, J.; Feng, S.J.; Chen, J.; Zhao, W.T.; Yang, Z.M. A Cadmium Stress-Responsive Gene AtFC1 Confers Plant Tolerance to Cadmium Toxicity. *BMC Plant Biol* **2017**, *17*, 187, doi:10.1186/s12870-017-1141-0.
56. Astolfi, S.; Ortolani, M.R.; Catarcione, G.; Paolacci, A.R.; Cesco, S.; Pinton, R.; Ciaffi, M. Cadmium Exposure Affects Iron Acquisition in Barley (Hordeum Vulgare) Seedlings. *Physiol Plant* **2014**, *152*, 646–659, doi:10.1111/ppl.12207.
57. Bahmani, R.; Modareszadeh, M.; Kim, D.; Hwang, S. Overexpression of Tobacco UBQ2 Increases Cd Tolerance by Decreasing Cd Accumulation and Oxidative Stress in Tobacco and Arabidopsis. *Environ Exp Bot* **2019**, *166*, 103805, doi:https://doi.org/10.1016/j.envexpbot.2019.103805.
58. Yu, R.; Li, D.; Du, X.; Xia, S.; Liu, C.; Shi, G. Comparative Transcriptome Analysis Reveals Key Cadmium Transport-Related Genes in Roots of Two Pak Choi (Brassica Rapa L. Ssp. Chinensis) Cultivars. *BMC Genomics* **2017**, *18*, 587, doi:10.1186/s12864-017-3973-2.
59. Rui, H.; Zhang, X.; Shinwari, K.; Zheng, L.; Shen, Z.G. Comparative Transcriptomic Analysis of Two Vicia Sativa L. Varieties with Contrasting Responses to Cadmium Stress Reveals the Important Role of Metal Transporters in Cadmium Tolerance. *Plant Soil* **2018**, *423*, 1–15, doi:10.1007/s11104-017-3501-9.
60. Shu, X.; Zhang, K.; Zhang, Q.; Wang, W. Ecophysiological Responses of Jatropha Curcas L. Seedlings to Simulated Acid Rain under Different Soil Types. *Ecotoxicol Environ Saf* **2019**, *185*, 109705, doi:https://doi.org/10.1016/j.ecoenv.2019.109705.
61. Milner, M.; Mitani-Ueno, N.; Yamaji, N.; Yokosho, K.; Craft, E.; Fei, Z.; Ebbs, S.; Zambrano, M.; Kochian, L. Root and Shoot Transcriptome Analysis of Two Ecotypes of Noccaea Caerulescens Uncovers the Role of NcNramp1 in Cd Hyperaccumulation. *Plant J* **2014**, *78*, doi:10.1111/tpj.12480.
62. Zhang, J.; Zhang, C.; Huang, S.; Chang, L.; Li, J.; Tang, H.; Dey, S.; Biswas, A.; Du, D.; Li, D.; et al. Key Cannabis Salt-Responsive Genes and Pathways Revealed by Comparative Transcriptome and Physiological Analyses of Contrasting Varieties. *Agronomy* 2021, *11*.
63. Feng, Z.; Bartholomew, E.S.; Liu, Z.; Cui, Y.; Dong, Y.; Li, S.; Wu, H.; Ren, H.; Liu, X. Glandular Trichomes: New Focus on Horticultural Crops. *Hortic Res* **2021**, *8*, 158, doi:10.1038/s41438-021-00592-1.
64. Chen, H.; Li, Y.; Ma, X.; Guo, L.; He, Y.; Ren, Z.; Kuang, Z.; Zhang, X.; Zhang, Z. Analysis of Potential Strategies for Cadmium Stress Tolerance Revealed by Transcriptome Analysis of Upland Cotton. *Sci Rep* **2019**, *9*, 86, doi:10.1038/s41598-018-36228-z.
65. Wei, W.; Peng, H.; Xie, Y.; Wang, X.; Huang, R.; Chen, H.; Ji, X. The Role of Silicon in Cadmium Alleviation by Rice Root Cell Wall Retention and Vacuole Compartmentalization under Different Durations of Cd Exposure. *Ecotoxicol Environ Saf* **2021**, *226*, 112810, doi:https://doi.org/10.1016/j.ecoenv.2021.112810.

66. Ghuge, S.A.; Nikalje, G.C.; Kadam, U.S.; Suprasanna, P.; Hong, J.C. Comprehensive Mechanisms of Heavy Metal Toxicity in Plants, Detoxification, and Remediation. *J Hazard Mater* **2023**, *450*, 131039, doi:https://doi.org/10.1016/j.jhazmat.2023.131039.
67. Ahmad, J.; Ali, A.A.; Baig, M.A.; Iqbal, M.; Haq, I.; Irfan Qureshi, M. Chapter 8 - Role of Phytochelatins in Cadmium Stress Tolerance in Plants. In; Hasanuzzaman, M., Prasad, M.N.V., Fujita, M.B.T.-C.T. and T. in P., Eds.; Academic Press, 2019; pp. 185–212 ISBN 978-0-12-814864-8.
68. Hendrix, S.; Schröder, P.; Keunen, E.; Huber, C.; Cuypers, A. Chapter Six - Molecular and Cellular Aspects of Contaminant Toxicity in Plants: The Importance of Sulphur and Associated Signalling Pathways. In *Phytoremediation*; Cuypers, A., Vangronsveld, J.B.T.-A. in B.R., Eds.; Academic Press, 2017; Vol. 83, pp. 223–276 ISBN 0065-2296.
69. Mahmud, J. Al; Hasanuzzaman, M.; Nahar, K.; Bhuyan, M.H.M.B.; Fujita, M. Insights into Citric Acid-Induced Cadmium Tolerance and Phytoremediation in Brassica Juncea L.: Coordinated Functions of Metal Chelation, Antioxidant Defense and Glyoxalase Systems. *Ecotoxicol Environ Saf* **2018**, *147*, 990–1001, doi:https://doi.org/10.1016/j.ecoenv.2017.09.045.
70. Peco, J.D.; Campos, J.A.; Romero-Puertas, M.C.; Olmedilla, A.; Higueras, P.; Sandalio, L.M. Characterization of Mechanisms Involved in Tolerance and Accumulation of Cd in Biscutella Auriculata L. *Ecotoxicol Environ Saf* **2020**, *201*, 110784, doi:https://doi.org/10.1016/j.ecoenv.2020.110784.
71. Clemens, S.; Peršoh, D. Multi-Tasking Phytochelatin Synthases. *Plant Science* **2009**, *177*, 266–271, doi:10.1016/j.plantsci.2009.06.008.
72. Bellini, E.; Bandoni, E.; Giardini, S.; Sorce, C.; Spanò, C.; Bottega, S.; Fontanini, D.; Kola, A.; Valensin, D.; Bertolini, A.; et al. Glutathione and Phytochelatins Jointly Allow Intracellular and Extracellular Detoxification of Cadmium in the Liverwort Marchantia Polymorpha. *Environ Exp Bot* **2023**, *209*, doi:10.1016/j.envexpbot.2023.105303.
73. Huang, L.; Li, W.C.; Tam, N.F.Y.; Ye, Z. Effects of Root Morphology and Anatomy on Cadmium Uptake and Translocation in Rice (Oryza Sativa L.). *Journal of Environmental Sciences* **2019**, *75*, 296–306, doi:https://doi.org/10.1016/j.jes.2018.04.005.
74. Zhao, F.-J.; Wang, P. Arsenic and Cadmium Accumulation in Rice and Mitigation Strategies. *Plant Soil* **2020**, *446*, 1–21, doi:10.1007/s11104-019-04374-6.
75. Li, M.; Barbaro, E.; Bellini, E.; Saba, A.; di Toppi, L.S.; Varotto, C. Ancestral Function of the Phytochelatin Synthase C-Terminal Domain in Inhibition of Heavy Metal-Mediated Enzyme Overactivation. *J Exp Bot* **2020**, *71*, 6655–6669, doi:10.1093/jxb/eraa386.
76. Li, M.; Leso, M.; Buti, M.; Bellini, E.; Bertoldi, D.; Saba, A.; Larcher, R.; Sanità di Toppi, L.; Varotto, C. Phytochelatin Synthase De-Regulation in Marchantia Polymorpha Indicates Cadmium Detoxification as Its Primary Ancestral Function in Land Plants and Provides a Novel Visual Bioindicator for Detection of This Metal. *J Hazard Mater* **2022**, *440*, 129844, doi:https://doi.org/10.1016/j.jhazmat.2022.129844.
77. Bellini, E.; Varotto, C.; Borsò, M.; Rugnini, L.; Bruno, L.; Di Toppi, L.S. Eukaryotic and Prokaryotic Phytochelatin Synthases Differ Less in Functional Terms than Previously Thought: A Comparative Analysis of Marchantia Polymorpha and Geitlerinema Sp. PCC 7407. *Plants* **2020**, *9*, 1–12, doi:10.3390/plants9070914.
78. Bhuyan, M.H.M.B.; Parvin, K.; Mohsin, S.M.; Mahmud, J.A.; Hasanuzzaman, M.; Fujita, M. Modulation of Cadmium Tolerance in Rice: Insight into Vanillic Acid-Induced Upregulation of Antioxidant Defense and Glyoxalase Systems. *Plants* 2020, *9*.
79. Fontanini, D.; Andreucci, A.; Castiglione, M.; Basile, A.; Sorbo, S.; Petraglia, A.; Degola, F.; Bellini, E.; Bruno, L.; Varotto, C.; et al. The Phytochelatin Synthase from Nitella Mucronata (Charophyta) Plays a Role in the Homeostatic Control of Iron(II)/(III). *Plant Physiology and Biochemistry* **2018**, *127*, doi:10.1016/j.plaphy.2018.03.014.
80. Degola, F.; De Benedictis, M.; Petraglia, A.; Massimi, A.; Fattorini, L.; Sorbo, S.; Basile, A.; Sanita' di Toppi, L. A Cd/Fe/Zn-Responsive Phytochelatin Synthase Is Constitutively Present in the

Ancient Liverwort Lunularia Cruciata (L.) Dumort. *Plant Cell Physiol* **2014**, *55*, doi:10.1093/pcp/pcu117.

81. Petraglia, A.; De Benedictis, M.; Degola, F.; Pastore, G.; Calcagno, M.; Ruotolo, R.; Mengoni, A.; Sanita' di Toppi, L. The Capability to Synthesize Phytochelatins and the Presence of Constitutive and Functional Phytochelatin Synthases Are Ancestral (Plesiomorphic) Characters for Basal Land Plants. *J Exp Bot* **2014**, *65*, doi:10.1093/jxb/ert472.
82. Bellini, E.; Betti, C.; Sanità di Toppi, L. Responses to Cadmium in Early-Diverging Streptophytes (Charophytes and Bryophytes): Current Views and Potential Applications. *Plants* 2021, *10*.
83. Maresca, V.; Sorbo, S.; Loppi, S.; Funaro, F.; Del Prete, D.; Basile, A. Biological Effects from Environmental Pollution by Toxic Metals in the "Land of Fires" (Italy) Assessed Using the Biomonitor Species Lunularia Cruciata L. (Dum). *Environmental Pollution* **2020**, *265*, 115000, doi:https://doi.org/10.1016/j.envpol.2020.115000.
84. Fasani, E.; Li, M.; Varotto, C.; Furini, A.; DalCorso, G. Metal Detoxification in Land Plants: From Bryophytes to Vascular Plants. STATE of the Art and Opportunities. *Plants* 2022, *11*.
85. Bellini, E.; Maresca, V.; Betti, C.; Castiglione, M.R.; Fontanini, D.; Capocchi, A.; Sorce, C.; Borsò, M.; Bruno, L.; Sorbo, S.; et al. The Moss Leptodictyum Riparium Counteracts Severe Cadmium Stress by Activation of Glutathione Transferase and Phytochelatin Synthase, but Slightly by Phytochelatins. *Int J Mol Sci* **2020**, *21*, doi:10.3390/ijms21051583.
86. Esposito, S.; Loppi, S.; Monaci, F.; Paoli, L.; Vannini, A.; Sorbo, S.; Maresca, V.; Fusaro, L.; Karam, E.; Lentini, M.; et al. In-Field and in-Vitro Study of the Moss Leptodictyum Riparium as Bioindicator of Toxic Metal Pollution in the Aquatic Environment: Ultrastructural Damage, Oxidative Stress and HSP70 Induction. *PLoS One* **2018**, *13*, e0195717, doi:10.1371/journal.pone.0195717.
87. Landi, S.; Esposito, S. Nitrate Uptake Affects Cell Wall Synthesis and Modeling. *Front Plant Sci* **2017**, *8*.
88. Singh, S.; Prasad, S.M. Effects of 28-Homobrassinoloid on Key Physiological Attributes of Solanum Lycopersicum Seedlings under Cadmium Stress: Photosynthesis and Nitrogen Metabolism. *Plant Growth Regul* **2017**, *82*, 161–173, doi:10.1007/s10725-017-0248-5.
89. Lentini, M.; De Lillo, A.; Paradisone, V.; Liberti, D.; Landi, S.; Esposito, S. Early Responses to Cadmium Exposure in Barley Plants: Effects on Biometric and Physiological Parameters. *Acta Physiol Plant* **2018**, *40*, 178, doi:10.1007/s11738-018-2752-2.
90. Yang, Y.; Xiong, J.; Tao, L.; Cao, Z.; Tang, W.; Zhang, J.; Yu, X.; Fu, G.; Zhang, X.; Lu, Y. Regulatory Mechanisms of Nitrogen (N) on Cadmium (Cd) Uptake and Accumulation in Plants: A Review. *Science of The Total Environment* **2020**, *708*, 135186, doi:https://doi.org/10.1016/j.scitotenv.2019.135186.
91. Ben Azaiez, F.E.; Ayadi, S.; Capasso, G.; Landi, S.; Paradisone, V.; Jallouli, S.; Hammami, Z.; Chamekh, Z.; Zouari, I.; Trifa, Y.; et al. Salt Stress Induces Differentiated Nitrogen Uptake and Antioxidant Responses in Two Contrasting Barley Landraces from MENA Region. *Agronomy* 2020, *10*.
92. Jallouli, S.; Ayadi, S.; Landi, S.; Capasso, G.; Santini, G.; Chamekh, Z.; Zouari, I.; Ben Azaiez, F.E.; Trifa, Y.; Esposito, S. Physiological and Molecular Osmotic Stress Responses in Three Durum Wheat (Triticum Turgidum Ssp Durum) Genotypes. *Agronomy* 2019, *9*.
93. Lee, H.J.; Abdula, S.E.; Jang, D.W.; Park, S.-H.; Yoon, U.-H.; Jung, Y.J.; Kang, K.K.; Nou, I.S.; Cho, Y.-G. Overexpression of the Glutamine Synthetase Gene Modulates Oxidative Stress Response in Rice after Exposure to Cadmium Stress. *Plant Cell Rep* **2013**, *32*, 1521–1529, doi:10.1007/s00299-013-1464-8.
94. Saini, S.; Kaur, N.; Pati, P.K. Phytohormones: Key Players in the Modulation of Heavy Metal Stress Tolerance in Plants. *Ecotoxicol Environ Saf* **2021**, *223*, 112578, doi:https://doi.org/10.1016/j.ecoenv.2021.112578.
95. Maresca, V.; Bellini, E.; Landi, S.; Capasso, G.; Cianciullo, P.; Carraturo, F.; Pirintsos, S.; Sorbo, S.; Sanità di Toppi, L.; Esposito, S.; et al. Biological Responses to Heavy Metal Stress in the Moss

Leptodictyum Riparium (Hedw.) Warnst. *Ecotoxicol Environ Saf* **2022**, *229*, 1–7, doi:10.1016/j.ecoenv.2021.113078.
96. Meister, A. Glutathione Metabolism. *Methods Enzymol* **1995**, *251*, 3–7, doi:10.1016/0076-6879(95)51106-7.
97. Pasternak, M.; Lim, B.; Wirtz, M.; Hell, R.; Cobbett, C.S.; Meyer, A.J. Restricting Glutathione Biosynthesis to the Cytosol Is Sufficient for Normal Plant Development. *The Plant Journal* **2008**, *53*, 999–1012, doi:https://doi.org/10.1111/j.1365-313X.2007.03389.x.
98. BELIN, C.; BASHANDY, T.; CELA, J.; DELORME-HINOUX, V.; RIONDET, C.; REICHHELD, J.P. A Comprehensive Study of Thiol Reduction Gene Expression under Stress Conditions in Arabidopsis Thaliana. *Plant Cell Environ* **2015**, *38*, 299–314, doi:https://doi.org/10.1111/pce.12276.
99. Xiang, C.; Oliver, D.J. Glutathione Metabolic Genes Coordinately Respond to Heavy Metals and Jasmonic Acid in Arabidopsis. *Plant Cell* **1998**, *10*, 1539–1550, doi:10.1105/tpc.10.9.1539.
100. Wachter, A.; Wolf, S.; Steininger, H.; Bogs, J.; Rausch, T. Differential Targeting of GSH1 and GSH2 Is Achieved by Multiple Transcription Initiation: Implications for the Compartmentation of Glutathione Biosynthesis in the Brassicaceae. *The Plant Journal* **2005**, *41*, 15–30, doi:https://doi.org/10.1111/j.1365-313X.2004.02269.x.
101. Yang, Y.; Lenherr, E.D.; Gromes, R.; Wang, S.; Wirtz, M.; Hell, R.; Peskan-Berghöfer, T.; Scheffzek, K.; Rausch, T. Plant Glutathione Biosynthesis Revisited: Redox-Mediated Activation of Glutamylcysteine Ligase Does Not Require Homo-Dimerization. *Biochemical Journal* **2019**, *476*, 1191–1203, doi:10.1042/BCJ20190072.
102. Watson, S.J.; Sowden, R.G.; Jarvis, P. Abiotic Stress-Induced Chloroplast Proteome Remodelling: A Mechanistic Overview. *J Exp Bot* **2018**, *69*, 2773–2781, doi:10.1093/jxb/ery053.
103. Kopriva, S.; Rennenberg, H. Control of Sulphate Assimilation and Glutathione Synthesis: Interaction with N and C Metabolism. *J Exp Bot* **2004**, *55*, 1831–1842, doi:10.1093/jxb/erh203.
104. Strohm, M.; Jouanin, L.; Kunert, K.J.; Pruvost, C.; Polle, A.; Foyer, C.H.; Rennenberg, H. Regulation of Glutathione Synthesis in Leaves of Transgenic Poplar (Populus Tremula X P. Alba) Overexpressing Glutathione Synthetase. *The Plant Journal* **1995**, *7*, 141–145, doi:https://doi.org/10.1046/j.1365-313X.1995.07010141.x.
105. Gill, S.S.; Anjum, N.A.; Hasanuzzaman, M.; Gill, R.; Trivedi, D.K.; Ahmad, I.; Pereira, E.; Tuteja, N. Glutathione and Glutathione Reductase: A Boon in Disguise for Plant Abiotic Stress Defense Operations. *Plant Physiology and Biochemistry* **2013**, *70*, 204–212, doi:https://doi.org/10.1016/j.plaphy.2013.05.032.
106. Sairam, R.K.; Saxena, D.C. Oxidative Stress and Antioxidants in Wheat Genotypes: Possible Mechanism of Water Stress Tolerance. *J Agron Crop Sci* **2000**, *184*, 55–61.
107. Romero-Puertas, M.C.; Corpas, F.J.; Sandalio, L.M.; Leterrier, M.; Rodríguez-Serrano, M.; Del Río, L.A.; Palma, J.M. Glutathione Reductase from Pea Leaves: Response to Abiotic Stress and Characterization of the Peroxisomal Isozyme. *New Phytol* **2006**, *170*, 43–52, doi:10.1111/j.1469-8137.2006.01643.x.
108. Marty, L.; Siala, W.; Schwarzländer, M.; Fricker, M.D.; Wirtz, M.; Sweetlove, L.J.; Meyer, Y.; Meyer, A.J.; Reichheld, J.-P.; Hell, R. The NADPH-Dependent Thioredoxin System Constitutes a Functional Backup for Cytosolic Glutathione Reductase in Arabidopsis. *Proceedings of the National Academy of Sciences* **2009**, *106*, 9109–9114, doi:10.1073/pnas.0900206106.
109. Kataya, A.R.A.; Reumann, S. Arabidopsis Glutathione Reductase 1 Is Dually Targeted to Peroxisomes and the Cytosol. *Plant Signal Behav* **2010**, *5*, 171–175, doi:10.4161/psb.5.2.10527.
110. Delorme-Hinoux, V.; Bangash, S.A.K.; Meyer, A.J.; Reichheld, J.-P. Nuclear Thiol Redox Systems in Plants. *Plant Science* **2016**, *243*, 84–95, doi:https://doi.org/10.1016/j.plantsci.2015.12.002.
111. Liu, L.; Li, W.; Song, W.; Guo, M. Remediation Techniques for Heavy Metal-Contaminated Soils: Principles and Applicability. *Science of The Total Environment* **2018**, *633*, 206–219, doi:https://doi.org/10.1016/j.scitotenv.2018.03.161.
112. Rizwan, M.; Ali, S.; Zia ur Rehman, M.; Rinklebe, J.; Tsang, D.C.W.; Bashir, A.; Maqbool, A.; Tack, F.M.G.; Ok, Y.S. Cadmium Phytoremediation Potential of Brassica Crop Species: A

Review. *Science of The Total Environment* **2018**, *631–632*, 1175–1191, doi:https://doi.org/10.1016/j.scitotenv.2018.03.104.

113. Luo, Z.-B.; He, J.; Polle, A.; Rennenberg, H. Heavy Metal Accumulation and Signal Transduction in Herbaceous and Woody Plants: Paving the Way for Enhancing Phytoremediation Efficiency. *Biotechnol Adv* **2016**, *34*, 1131–1148, doi:https://doi.org/10.1016/j.biotechadv.2016.07.003.
114. Krämer, U. Metal Hyperaccumulation in Plants. *Annu Rev Plant Biol* **2010**, *61*, 517–534, doi:10.1146/annurev-arplant-042809-112156.
115. Meighan, M.M.; Fenus, T.; Karey, E.; MacNeil, J. The Impact of EDTA on the Rate of Accumulation and Root/Shoot Partitioning of Cadmium in Mature Dwarf Sunflowers. *Chemosphere* **2011**, *83*, 1539–1545, doi:10.1016/j.chemosphere.2011.01.035.
116. Marmiroli, M.; Visioli, G.; Maestri, E.; Marmiroli, N. Correlating SNP Genotype with the Phenotypic Response to Exposure to Cadmium in Populus Spp. *Environ Sci Technol* **2011**, *45*, 4497–4505, doi:10.1021/es103708k.
117. Pietrini, F.; Zacchini, M.; Iori, V.; Pietrosanti, L.; Bianconi, D.; Massacci, A. Screening of Poplar Clones for Cadmium Phytoremediation Using Photosynthesis, Biomass and Cadmium Content Analyses. *Int J Phytoremediation* **2010**, *12*, 105–120, doi:10.1080/15226510902767163.
118. Wu, F.; Yang, W.; Zhang, J.; Zhou, L. Cadmium Accumulation and Growth Responses of a Poplar (Populus DeltoidsxPopulus Nigra) in Cadmium Contaminated Purple Soil and Alluvial Soil. *J Hazard Mater* **2010**, *177*, 268–273, doi:10.1016/j.jhazmat.2009.12.028.
119. Di Lonardo, S.; Capuana, M.; Arnetoli, M.; Gabbrielli, R.; Gonnelli, C. Exploring the Metal Phytoremediation Potential of Three Populus Alba L. Clones Using an in Vitro Screening. *Environmental Science and Pollution Research* **2011**, *18*, 82–90, doi:10.1007/s11356-010-0354-7.
120. Redjala, T.; Zelko, I.; Sterckeman, T.; Legué, V.; Lux, A. Relationship between Root Structure and Root Cadmium Uptake in Maize. *Environ Exp Bot* **2011**, *71*, 241–248, doi:https://doi.org/10.1016/j.envexpbot.2010.12.010.
121. Thakur, S.; Singh, L.; Wahid, Z.; Siddiqui, M.; Atnaw, S.; Md Din, M.F. Plant-Driven Removal of Heavy Metals from Soil: Uptake, Translocation, Tolerance Mechanism, Challenges, and Future Perspectives. *Environ Monit Assess* **2016**, *188*, doi:10.1007/s10661-016-5211-9.
122. Kumar Yadav, K.; Gupta, N.; Kumar, A.; Reece, L.M.; Singh, N.; Rezania, S.; Ahmad Khan, S. Mechanistic Understanding and Holistic Approach of Phytoremediation: A Review on Application and Future Prospects. *Ecol Eng* **2018**, *120*, 274–298, doi:https://doi.org/10.1016/j.ecoleng.2018.05.039.
123. Laghlimi, M.; Baghdad, B.; EL Hadi, H.; Bouabdli, A. Phytoremediation Mechanisms of Heavy Metal Contaminated Soils: A Review. *Open J Ecol* **2015**, *5*, 375–388, doi:10.4236/oje.2015.58031.
124. FAHR, M.; Laplaze, L.; BENDAOU, N.; HOCHER, V.; EL MZIBRI, M.; BOGUSZ, D.; SMOUNI, A. Effect of Lead on Root Growth. *Front Plant Sci* **2013**, *4*.
125. Gupta, N.; Yadav, K.K.; Kumar, V.; Kumar, S.; Chadd, R.P.; Kumar, A. Trace Elements in Soil-Vegetables Interface: Translocation, Bioaccumulation, Toxicity and Amelioration - A Review. *Sci Total Environ* **2019**, *651*, 2927–2942, doi:10.1016/j.scitotenv.2018.10.047.
126. Gupta, N.; Ram, H.; Kumar, B. Mechanism of Zinc Absorption in Plants: Uptake, Transport, Translocation and Accumulation. *Rev Environ Sci Biotechnol* **2016**, *15*, 89–109, doi:10.1007/s11157-016-9390-1.
127. Kim, R.-Y.; Yoon, J.-K.; Kim, T.-S.; Yang, J.; Owens, G.; Kim, K.-R. Bioavailability of Heavy Metals in Soils: Definitions and Practical Implementation—a Critical Review. *Environ Geochem Health* **2015**, *37*, doi:10.1007/s10653-015-9695-y.
128. Sebastian, A.; Prasad, M.N. V Exogenous Citrate and Malate Alleviate Cadmium Stress in Oryza Sativa L.: Probing Role of Cadmium Localization and Iron Nutrition. *Ecotoxicol Environ Saf* **2018**, *166*, 215–222, doi:https://doi.org/10.1016/j.ecoenv.2018.09.084.
129. Wu, Z.; Zhao, X.; Sun, X.; Tan, Q.; Tang, Y.; Nie, Z.; Hu, C. Xylem Transport and Gene Expression Play Decisive Roles in Cadmium Accumulation in Shoots of Two Oilseed Rape Cultivars

(Brassica Napus). *Chemosphere* **2015**, *119*, 1217–1223, doi:https://doi.org/10.1016/j.chemosphere.2014.09.099.
130. Hall, J.L. Cellular Mechanisms for Heavy Metal Detoxification and Tolerance. *J Exp Bot* **2002**, *53*, 1–11, doi:10.1093/jexbot/53.366.1.
131. Kumar, A.; Dubey, A.; Kumar, V.; Ansari, M.; Narayan, S.; . M.; Kumar, S.; Pandey, V.; Shirke, P.; Pande, V.; et al. Over-Expression of Chickpea Glutaredoxin (CaGrx) Provides Tolerance to Heavy Metals by Reducing Metal Accumulation and Improved Physiological and Antioxidant Defence System. *Ecotoxicol Environ Saf* **2020**, *192*, 110252, doi:10.1016/j.ecoenv.2020.110252.
132. Cointry, V.; Vert, G. The Bifunctional Transporter-receptor IRT1 at the Heart of Metal Sensing and Signaling. *New Phytologist* **2019**, *223*, doi:10.1111/nph.15826.
133. Narayan, O.; Verma, N.; Jogawat, A.; Dua, M.; Johri, A. *Role of Sulphate Transporter (PiSulT) of Endophytic Fungus Serendipita Indica in Plant Growth and Development*; 2020;
134. Narayan, O.; Verma, N.; Jogawat, A.; Dua, M.; Johri, A. Sulfur Transfer from the Endophytic Fungus Serendipita Indica Improves Maize Growth and Requires the Sulfate Transporter SiSulT. *Plant Cell* **2021**, *33*, doi:10.1093/plcell/koab006.
135. Yadav, B.; Jogawat, A.; Lal, S.K.; Lakra, N.; Mehta, S.; Shabek, N.; Narayan, O. Plant Mineral Transport Systems and the Potential for Crop Improvement. *Planta* **2021**, *253*, doi:10.1007/s00425-020-03551-7.
136. Dubeaux, G.; Julie, N.; Zelazny, E.; Vert, G. Metal Sensing by the IRT1 Transporter-Receptor Orchestrates Its Own Degradation and Plant Metal Nutrition. *Mol Cell* **2018**, *69*, 953-964.e5, doi:10.1016/j.molcel.2018.02.009.
137. Wu, Q.; Huang, L.; su, N.; Shabala, L.; Wang, H.; Huang, X.; Wen, R.; Yu, M.; Cui, J.; Shabala, S. Calcium-Dependent Hydrogen Peroxide Mediates Hydrogen-Rich Water-Reduced Cadmium Uptake in Plant Roots. *Plant Physiol* **2020**, *183*, pp.00377.2020, doi:10.1104/pp.20.00377.
138. Takahashi, R.; Ishimaru, Y.; Senoura, T.; Shimo, H.; Ishikawa, S.; Arao, T.; Nakanishi, H.; Nishizawa, N. The OsNRAMP1 Iron Transporter Is Involved in Cd Accumulation in Rice. *J Exp Bot* **2011**, *62*, 4843–4850, doi:10.1093/jxb/err136.
139. Lang, M.; Hao, M.; Fan, Q.; Wang, W.; Mo, S.; Zhao, W.; Zhou, J. Functional Characterization of BjCET3 and BjCET4, Two New Cation-Efflux Transporters from Brassica Juncea L. *J Exp Bot* **2011**, *62*, 4467–4480, doi:10.1093/jxb/err137.
140. Li, J.; Wang, Y.; Zheng, L.; Li, Y.; Zhou, X.; Li, J.; Gu, D.; Xu, E.; Lu, Y.; Chen, X.; et al. The Intracellular Transporter AtNRAMP6 Is Involved in Fe Homeostasis in Arabidopsis. *Front Plant Sci* **2019**, *10*.
141. Fu, S.; Lu, Y.; Zhang, X.; Yang, G.; Chao, D.; Wang, Z.; Shi, M.; Chen, J.; Chao, D.-Y.; Li, R.; et al. The ABC Transporter ABCG36 Is Required for Cadmium Tolerance in Rice. *J Exp Bot* **2019**, *70*, 5909–5918, doi:10.1093/jxb/erz335.
142. Wang, H.; Liu, Y.; Peng, Z.; Li, J.; Huang, W.; Liu, Y.; Wang, X.; Xie, S.; Sun, L.; Han, E.; et al. Ectopic Expression of Poplar ABC Transporter PtoABCG36 Confers Cd Tolerance in Arabidopsis Thaliana. *Int J Mol Sci* 2019, *20*.
143. Kim, D.Y.; Bovet, L.; Maeshima, M.; Martinoia, E.; Lee, Y. The ABC Transporter AtPDR8 Is a Cadmium Extrusion Pump Conferring Heavy Metal Resistance. *Plant Journal* **2007**, *50*, 207–218, doi:10.1111/j.1365-313X.2007.03044.x.
144. Brunetti, P.; Zanella, L.; De Paolis, A.; Di Litta, D.; Cecchetti, V.; Falasca, G.; Barbieri, M.; Altamura, M.M.; Costantino, P.; Cardarelli, M. Cadmium-Inducible Expression of the ABC-Type Transporter AtABCC3 Increases Phytochelatin-Mediated Cadmium Tolerance in Arabidopsis. *J Exp Bot* **2015**, *66*, 3815–3829, doi:10.1093/jxb/erv185.
145. Song, W.-Y.; Park, J.; Mendoza Cozatl, D.; Grotemeyer, M.; Shim, D.; Hörtensteiner, S.; Geisler, M.; Weder, B.; Rea, P.; Rentsch, D.; et al. Arsenic Tolerance in Arabidopsis Is Mediated by Two ABCC-Type Phytochelatin Transporters. *Proc Natl Acad Sci U S A* **2010**, *107*, 21187–21192, doi:10.1073/pnas.1013964107.

146. Neri, A.; Traversari, S.; Andreucci, A.; Francini, A.; Sebastiani, L. The Role of Aquaporin Overexpression in the Modulation of Transcription of Heavy Metal Transporters under Cadmium Treatment in Poplar. *Plants* **2021**, *10*, 1–17, doi:10.3390/plants10010054.
147. Mikkelsen, M.; Pedas, P.; Stokholm, M.; Vincze, E.; Mills, R.; Borg, S.; Møller, A.; Schjoerring, J.; Williams, L.; Baekgaard, L.; et al. Barley HvHMA1 Is a Heavy Metal Pump Involved in Mobilizing Organellar Zn and Cu and Plays a Role in Metal Loading into Grains. *PLoS One* **2012**, *7*, e49027, doi:10.1371/journal.pone.0049027.
148. Eren, E.; Argüello, J. Arabidopsis HMA2, a Divalent Heavy Metal-Transporting PIB-Type ATPase, Is Involved in Cytoplasmic Zn2+ Homeostasis. *Plant Physiol* **2004**, *136*, 3712–3723, doi:10.1104/pp.104.046292.
149. Sinclair, S.; Senger, T.; Talke, I.; Cobbett, C.; Haydon, M.; Kraemer, U. Systemic Upregulation of MTP2- and HMA2-Mediated Zn Partitioning to the Shoot Supplements Local Zn Deficiency Responses of Arabidopsis. *Plant Cell* **2018**, doi:10.1105/tpc.18.00207.
150. Morel-Rouhier, M.; Crouzet, J.; Gravot, A.; Auroy, P.; Leonhardt, N.; Vavasseur, A.; Richaud, P. AtHMA3, a P1B-ATPase Allowing Cd/Zn/Co/Pb Vacuolar Storage in Arabidopsis. *Plant Physiol* **2008**, *149*, 894–904, doi:10.1104/pp.108.130294.
151. Sasaki, A.; Yamaji, N. Overexpression of OsHMA3 Enhances Cd Tolerance and Expression of Zn Transporter Genes in Rice. *J Exp Bot* **2014**, *65*, doi:10.1093/jxb/eru340.
152. Satoh-Nagasawa, N.; Mori, M.; Nakazawa, N.; Kawamoto, T.; Nagato, Y.; Sakurai, K.; Takahashi, H.; Watanabe, A.; Akagi, H. Mutations in Rice (Oryza Sativa) Heavy Metal ATPase 2 (OsHMA2) Restrict the Translocation of Zinc and Cadmium. *Plant Cell Physiol* **2012**, *53*, 213–224, doi:10.1093/pcp/pcr166.
153. de caroli, M.; Furini, A.; Dalcorso, G.; Rojas, M.; Di Sansebastiano, G. Endomembrane Reorganization Induced by Heavy Metals. *Plants* **2020**, *9*, 482, doi:10.3390/plants9040482.
154. The Plant List (accessed on 1 January 2024).
155. Naithani HB, N.S. *Indian Poplars with Special Reference to Indigenous Species*; 2012;
156. Naithani, H.B.; Chandra, S.; Pal, M. Indian Poplars with Special Reference to Indigenous Species. *The Indian Forester* **2001**, *127*, 230–237.
157. Eckenwalder, J.E. Taxonomic Signal and Noise in Multivariate Interpopulational Relationships in Populus Mexicana (Salicaceae). *Syst Bot* **1996**, *21*, 261–271, doi:10.2307/2419658.
158. Cronk, Q.C.B. Plant Eco-Devo: The Potential of Poplar as a Model Organism. *New Phytol* **2005**, *166*, 39–48, doi:10.1111/j.1469-8137.2005.01369.x.
159. Stobrawa, K. Poplars (Populus Spp.): Ecological Role, Applications and Scientific Perspectives in the 21st Century (Review Paper). *Balt For* **2014**, *20*, 204–213.
160. Schwarz, M.; Phillips, C.; Marden, M.; McIvor, I.; Douglas, G.; Watson, A. Modelling of Root Reinforcement and Erosion Control by 'Veronese' Poplar on Pastoral Hill Country in New Zealand. *N Z J For Sci* **2016**, *46*, doi:10.1186/s40490-016-0060-4.
161. Whitham, T.G.; Difazio, S.P.; Schweitzer, J.A.; Shuster, S.M.; Allan, G.J.; Bailey, J.K.; Woolbright, S.A. Extending Genomics to Natural Communities and Ecosystems. *Science* **2008**, *320*, 492–495, doi:10.1126/science.1153918.
162. Kivinen, S.; Koivisto, E.; Keski-Saari, S.; Poikolainen, L.; Tanhuanpää, T.; Kuzmin, A.; Viinikka, A.; Heikkinen, R.; Pykälä, J.; Virkkala, R.; et al. A Keystone Species, European Aspen (Populus Tremula L.), in Boreal Forests: Ecological Role, Knowledge Needs and Mapping Using Remote Sensing. *For Ecol Manage* **2020**, *462*, 118008, doi:10.1016/j.foreco.2020.118008.
163. Lemus, R.; Lal, R. Bioenergy Crops and Carbon Sequestration. *Critical Reviews in Plant Sciences - CRIT REV PLANT SCI* **2005**, *24*, 1–21, doi:10.1080/07352680590910393.
164. Zhang, X.; Hung, T.M.; Phuong, P.T.; Ngoc, T.M.; Min, B.-S.; Song, K.-S.; Seong, Y.H.; Bae, K. Anti-Inflammatory Activity of Flavonoids from Populus Davidiana. *Arch Pharm Res* **2006**, *29*, 1102–1108, doi:10.1007/BF02969299.

165. Zhang, X.; Thuong, P.T.; Min, B.-S.; Ngoc, T.M.; Hung, T.M.; Lee, I.S.; Na, M.; Seong, Y.-H.; Song, K.-S.; Bae, K. Phenolic Glycosides with Antioxidant Activity from the Stem Bark of Populus Davidiana. *J Nat Prod* **2006**, *69*, 1370–1373, doi:10.1021/np060237u.
166. Vardar-Ünlü, G.; Silici, S.; Unlu, M. Composition and in Vitro Antimicobial Activity of Populus Buds and Poplar-Type Propolis. *World J Microbiol Biotechnol* **2008**, *24*, 1011–1017, doi:10.1007/s11274-007-9566-5.
167. Liu, Y.-Y.; Huang, D.-L.; Dong, Y.; Qin, D.-P.; Yan, Y.-M.; Cheng, Y.-X. Neuroprotective Norsesquiterpenoids and Triterpenoids from Populus Euphratica Resins. *Molecules* **2019**, *24*, doi:10.3390/molecules24234379.
168. Belanger, A.; Grenier, A.; Simard, F.; Gendreau, I.; Pichette, A.; Legault, J.; Pouliot, R. Dihydrochalcone Derivatives from Populus Balsamifera L. Buds for the Treatment of Psoriasis. *Int J Mol Sci* **2019**, *21*, 256, doi:10.3390/ijms21010256.
169. Devappa, R.K.; Rakshit, S.; Dekker, R. Forest Biorefinery: Potential of Poplar Phytochemicals as Value-Added Co-Products. *Biotechnol Adv* **2015**, *33*, 681–716, doi:10.1016/j.biotechadv.2015.02.01.
170. Sannigrahi, P.; Ragauskas, A.; Tuskan, G. Poplar as a Feedstock for Biofuels: A Review of Compositional Characteristics. *Biofuels, Bioproducts and Biorefining* **2010**, *4*, 209–226, doi:10.1002/bbb.206.
171. Pivetz, B. Phytoremediation of Contaminated Soil and Ground Water at Hazardous Waste Sites. *EPA Ground Water Issue* **2001**, 1–36.
172. Hanikenne, M.; Nouet, C. Metal Hyperaccumulation and Hypertolerance: A Model for Plant Evolutionary Genomics. *Curr Opin Plant Biol* **2011**, *14*, 252–259, doi:https://doi.org/10.1016/j.pbi.2011.04.003.
173. Lu, L.; Tian, S.; Yang, X.; Wang, X.; Brown, P.; Li, T.; He, Z. Enhanced Root-to-Shoot Translocation of Cadmium in the Hyperaccumulating Ecotype of Sedum Alfredii. *J Exp Bot* **2008**, *59*, 3203–3213, doi:10.1093/jxb/ern174.
174. Meighan, M.M.; Fenus, T.; Karey, E.; MacNeil, J. The Impact of EDTA on the Rate of Accumulation and Root/Shoot Partitioning of Cadmium in Mature Dwarf Sunflowers. *Chemosphere* **2011**, *83*, 1539–1545, doi:10.1016/j.chemosphere.2011.01.035.
175. Pulford, I.D.; Watson, C. Phytoremediation of Heavy Metal-Contaminated Land by Trees - A Review. *Environ Int* **2003**, *29*, 529–540, doi:10.1016/S0160-4120(02)00152-6.
176. Sebastiani, L.; Scebba, F.; Tognetti, R. Heavy Metal Accumulation and Growth Responses in Poplar Clones Eridano (Populus Deltoides × Maximowiczii) and I-214 (P. × Euramericana) Exposed to Industrial Waste. *Environ Exp Bot* **2004**, *52*, 79–88, doi:https://doi.org/10.1016/j.envexpbot.2004.01.003.
177. Ali, H.; Khan, E.; Sajad, M.A. Phytoremediation of Heavy Metals—Concepts and Applications. *Chemosphere* **2013**, *91*, 869–881, doi:https://doi.org/10.1016/j.chemosphere.2013.01.075.
178. Di Baccio, D.; Castagna, A.; Tognetti, R.; Ranieri, A.; Sebastiani, L. Differential Ozone Sensitivity Interferes with Cadmium Stress in Poplar Clones. *Biol Plant* **2012**, *57*, 313, doi:10.1007/s10535-012-0274-0.
179. Di Baccio, D.; Castagna, A.; Tognetti, R.; Ranieri, A.; Sebastiani, L. Early Responses to Cadmium of Two Poplar Clones That Differ in Stress Tolerance. *J Plant Physiol* **2014**, *171*, 1693–1705, doi:10.1016/j.jplph.2014.08.007.
180. Romeo, S.; Francini, A.; Ariani, A.; Sebastiani, L. Phytoremediation of Zn: Identify the Diverging Resistance, Uptake and Biomass Production Behaviours of Poplar Clones under High Zinc Stress. *Water Air Soil Pollut* **2014**, *225*, 1–12, doi:10.1007/s11270-013-1813-9.
181. Elobeid, M.; Göbel, C.; Feussner, I.; Polle, A. Cadmium Interferes with Auxin Physiology and Lignification in Poplar. *J Exp Bot* **2011**, *63*, 1413–1421, doi:10.1093/jxb/err384.
182. He, J.; Qin, J.; Long, L.; Ma, Y.; Li, H.; Li, K.; Jiang, X.; Liu, T.-X.; Polle, A.; Liang, Z.; et al. Net Cadmium Flux and Accumulation Reveal Tissue-Specific Oxidative Stress and Detoxification in Populus × Canescens. *Physiol Plant* **2011**, *143*, 50–63, doi:10.1111/j.1399-3054.2011.01487.x.

183. Laureysens, I.; Blust, R.; De Temmerman, L.; Lemmens, C.; Ceulemans, R. Clonal Variation in Heavy Metal Accumulation and Biomass Production in a Poplar Coppice Culture: I. Seasonal Variation in Leaf, Wood and Bark Concentrations. *Environmental Pollution* **2004**, *131*, 485–494, doi:https://doi.org/10.1016/j.envpol.2004.02.009.
184. Laureysens, I.; De Temmerman, L.; Hastir, T.; Van Gysel, M.; Ceulemans, R. Clonal Variation in Heavy Metal Accumulation and Biomass Production in a Poplar Coppice Culture. II. Vertical Distribution and Phytoextraction Potential. *Environmental Pollution* **2005**, *133*, 541–551, doi:https://doi.org/10.1016/j.envpol.2004.06.013.
185. Milner, M.; Kochian, L. Milner, M.J. & Kocian, L.V. Investigating Heavy-Metal Hyperaccumulation Using Thlaspi Caerulescens as a Model System. Ann. Bot. (Lond.) 102, 3-13. *Ann Bot* **2008**, *102*, 3–13, doi:10.1093/aob/mcn063.
186. Pietrini, F.; Zacchini, M.; Iori, V.; Pietrosanti, L.; Bianconi, D.; Massacci, A. Screening of Poplar Clones for Cadmium Phytoremediation Using Photosynthesis, Biomass and Cadmium Content Analyses. *Int J Phytoremediation* **2010**, *12*, 105–120, doi:10.1080/15226510902767163.
187. Rockwood, D.; Naidu, C. V; Carter, D.R.; Rahmani, M.; Spriggs, T.A.; Lin, C.; Alker, G.R.; Isebrands, J.G.; Segrest, S. Short-Rotation Woody Crops and Phytoremediation: Opportunities for Agroforestry? *Agroforestry Systems* **2004**, *61–62*, 51–63, doi:10.1023/B:AGFO.0000028989.72186.e6.
188. Tuskan, G.A.; Difazio, S.; Jansson, S.; Bohlmann, J.; Grigoriev, I.; Hellsten, U.; Putnam, N.; Ralph, S.; Rombauts, S.; Salamov, A.; et al. The Genome of Black Cottonwood, Populus Trichocarpa (Torr. & Gray). *Science* **2006**, *313*, 1596–1604, doi:10.1126/science.1128691.
189. Castiglione, S.; Todeschini, V.; Franchin, C.; Torrigiani, P.; Gastaldi, D.; Cicatelli, A.; Rinaudo, C.; Berta, G.; Biondi, S.; Lingua, G. Clonal Differences in Survival Capacity, Copper and Zinc Accumulation, and Correlation with Leaf Polyamine Levels in Poplar: A Large-Scale Field Trial on Heavily Polluted Soil. *Environmental Pollution* **2009**, *157*, 2108–2117, doi:https://doi.org/10.1016/j.envpol.2009.02.011.
190. Marmiroli, M.; Visioli, G.; Maestri, E.; Marmiroli, N. Correlating SNP Genotype with the Phenotypic Response to Exposure to Cadmium in Populus Spp. *Environ Sci Technol* **2011**, *45*, 4497–4505, doi:10.1021/es103708k.
191. Durand, T.C.; Sergeant, K.; Planchon, S.; Carpin, S.; Label, P.; Morabito, D.; Hausman, J.-F.; Renaut, J. Acute Metal Stress in Populus Tremula x P. Alba (717-1B4 Genotype): Leaf and Cambial Proteome Changes Induced by Cadmium 2+. *Proteomics* **2010**, *10*, 349–368, doi:10.1002/pmic.200900484.
192. Kieffer, P.; Dommes, J.; Hoffmann, L.; Hausman, J.-F.; Renaut, J. Quantitative Changes in Protein Expression of Cadmium-Exposed Poplar Plants. *Proteomics* **2008**, *8*, 2514–2530, doi:10.1002/pmic.200701110.
193. Polle, A.; Klein, T.; Kettner, C. Impact of Cadmium on Young Plants of Populus Euphratica and P. × Canescens, Two Poplar Species That Differ in Stress Tolerance. *New For (Dordr)* **2013**, *44*, 13–22, doi:10.1007/s11056-011-9301-9.
194. Zacchini, M.; Iori, V.; Mugnozza, G.; Pietrini, F.; Massacci, A. Cadmium Accumulation and Tolerance in Populus Nigra and Salix Alba. *Biol Plant* **2011**, *55*, 383–386, doi:10.1007/s10535-011-0060-4.
195. He, J.; Ma, C.; Ma, Y.; Li, H.; Kang, J.; Liu, T.; Polle, A.; Peng, C.; Luo, Z. Bin Cadmium Tolerance in Six Poplar Species. *Environmental Science and Pollution Research* **2013**, *20*, 163–174, doi:10.1007/s11356-012-1008-8.
196. Cao, X.; Jia, J.; Li, H.; Li, M.; Luo, J.; Liang, Z.; Liu, T.-X.; Liu, W.; Peng, C.; Luo, Z.-B. Photosynthesis, Water Use Efficiency and Stable Carbon Isotope Composition Are Associated with Anatomical Properties of Leaf and Xylem in Six Poplar Species. *Plant Biol (Stuttg)* **2011**, *14*, 612–620, doi:10.1111/j.1438-8677.2011.00531.x.
197. Hoffmann, E. de; Stroobant, V. *Mass Spectrometry: Principles and Applications*; J. Wiley Chichester, West Sussex, Engl. ; Hoboken, N.., Ed.; 3rd editio.; 2007;

198. Carraro, S.; Giordano, G.; Reniero, F.; Perilongo, G.; Baraldi, E. Metabolomics: A New Frontier for Research in Pediatrics. *J Pediatr* **2009**, *154*, 638–644, doi:10.1016/j.jpeds.2009.01.014.
199. Emwas, A.-H.; Salek, R.; Griffin, J.; Merzaban, J. NMR-Based Metabolomics in Human Disease Diagnosis: Applications, Limitations, and Recommendations. *Metabolomics* **2013**, *9*, doi:10.1007/s11306-013-0524-y.
200. Fenn, J.B.; Mann, M.; Meng, C.K.; Wong, S.F.; Whitehouse, C.M. Electrospray Ionization for Mass Spectrometry of Large Biomolecules. *Science* **1989**, *246*, 64–71, doi:10.1126/science.2675315.
201. Bruins, A.P. Mechanistic Aspects of Electrospray Ionization. *J Chromatogr A* **1998**, *794*, 345–357, doi:https://doi.org/10.1016/S0021-9673(97)01110-2.
202. Bruins, A.P.; Covey, T.R.; Henion, J.D. Ion Spray Interface for Combined Liquid Chromatography/Atmospheric Pressure Ionization Mass Spectrometry. *Anal Chem* **1987**, *59*, 2642–2646, doi:10.1021/ac00149a003.
203. Banerjee, S.; Mazumdar, S. Electrospray Ionization Mass Spectrometry: A Technique to Access the Information beyond the Molecular Weight of the Analyte. *Int J Anal Chem* **2012**, *2012*, 282574, doi:10.1155/2012/282574.
204. Pitt, J.J. Principles and Applications of Liquid Chromatography-Mass Spectrometry in Clinical Biochemistry. *Clin Biochem Rev* **2009**, *30*, 19–34.
205. McMaster, M.C. *LC/MS: A Practical User's Guide*; John Wiley, Hoboken, N.J., Ed.; 2005; ISBN 9780471655312.
206. Schmidt, M.L. QuEChERS (Quick, Easy, Cheap, Effective, Rugged, and Safe) Extraction – Gas Chromatography for the Analysis of Drugs.; 2015.
207. Simmons, D.B.D.; Hayward, A.R.; Hutchinson, T.C.; Emery, R.J.N. Identification and Quantification of Glutathione and Phytochelatins from Chlorella Vulgaris by RP-HPLC ESI-MS/MS and Oxygen-Free Extraction. *Anal Bioanal Chem* **2009**, *395*, 809–817, doi:10.1007/s00216-009-3016-1.
208. Mou, R.-X.; Cao, Z.-Y.; Lin, X.-Y.; Wu, L.; Cao, Z.-Z.; Zhu, Z.-W.; Chen, M.-X. Characterization of the Phytochelatins and Their Derivatives in Rice Exposed to Cadmium Based on High-Performance Liquid Chromatography Coupled with Data-Dependent Hybrid Linear Ion Trap Orbitrap Mass Spectrometry. *Rapid Commun Mass Spectrom* **2016**, *30*, 1891–1900, doi:10.1002/rcm.7669.
209. Sneller, F.E.C.; Van Heerwaarden, L.M.; Kraaijeveld-Smit, F.J.L.; Ten Bookum, W.M.; Koevoets, P.L.M.; Schat, H.; Verkleij, J.A.C. Toxicity of Arsenate in Silene Vulgaris, Accumulation and Degradation of Arsenate-Induced Phytochelatins. *New Phytologist* **1999**, *144*, 223–232, doi:10.1046/j.1469-8137.1999.00512.x.
210. Minocha, R.; Thangavel, P.; Dhankher, O.P.; Long, S. Separation and Quantification of Monothiols and Phytochelatins from a Wide Variety of Cell Cultures and Tissues of Trees and Other Plants Using High Performance Liquid Chromatography. *J Chromatogr A* **2008**, *1207*, 72–83, doi:10.1016/j.chroma.2008.08.023.
211. Bräutigam, A.; Wesenberg, D.; Preud'homme, H.; Schaumlöffel, D. Rapid and Simple UPLC-MS/MS Method for Precise Phytochelatin Quantification in Alga Extracts. *Anal Bioanal Chem* **2010**, *398*, 877–883, doi:10.1007/s00216-010-3970-7.
212. Berlich, M.; Menge, S.; Bruns, I.; Schmidt, J.; Schneider, B.; Krauss, G.-J. Coumarins Give Misleading Absorbance with Ellman's Reagent Suggestive of Thiol Conjugates. *Analyst* **2002**, *127*, 333–336, doi:10.1039/b110988j.
213. Liu, P.; Cai, W.-J.; Yu, L.; Yuan, B.-F.; Feng, Y.-Q. Determination of Phytochelatins in Rice by Stable Isotope Labeling Coupled with Liquid Chromatography-Mass Spectrometry. *J Agric Food Chem* **2015**, *63*, 5935–5942, doi:10.1021/acs.jafc.5b01797.
214. Huang, Y.-Q.; Wang, Q.-Y.; Liu, J.-Q.; Hao, Y.-H.; Yuan, B.-F.; Feng, Y.-Q. Isotope Labelling--Paired Homologous Double Neutral Loss Scan-Mass Spectrometry for Profiling of Metabolites with a Carboxyl Group. *Analyst* **2014**, *139*, 3446–3454, doi:10.1039/c4an00312h.

215. Wood, B.A.; Feldmann, J. Quantification of Phytochelatins and Their Metal(Loid) Complexes: Critical Assessment of Current Analytical Methodology. *Anal Bioanal Chem* **2012**, *402*, 3299–3309, doi:10.1007/s00216-011-5649-0.
216. El-Zohri, M.H.A.; Cabala, R.; Frank, H. Quantification of Phytochelatins in Plants by Reversed-Phase HPLC-ESI-MS-MS. *Anal Bioanal Chem* **2005**, *382*, 1871–1876, doi:10.1007/s00216-005-3331-0.
217. Cao, Z.-Y.; Sun, L.-H.; Mou, R.-X.; Zhou, R.; Zhu, Z.-W.; Chen, M.-X. A Novel Method for the Simultaneous Analysis of Seven Biothiols in Rice (Oryza Sativa L.) Using Hydrophilic Interaction Chromatography Coupled with Electrospray Tandem Mass Spectrometry. *J Chromatogr B Analyt Technol Biomed Life Sci* **2015**, *976–977*, 19–26, doi:10.1016/j.jchromb.2014.11.007.
218. Bellini, E.; Borsò, M.; Betti, C.; Bruno, L.; Andreucci, A.; Ruffini Castiglione, M.; Saba, A.; Sanità di Toppi, L. Characterization and Quantification of Thiol-Peptides in Arabidopsis Thaliana Using Combined Dilution and High Sensitivity HPLC-ESI-MS-MS. *Phytochemistry* **2019**, *164*, 215–222, doi:10.1016/j.phytochem.2019.05.007.
219. Loyola-Vargas, V.M.; Broeckling, C.D.; Badri, D.; Vivanco, J.M. Effect of Transporters on the Secretion of Phytochemicals by the Roots of Arabidopsis Thaliana. *Planta* **2007**, *225*, 301–310, doi:10.1007/s00425-006-0349-2.
220. Kubier, A.; Wilkin, R.T.; Pichler, T. Cadmium in Soils and Groundwater: A Review. *Appl Geochem* **2019**, *108*, 1–16, doi:10.1016/j.apgeochem.2019.104388.
221. Ma, L. and Rao, G. Chemical Fractionation of Cadmium, Copper, Nickel, and Zinc in Contaminated Soils. *J Environ Qual* **1997**, *26*, 259–264, doi:10.1007/s10661-015-4533-3.
222. Strasser, R.; Srivastava, A.; Tsimilli-Michael, M. The Fluorescence Transient as a Tool to Characterize and Screen Photosynthetic Samples. *Probing photosynthesis: Mechanism, regulation and adaptation* **2000**.
223. Goodno, C.C. Inhibition of Myosin ATPase by Vanadate Ion. *Proc Natl Acad Sci U S A* **1979**, *76*, 2620–2624, doi:10.1073/pnas.76.6.2620.
224. Miao, Y.C.; Liu, C.J. ATP-Binding Cassette-like Transporters Are Involved in the Transport of Lignin Precursors across Plasma and Vacuolar Membranes. *Proc Natl Acad Sci U S A* **2010**, *107*, 22728–22733, doi:10.1073/pnas.1007747108.
225. Sanita' di Toppi, L.; Gabbrielli, R. Response to Cadmium in Higher Plants. *Environ Exp Bot* **1999**, *41*, doi:10.1016/S0098-8472(98)00058-6.
226. Kneer, R.; Zenk, M.H. The Formation of Cd-Phytochelatin Complexes in Plant Cell Cultures. *Phytochemistry* **1997**, *44*, 69–74, doi:https://doi.org/10.1016/S0031-9422(96)00514-6.
227. Bellini, E.; Sorce, C.; Andreucci, A.; Vitelli, V.; Saba, A.; Li, M.; Varotto, C.; Sanità di Toppi, L. Intracellular and Extracellular Thiol-Peptides Modulate the Response of Marchantia Polymorpha to Physiological Needs, Excess, and Starvation of Zinc, Copper, and Iron. *Plant Biosyst* **2024**, *158*, 754–762, doi:10.1080/11263504.2024.2357302.
228. Dai, H.; Wei, A.-Z.; Yang, T.; Gu, T.; Zhao, H.; Wu, S.-Q.; Chen, W.-Q.; Huo, K.-K. Cadmium Uptake, Localization and Detoxification in Populus × Canescens.; 2013.
229. Ge, W.; Jiao, Y.Q.; Sun, B.L.; Qin, R.; Jiang, W.S.; Liu, D.H. Cadmium-Mediated Oxidative Stress and Ultrastructural Changes in Root Cells of Poplar Cultivars. *South African Journal of Botany* **2012**, *83*, 98–108, doi:10.1016/j.sajb.2012.07.026.
230. Dos Santos Utmazian, M.N.; Wieshammer, G.; Vega, R.; Wenzel, W.W. Hydroponic Screening for Metal Resistance and Accumulation of Cadmium and Zinc in Twenty Clones of Willows and Poplars. *Environmental Pollution* **2007**, *148*, 155–165, doi:10.1016/j.envpol.2006.10.045.
231. Mohamed, A.A.; Castagna, A.; Ranieri, A.; Sanità di Toppi, L. Cadmium Tolerance in Brassica Juncea Roots and Shoots Is Affected by Antioxidant Status and Phytochelatin Biosynthesis. *Plant Physiology and Biochemistry* **2012**, *57*, 15–22, doi:10.1016/j.plaphy.2012.05.002.

232. Foyer, C. H. and Noctor, G. The Molecular Biology and Metabolism of Glutathione. In *Significance of glutathione to plant adaptation to the environment*; Grill, D., Dekok, L. J. and Tausz, M., Ed.; Kluwer Academic Publishers, Dordrecht, Netherlands, 2001; pp. 27–56.
233. Schafer, F.Q.; Buettner, G.R. Redox Environment of the Cell as Viewed through the Redox State of the Glutathione Disulfide/Glutathione Couple. *Free Radic Biol Med* **2001**, *30*, 1191–1212, doi:10.1016/s0891-5849(01)00480-4.
234. Połeć-Pawlak, K.; Ruzik, R.; Lipiec, E. Investigation of Cd(II), Pb(II) and Cu(I) Complexation by Glutathione and Its Component Amino Acids by ESI-MS and Size Exclusion Chromatography Coupled to ICP-MS and ESI-MS. *Talanta* **2007**, *72*, 1564–1572, doi:10.1016/j.talanta.2007.02.008.
235. Delalande, O.; Desvaux, H.; Godat, E.; Valleix, A.; Junot, C.; Labarre, J.; Boulard, Y. Cadmium-Glutathione Solution Structures Provide New Insights into Heavy Metal Detoxification. *FEBS J* **2010**, *277*, 5086–5096, doi:10.1111/j.1742-4658.2010.07913.x.
236. Uraguchi, S.; Nagai, K.; Naruse, F.; Otsuka, Y.; Ohshiro, Y.; Nakamura, R.; Takanezawa, Y.; Kiyono, M. Development of Affinity Bead-Based in Vitro Metal-Ligand Binding Assay Reveals Dominant Cadmium Affinity of Thiol-Rich Small Peptides Phytochelatins beyond Glutathione. *Metallomics* **2021**, *13*, doi:10.1093/mtomcs/mfab068.
237. Schmöger, M.E.; Oven, M.; Grill, E. Detoxification of Arsenic by Phytochelatins in Plants. *Plant Physiol* **2000**, *122*, 793–801, doi:10.1104/pp.122.3.793.
238. Franić, M.; Galić, V.; Mazur, M.; Šimić, D. Effects of Excess Cadmium in Soil on JIP-Test Parameters, Hydrogen Peroxide Content and Antioxidant Activity in Two Maize Inbreds and Their Hybrid. *Photosynthetica* **2018**, *56*, 660–669, doi:10.1007/s11099-017-0710-7.
239. Deng, J.; Fu, D.; Hu, W.; Lu, X.; Wu, Y.; Bryan, H. Physiological Responses and Accumulation Ability of Microcystis Aeruginosa to Zinc and Cadmium: Implications for Bioremediation of Heavy Metal Pollution. *Bioresour Technol* **2020**, *303*, 122963, doi:https://doi.org/10.1016/j.biortech.2020.122963.
240. Salt, D.E.; Rauser, W.E. MgATP-Dependent Transport of Phytochelatins Across the Tonoplast of Oat Roots. *Plant Physiol* **1995**, *107*, 1293–1301, doi:10.1104/pp.107.4.1293.
241. Wanke, D.; Kolukisaoglu, H.U. An Update on the ABCC Transporter Family in Plants: Many Genes, Many Proteins, but How Many Functions? *Plant Biol (Stuttg)* **2010**, *12 Suppl 1*, 15–25, doi:10.1111/j.1438-8677.2010.00380.x.
242. Procko, E.; O'Mara, M.L.; Bennett, W.F.D.; Tieleman, D.P.; Gaudet, R. The Mechanism of ABC Transporters: General Lessons from Structural and Functional Studies of an Antigenic Peptide Transporter. *FASEB J* **2009**, *23*, 1287–1302, doi:10.1096/fj.08-121855.
243. Frémont, A.; Sas, E.; Sarrazin, M.; Gonzalez, E.; Brisson, J.; Pitre, F.E.; Brereton, N.J.B. Phytochelatin and Coumarin Enrichment in Root Exudates of Arsenic-Treated White Lupin. *Plant Cell Environ* **2022**, *45*, 936–954, doi:10.1111/pce.14163.
244. Song, W.-Y.; Park, J.; Eisenach, C.; Maeshima, M.; Lee, Y.; Martinoia, E. ABC Transporters and Heavy Metals. **2014**, 1–17, doi:10.1007/978-3-319-06511-3_1.
245. Satofuka, H.; Fukui, T.; Takagi, M.; Atomi, H.; Imanaka, T. Metal-Binding Properties of Phytochelatin-Related Peptides. *J Inorg Biochem* **2001**, *86*, 595–602, doi:10.1016/S0162-0134(01)00223-9.
246. Jozefczak, M.; Remans, T.; Vangronsveld, J.; Cuypers, A. Glutathione Is a Key Player in Metal-Induced Oxidative Stress Defenses. *Int J Mol Sci* **2012**, *13*, 3145–3175, doi:10.3390/ijms13033145.